Magisterarbeit

Advanced Oxidation Processes at the bench scale unit level:

Characterisation and experimental investigations of

Ethylenediamintetraacetic acid (EDTA)

Erstellt für

VTU Technology GmbH

Vorgelegt von:
Magdalena Drózd
0535376

Betreuer/Gutachter:

Ao.Univ.-Prof.Dipl.-Ing.Dr.techn. Josef Draxler
Dipl.-Ing. Dr. Julia Zelenka

Leoben, März 2009

EIDESSTATTLICHE ERKLÄRUNG

Ich erkläre an Eides statt, dass ich diese Arbeit selbständig verfasst, andere als die angegebenen Quellen und Hilfsmittel nicht benutzt und mich auch sonst keiner unerlaubten Hilfsmittel nicht bedient habe.

AFFIDAVIT

I declare in lieu of oath, that I wrote this thesis and performed the associated research myself, using only literature cited in this volume.

Leoben, März 2009

Kurzfassung

Advanced Oxidation Processes Laboranlage:
Charakterisierung und experimentelle Untersuchungen am Beispiel des Komplexbildners Ethylenediamintetraessigsäure

Advanced Oxidation Processes (AOPs) spielen eine bedeutende Rolle bei der Aufbereitung von Abwasser mit persistenten Inhaltsstoffen, welche durch herkömmliche Abwasserbehandlungsverfahren nur schwer oder gar nicht abgebaut werden können. Ethylendiamintetraessigsäure (EDTA), ein persistenter Komplexbildner, der in zahlreichen Industriebranchen eingesetzt wird, mit der Eignung Schwermetalle aus Bodensedimenten zu mobilisieren, diente dieser Arbeit als Modellsubstanz.

Die gegenwärtige Diplomarbeit behandelt die Charakterisierung einer AOP-Laboranlage für photochemische, elektrochemische und katalytische Oxidationsprozesse. Es wurden die Verweilzeitverteilungen unterschiedlicher Reaktoren und einer Elektrolysezelle vermessen, sowie Photonenflüsse in Photoreaktoren bei einer Wellenlänge von λ = 254. In einem weiteren Teil der Arbeit wurde die Herstellung von kathodisch produziertem Wasserstoffperoxid (H_2O_2) an granuliertem Glaskohlenstoff näher betrachtet.

Abschließend wurden mit der oben erwähnten Modellsubstanz Abbauuntersuchungen zur direkten anodsichen Oxidation, zur Fe(II)-EDTA-Photolyse und zum Kombinationsverfahren „Anodische Oxidation mit kathodisch produziertem H_2O_2 welches durch Photolyse aktiviert wird" (Anox/H_2O_{2cath}/UV) durchgeführt.

Die Verfahrenseffektivität wurde in Beziehung auf die verwendeten Reaktoren und dem eingestellten Volumenstrom der EDTA-Lösung in der Versuchsanlage analysiert. Die Gegenüberstellung der unterschiedlichen EDTA-Abbaumethoden und deren wirtschaftliche Betrachtung wurde mittels Strom- und Strahlerleistungsausbeute, sowie anhand des spezifischen Energiebedarfs, welcher aus den Messergebnissen ermittelt wurde, bewertet.

Abstract

Advanced Oxidation Processes at the bench scale unit level: Characterisation and experimental investigations of ethylenediamintetraacetic acid (EDTA)

Advanced Oxidation Processes (AOPs) have gained in great importance in recent years as an alternative method of wastewater treatment. Problems with pollutants not amenable to biological treatments and with high chemical stability especially revealed the prominent role of that class of oxidation techniques.

Ethylenediamintetraacetic acid (EDTA), a common applied complexing agent in many industrial branches, not only has a high resistance to environmental degradation, but also an ability to bind heavy metal ions, which could cause hazardous effects.

This master thesis includes the characterization of Advanced Oxidation Processes at the bench scale unit, consisting of a low pressure mercury lamp from *Heraeus* with power output of 35 W and maximum emission at λ = 254 nm, *EC Electro MP-Cell* with iridium oxide plate as an anode and glassy carbon as a cathode. In addition there were four exchangeable reactors used. The residence time distribution and photon flow in various reactors were investigated, as well as hydrogen peroxide production on the cathode.

Three different AOPs techniques were applied in the studied EDTA degradation process: direct EDTA oxidation on the anode, Fe(II)-EDTA photolysis and Anox/$H_2O_2^{Cath}$/UV method. Effectiveness of these processes was analyzed according to the implemented reactor and the flow rate of EDTA solution in a bench scale unit. To enable comparison of the various processes from the economical point of view, current efficiency and radiant power efficiency and specific energy demands were calculated from the achieved experimental data.

Table of contents

8. Experimental results – reactors' characterisation 48

9. Experimental results – EDTA degradation 73

1. Introduction

1.1. Problem identification

Increasing environmental awareness is leading to higher restrictions imposed on the emitted pollution. The level of water contamination with EDTA – a common applied complexing agent in many industrial branches - is mostly underestimated. Despite EDTA's low concentration in surface waters (usually about several dozen µg/l), its high resistance to environmental degradation and ability to bind heavy metal ions could cause hazardous effects. According to European Union Water Framework Directive 2000/60/EG and its environmental quality norm recommendation for other relevant substances, EDTA concentration in surface waters should not exceed 10 µg/l. [1],[2]

As EDTA can be biologically degraded under only a number of specific conditions like relatively high hydraulic and sludge retention time, an alkaline pH value of the wastewater, a relatively high EDTA concentration and no complex bonding with heavy metal ions, in the present study the Advanced Oxidation Processes (AOPs) were investigated as an alternative decomposition method. AOPs, sometimes also called Advanced Oxidation Technologies (AOTs) or Enhanced Oxidation Processes (EOPs), rely mainly on the formation of reactive and short-lived oxygen containing intermediates such as hydroxyl radicals (•OH). Besides photochemical and solar photocatalytic processes many other technologies are included in AOPs, for example electrochemical oxidation of organic water contaminants, catalytic processes and non-thermal plasma treatment methods for exhaust air processing. The greatest advantage of AOPs is that they are „not-invasive" methods, no sludge formation is involved, no subsequental disposal has to be taken into account, only a minimum treatment of residues is necessary. There are several alternatives in the selection of the auxiliary oxidant (H_2O_2, O_3) as well as implementation of synergistic treatment concepts with conventional technologies (carbon adsorption, biological treatment). The possibility of applying batch or plug flow modes, also at large volume flows, low preventative maintenance and operating requirements together with reliable safety during operation make AOPs a very interesting option for the wastewater treatment branch.

EDTA degradation using AOPs instruments was broadly investigated, applying diverse combinations, among them H_2O_2/UV and $Fe^{2+}(Fe^{3+})$/UV were the best known ones. In present work three different ways of EDTA decomposition were researched: direct anodic oxidation on the anode, Fe(II)–EDTA photolysis and Anox/$H_2O_2^{Cath}$/UV process. All the experiments were carried out at the *VTU Technology* laboratory with application of various reactors.

It is well-known that any chemical reaction depends strongly on the reactor set-up. When it comes to the photochemical reactions, that fact has even greater importance. The research on the EDTA degradation involved such instruments as coil reactor, small and large plug flow reactor and continuous stirred-tank reactor, which was also used as a batch reactor. To be able to optimise the experiments the characterisation for all these reactors was necessary.

That included description of residence time distribution at different flow rates, photon flow and radiant energy determination and also hydrogen peroxide production on the cathode in the electrolysis cell.

The bench scale unit characterisation constituted the first part of the investigation and allowed to carry out the second and main part of the research: EDTA degradation with AOPs instruments. [3], [4]

1.2.   Goals and targets

This master thesis aims to:

1. Characterise the AOPs bench scale unit expressed by:

    - residence time distribution in various reactor types

    - photon flow in various reactor types at low mercury UV lamp radiation

    - hydrogen peroxide production on the cathode in *EC Electro MP-Cell*

2. Discuss the possibility of application of Advanced Oxidation Processes as an instrument of EDTA mineralization according to results achieved at the bench scale experiments:

    - direct anodic EDTA oxidation

    - Fe(II) – EDTA photolysis

    - Anox/$H_2O_2^{Cath}$/UV process

2. Principles of electrochemistry

2.1. Electrolysis cell and reactor

All of the electrochemical processes and substance conversions take place in an electrochemical cell. The electrolysis cell could be described as a chemical reactor, in which an electric current is used to bring about an otherwise non-spontaneous chemical reaction. Such an electrolysis cell consists of:

- electrolyte
- electrodes, which are immersed in the electrolyte
- electronics with electrical connections
- electrolysis cell body [5], [6]
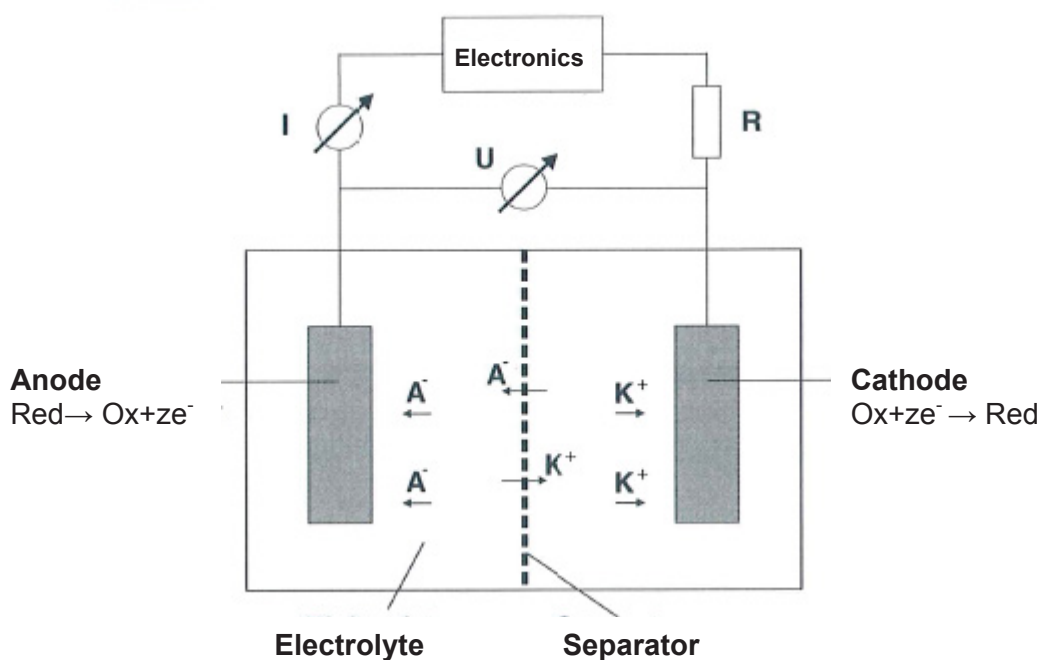
Figure 2.1: Common set-up of the electrolysis cell [5]

2.1.1. Electrodes

Electrodes are made of conductor material through which electrons leave or enter electrochemical cell and simultaneously enable the deposit of ions at their surface. The electrochemical reactions take place at the surface of electrodes.

The electrode can act as a source of electrons transferred to the species in the solution. In that case we can speak about reduction, which take place on the electrode called 'cathode'. The reduction reaction is described with Eq. 2.1:

Eq. 2.1 $$Ox + ze^- \rightarrow Red$$

The electrode, which act as a sink of electrons transferred from species into the solution is the 'anode'. On the anode an oxidising reaction takes place:

Eq. 2.2   Red → Ox + ze$^-$

To make electron transfer possible, there must be correspondence between the energies of the electron orbitals where transfer takes place in the donor and acceptor. In the electrode this level is the highest filled orbital, which in metal is the Fermi energy level and in soluble species – the orbital of the valence electron to be given or received.

Therefore:

- for a reduction, there is a minimum energy that the transferable electrons from the electrode must have before transfer can occur (negative potential)

- for an oxidation, there is a maximum energy that the lowest unoccupied level in the electrode can have in order to receive electrons from species in solution (sufficiently positive potential) [7],[8]

Electrode types

The electrodes vary in their size, design and material of which they consist. The most important requirements, which the electrode material has to be fulfill are:

- high conductivity
- adequate chemical resistance against electrolyte and electrolysis products
- good mechanical strength and machinability
- stability
- high electrical activity
- reasonable price [7],[5]

There are many electrode materials and the choice of the right one depends on the useful potential range of the electrode in the particular solvent and the qualities and purity of the material.

The most frequently materials are:

- metal electrodes
- carbon electrodes
- other solid materials: semiconductors, for example metal oxides and conducting organic salts
- mercury drop electrodes (liquid nature)

A metal electrode is the most typical one. A general advantage is that the high conductivity of metal electrodes results in low background currents. It could be applied as a foil, mesh or wire, but it is preferable to present it to the solution in a compact way.

Carbon electrodes exist in various conducting forms. Carbon has a high surface activity and therefore is susceptible to poisoning by organic compounds. Bonds with hydrogen, hydroxyl and carboxyl groups can be formed on the carbon surface. Carbon in the form of glassy carbon is widely used, especially when a chemical inert electrode without the catalytic power of platinum is required. [7],[8],[9]

2.1.2. Electrolyte

The main function of electrolytes is transporting of ions between electrodes. The important properties of an electrolytes are good ionic mobility, they should be also chemically inert. Another aspect is ionic conductivity, which is in the large part responsible for cell voltage lost.

Electrolytes are usually applied in form of fluids, using water as a solvent.

The charge transfer follows in two pathways:

- through **anions** – which are negative charged electrons and migrate to anode

- through **cations** – which are positive charged electrons and migrate to cathode

Apart from transporting the charge, the electrolyte also plays another role: it is responsible for the transport of educts and products to and from the electrodes and the products. Additionally, there are reactions taking place in the electrolyte itself. Last, but not least, the electrolytes can also act as heat exchanger. [5]

2.2. Electrochemical reactions and reaction techniques

During electrochemical reactions the electrodes will accept (cathode) or release (anode) the charge. That is the reason to call electrochemical reactions as cathodic or anodic part reactions. The total electrochemical reaction is in charge balance neutral. In the electrochemistry exists the law of charge permanence: during the electrochemical reactions no charge can be lost or created.

As an example of part reaction on the cathode and anode the water electrolysis is presented:

Eq. 2.3: $$3H_2O \rightarrow \frac{1}{2}O_2 + 2H_3O^+ + 2e^-$$ (anode)

Eq. 2.4: $$2H_3O^+ + 2e^- \rightarrow H_2 + 2H_2O$$ (cathode)

Eq. 2.5: $$H_2O \rightarrow H_2 + \frac{1}{2}O_2$$ (total reaction)
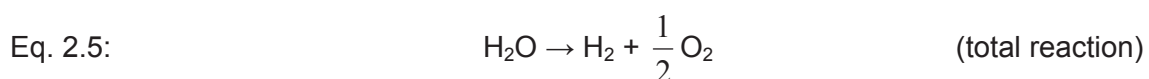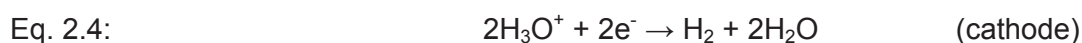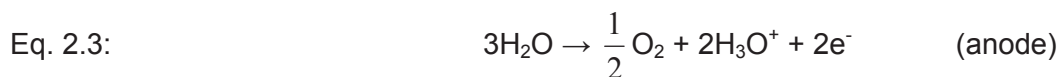
As we can see from Eq. 2.3 and Eq. 2.4 at the anode the oxygen formation takes place and at the cathode the hydrogen will be produced.

All of reactions in the electrolysis cell run at the phase boarder, between electrode and electrolyte. This reaction layer is also called 'the double layer'. At the double layer two different phases (electrode and electrolyte) stay in the contact, so we can speak about heterogenic reaction, with physical-chemical activities. The reaction techniques describe the whole process step by step: the chemical reaction as well as adsorption and desorption of educt and product molecules and of course electrochemical reaction with charge transfer itself.
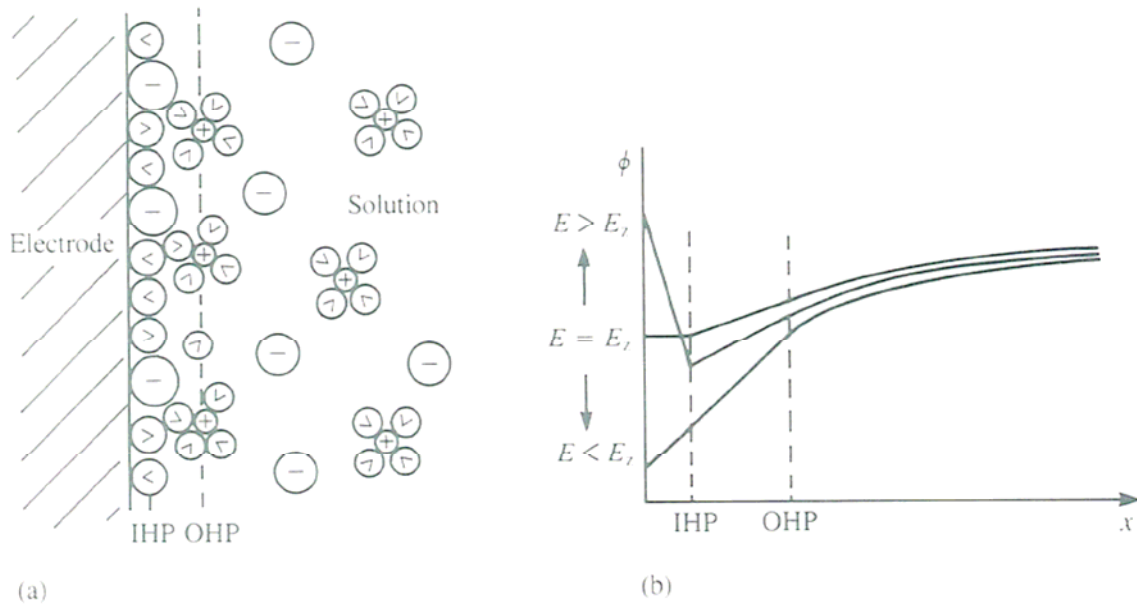
Figure 2.2: The Bockris model of the double layer.(a) Arrangement of ions and solvent molecules (b) Variation of the electrostatic potential, φ, with distance, x, from electrode. IHP first solvatation layer, OHP second solvatation layer [8]

During the reaction the educts concentration drops in the reaction layer and it has to be re-supplied from the electrolyte solution. At the same time the formed product has to be removed. That is why in electrochemical reactions, additionally the transport processes have to be considered.[5]

2.3. Electrochemical potential and Nernst equation

The electrochemical potential

The contribution of an electric potential to the chemical potential is calculated by noting that the electrical work of adding a charge *ze* to the potential ϕ is equal to $ze\phi$, and therefore the work per mole is $ze\phi F$, where *F* is Faraday's constant, *z* the number of electrons and *e* the elementary charge. Because at electrochemical reactions temperature and pressure are constant the maximum electrical work can be identified with the change in Gibbs energy. The difference in chemical potential of an ion with and without the electrical potential present is $z\phi F$. The chemical potential of an ion in the presence of an electric potential is called its electrochemical potential $\overline{\mu}$ and is described with Eq. 2.6:

Eq. 2.6:
$$\overline{\mu} = \mu + z\phi F$$

where μ is the chemical potential of the species when electrical potential is zero. When *z* = 0 (a neutral species), the electrochemical potential is equal to the chemical one. In phases of variable composition, the values of the Gibbs energy, *G*, are determined by Eq. 2.7 [10],[11]:

Eq. 2.7:
$$G = \sum n_k \mu_k$$

<u>Nernst equation</u>

The Nernst equation relates the activities of the species involved with the electrode potential, E, of the half-reaction and its standard electrode potential E^0, which is the value of the potential relative to the standard hydrogen electrode when the activities of all species are consistently. For the general half-reaction equation:

Eq. 2.8: $\sum \upsilon_i Oxid_i + ze^- \rightarrow \sum \upsilon_i Red_i$
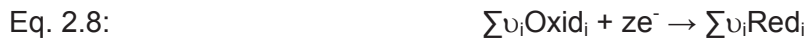
where z is the stoichiometric number of electrons transferred for each species. Nernst equation is described as follows:

Eq. 2.9: $E = E_0 - \dfrac{RT}{zF} \sum v_i \ln \dfrac{a_{Oxid}}{a_{Red}}$,

where a_{Oxid} and a_{Red} are the chemical activities of the redox couple. The v_i has positive values for products (reduced species) and negative values for reagents (oxidised species).

An electrochemical cell is a combination of two electrodes, and one of each can be considered as making a characteristic contribution to the overall cell potential. To define the standard potential E^0 of the electrode it has to be compared with a reference electrode, which has a stable and well-known potential. The examples of the standard reference electrodes are: the hydrogen electrode (SHE), the calomel electrode or glass electrode. [8],[11]

2.4.   Cell voltage and specific energy demand

The cell voltage does not consist not only of the drop of voltage between cathode and anode but also of voltage losses, which are caused, amongst other, by ohm's resistance. The cell voltage of any operating electrolysis is composed of following drops of potential:

- Equilibrium potential difference of the cell reaction $U_{0,c}$
- anodic overpotential η_a
- cathodic overpotential η_c
- ohmic voltage drop ΔU_Ω between cathode and anode
- in case of electrolyet separation: diaphragm voltage potential drop U_d

An example of potential run between two electrodes presents Figure 2.3.
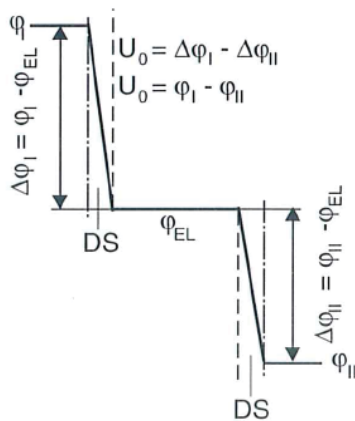
Figure 2.3: Potential run between two electrodes, which stay in electrochemical equilibrum [5]

The total voltage of the electrolysis cell could be described with following equation:

Eq. 2.10: $U_{cell} = U_{0,c} + \eta_a - \eta_c + \Delta U_\Omega + U_d$

The equilibrium potential of the cell reaction, $U_{0,c}$, is determinate by the Gibbs free enthalpy of the cell reaction and can be calculated fairly accurately by adding the equilibrium electrode potentials E^0_i for the electrode reactions corrected for the concentrations or partial pressures of the potential –determining species according to Nernst's equation. [12]

Eq. 2.11: $$U_{0,c} = \frac{\Delta G}{zF} = (E_A - E_C) = \left[E_a^0 + \frac{RT}{zF} \ln\left(\frac{c_{ox}}{c_{red}} \right) \right]_a - \left[E_c^0 + \frac{RT}{zF} \ln\left(\frac{c_{ox}}{c_{red}} \right) \right]_c$$

In the praxis the simplified correlation is applied:

Eq. 2.12: $U_{cell} = U_{0c} + I_a R_o$

U_{0c} could be treated as a constant, which depends only on the electrolytic process. On the other hand, R_o depends on construction details of electrolysis cell and the electrolyt's character, compound, temperature, is than actually the *"characteristics"* of the cell. [9]

To define how much kWh was absorbed during an electrochemical process, the average voltage U_{cell} of the electrolysis cell has to be determined. The absorbed energy is described with equation

Eq. 2.13 $E_w = I_a t_h U_{cell}$ [W]

where U_{cell} is the total electrolysis cell potential, I_a is the electricity current and t_h is the time. The specific energy demand refers to the in the effect achieved amount of product at given current and time. It could be presented in kWh/kg or kWh/m^3, depending on that if we use molar mass or molar volume. [9]

Eq. 2.14: $$E_S = \frac{E_w}{m_{prod}}$$

2.5.   Ohm's law, conductivity

Ohm's law describes the dependence between voltage U, resistance R and current I:

Eq. 2.15: $$I = \frac{U}{R}$$ [A]

The resistance R depends on the electrolyte, amount of ions in unit of volume and their mobility. The resistance of a sample increases with its length l and decreases with its cross-sectional are q:

Eq. 2.16: $$R = \frac{\rho \cdot l}{q}$$ [Ohm]

The resistivity, ρ, is a property of the solution and is specific for every conductor. For electrolytes it could be defined as the resistance, which is performed in fluid's cube of 1 cm ridge length.

The reciprocal of resistance and resistvity is the conductance G and conductivity κ. Therefore:

Eq. 2.17: $$G = \frac{1}{R} = \kappa \frac{q}{l}$$

The units of conductance are 1/ohm which is also known as the siemens S. [7],[13]

2.6.   Faraday's laws

The number of reactants molecules involved in an electrode reaction is related stoichiometrically to the number of charges (electrons) flowing in the circuit. This dependence is illustrated by Faraday's laws.

Faraday's first law*:*

In electrolysis, the quantities of substance involved in the chemical change are proportional to the quantity of electricity which passes through electrolyte.[10]

This definition is characterised by Eq. 2.18

Eq. 2.18:   m = kIt = kQ

where m is the mass of the substance altered at an electrode and Q is the total electric charge passed through the substance

Faraday's second law:

The masses of different substances set free or dissolved by a given amount of electricity are proportional to their chemical equivalents. [10]

is described with Eq. 2.19

Eq. 2.19:
$$m = \frac{MQ}{zF}$$

where M is the molar mass of the substance and z is the valence number of ions of the substance. The Faraday's constant, F, is the magnitude of the charge per mole of electrons and its value is calculated as following [6]:

Eq. 2.20: $F = 1,602 \times 10^{-19}C \times 10^{23}/(mol\ e^-) = 9,6485 \times 10^4 C/(mol\ e^-)$

2.7.   Current density and efficiency

The current density presents the density of flowing charge. It is the current I, which occurs to the cross-section area A.

Eq. 2.21:
$$i = \frac{I}{A} \qquad [Acm^{-2}]$$

The current efficiency is calculated from the ratio of efficient deposited amount of product m_{eff} to the theoretical value m_{th}, which should be achieved.[13]

Eq. 2.22:
$$\beta = \frac{m_{eff}}{m_{theor}}$$

3. Principles of photochemistry

Photochemistry comprises the chemical reactions of atoms or molecules that have been electronically excited by absorption of light with wavelength in the range of 200 nm to ca. 700 nm. In a primary process, products are formed directly from the excited state of reactant (fluorescence), while products of secondary processes originate from intermediates that are formed directly from the excited state of a reactant (photosynthesis, photochemical chain reactions). It is important to consider the timescales of excited state formation and decay before describing the mechanism of photochemical reactions, as the competing with the formation of photochemical products is a host of primary photophysical processes that can deactivate the excited state.[11],[12] The most common photophysical processes are presented in Table 1.

Table 1 Common photophysical processes [11]

Primary absorption	S + hv → S*
Fluorescence	S* → S+hv
Stimulated emission	S* + hv → S + 2hv
Intersystem crossing (ISC)	S* → T*
Phosphorescence	T* → S+ hv
Internal conversion (IC)	S* → S
Collision-induced emission	S* + M → S + M + hv
Collisional deactivation	T* + M → S +M

3.1.   Planck's law

Max Planck studied black-body radiation from the viewpoint of thermodynamics. He found out that the energy of each electromagnetic oscillator is limited to discrete values and cannot be varied arbitrarily. The limitation of energies to discrete values is called the quantisation of energy. In particular, Planck found that he could account for the observed distribution of energy if he supposed that the permitted energies of an electromagnetic oscillator of frequency ν are integer multiples of $h\nu$:

Eq. 3.1: $$E = nh\nu = h\frac{c}{\lambda} \text{ , } n\text{=}0,1,2$$

where *h* is a fundamental constant known as the Planck's constant. The value of ν , which is an undetermined parameter in the theory, may be obtained by varying its value until a best fit is obtained. The currently accepted value for *h* is 6,626x10^{-34} Js. [11]

3.2.   Photon flow

The photon flow, Φ_P, is the number of photons per unit time and is described with Eq. 3.2:

Eq. 3.2:
$$\Phi_P = \frac{dN}{dt}$$

When the number of photons is constant over the time, the simplified expression could be applied [14]:

Eq. 3.3:
$$\Phi_P = \frac{N_P}{t}\ [s^{-1}].$$

3.3.   Lambert – Beer law

The ratio of the transmitted intensity, I, to the incident intensity, I_0, at a given frequency is called the transmittance, T, and is described by equation:

Eq. 3.4:
$$T = \frac{I}{I_0}$$

The transmitted intensity varies with the length, d, of the sample and the molar concentration, c, of the absorbing species in accord with the Lambert-Beer law:

Eq. 3.5:
$$I = I_0 \cdot 10^{-\varepsilon \cdot c \cdot d}$$

The quantity ε is called molar absorption coefficient (formerly 'extinction coefficienty'). The molar absorption coefficient depends on the frequency of the incident radiation and is greater where the absorption is most intense.

The absorbance, A , of the sample at a given wave length is

Eq. 3.6:
$$A = \log\frac{I_0}{I} = -\log T = -\varepsilon \cdot c \cdot d$$

The Lambert-Beer law implies that the intensity of electromagnetic radiation transmitted through a sample at a given wave length decreases exponentially with the sample thickness and the molar concentration. [11]

3.4.   Quantum yield

Quantum yield of a photophysical or photochemical event is a quantitive measure of the efficiency of this process. It is a unit-less constant and it can achieve values between zero and one.

Quantum yield could be defined as a

Number n of events per unit time divided by the number of photons absorbed during this period [3]

Eq. 3.7:
$$\Phi_\lambda = \frac{dn(event)/dt}{\phi_P^{abs}}$$

Quantum yields may depend on the wavelength of the absorbed UV/VIS radiation, but there are many photochemical systems, which have a constant quantum yield Φ over a defined wavelength range. Such chemical systems can be easily used as a chemical actinometers (more in Chapter 6.2).

For batch reactors Eq. 3.7: could be also be written as

Eq. 3.8:
$$\Phi_\lambda = \frac{\Delta c_i \cdot V}{\Phi_P \cdot t} \quad [\text{mol/einstein}]$$

and for the plug flow reactors as

Eq. 3.9:
$$\Phi_\lambda = \frac{\Delta c_i \cdot \dot{V}}{\Phi_P}$$

3.5.   Radiant power

Radiant power, P, also called radiant (energy) flux is generally used in sense of the „*rate of transfer of fluid, particles or energy across a given surface*" and is presented by the

Eq. 3.10:
$$P = \frac{Q}{t}$$

where the radiant energy, Q, is constant over the time considered. Eq. 3.10 could be also presented using Planck's equation [3]:

Eq. 3.11:
$$P = \Phi_P \frac{h \cdot c}{\lambda} N_A$$

3.6.   Specific energy demand

The specific energy demand, E_{EM}, could be used to compare various photochemical reactors or different photochemical processes. It is defined as a ratio between the total amount of energy supplied to the AOP treatment system and mass unity of the pollutant.[3] The mathematical formula for idealized batch reactor is presented with Eq. 3.12

Eq. 3.12:
$$E_{EM} = \frac{P_{el} \cdot t \cdot 10^3}{V_R \cdot M_M (c_{t=0} - c_t)}$$

and for the ideal plug flow reactor with Eq. 3.13:

Eq. 3.13:
$$E_{EM} = \frac{P_{el}}{\dot{V} \cdot M_M (c_{t=0} - c_t)}$$
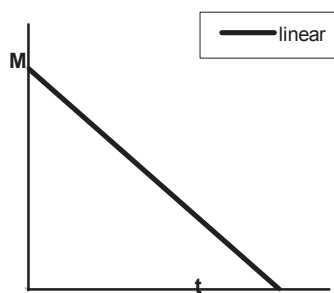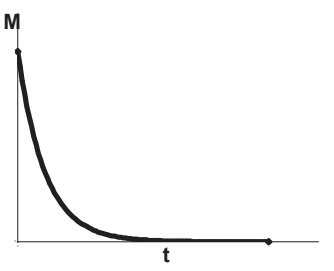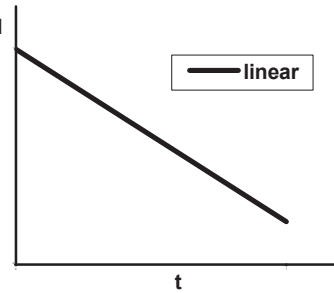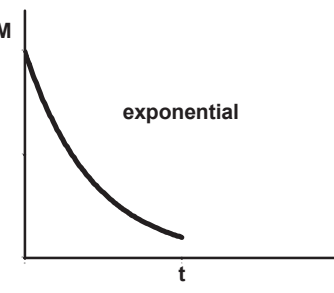
3.7.   Photochemical reactions

Photochemical reactions do not have a specific reaction order. Ground state (dark) reactions can run according to zero, first or second order. The kinetic behavior of a photochemical reaction depends strongly on the absorptions conditions – under total absorbance (high absorption coefficient) the decrease of the reactant concentration caused by irradiation is linear. In very dilute solutions under conditions with a very low absorption coefficient only a small fraction of the incident photon irradiance is absorbed by the reactant leading ultimately to its exponential decreases. [3] The comparison of the reaction rate constants is presented in Table 2.

Table 2: Comparison of the reaction rate expressions of simple thermal and photochemical reactions in a solution. A –area exposed to irradiation; V – irradiated volume; d – path length of irradiation; $E_{P,0}$ – incident photon irradiance, $E_{P,abs}$ – total absorbed photon irradiance; Φ_M – quantum yield of the photochemical conversion of M to photoproduct P at wavelength λ .[3]

Reaction of substance M	Rate constant, unit	Reaction rate	Graphical representation
M → P Reaction order: 0	k_0 [mol l^{-1}s^{-1}]	$-\dfrac{dc_M}{dt} = k_0$ $c_{M,t} = c_{M,t=0} - k_0 t$	
M → P Reaction order: 1	k_1 [s^{-1}]	$-\dfrac{dc_M}{dt} = k_1$ $c_M = c_{M,t=0} \cdot e^{-k_1 t}$	
M + hν → M* → P Photochemical reaction	if $A = \varepsilon_M c_M d > 2$ then $E_{p,abs} = E_{p,0}$	$-\dfrac{dc_M}{dt} = \Phi_M E_{P,0} t \dfrac{A}{N_A V_R}$ $c_{M,t} = c_{M,t=0} - \Phi_M E_{P,0} t \dfrac{A}{N_A V_R}$	
	if $A = \varepsilon_M c_M d \ll 1$ then $F = 1 - 10^{-\varepsilon_M c_M d} \cong 2{,}303 \varepsilon_M c_M d$	$-\dfrac{dc_M}{dt} = 2{,}303 \Phi_M E_{P,0} \varepsilon_M d c_M \dfrac{A}{N_A V_R}$ $c_{M,t} = c_{M,t=0} \exp\!\left(-(2{,}303 \Phi_M E_{P,0} \varepsilon_M d c_M \dfrac{A}{N_A V_R})t\right)$	

4. AOPs

Advanced Oxidation Processes have become broadly applied oxidation methods in the waste water treatment. Although they differ from each other, AOPs could be characterised by the same chemical feature: the capability of exploiting the high reactivity of •OH radicals in driving oxidation processes in near ambient temperature and pressure. AOPs are suitable for achieving the complete abatement and for mineralisation of even less reactive pollutants.

•OH radicals are extraordinarily reactive species, short-lived, non-selective reagents, which are easy to produce. The mean lifetime of •OH depends on their chemical environment and is estimated to be in the order of 10 micros in the presence of dissolved organic matter. The reduction potential E of •OH radicals has value •OH, H^+/H_2O = 2,730 V and is one of the strongest oxidants (see Table 3). They attack the most part of organic molecules with very high rate constants usually in the order of 10^6–$10^9\,M^{-1}\,s^{-1}$. [3],[16].

Table 3 Reduction potentials of selected oxidizing species [3]

Oxidation species	Reduction potential (V)
Fluorine $F^\bullet/F$	3,600
Hydroxyl radical •OH, H^+/H_2O	2,730
Sulfate radical $SO_4^{\bullet-}/SO_4^{2-}$	2,430
Chlorine radicals $Cl^\bullet/Cl-$	2,200 – 2,600
Ozone, O_3, H^+/H_2O	2,07
Hydrogen peroxide, H_2O_2, H^+/H_2O	1,77

As the hydroxyl radicals are so reactive and unstable, they must be continuously produced by means of photochemical or chemical reactions, which are listed below:

- H_2O_2/Fe^{2+} (Fenton)
- H_2O_2/Fe^{3+} (Fenton-like)
- $H_2O_2/\,Fe^{2+}\,(Fe^{3+})/UV$ (photo assisted Fenton)
- $TiO_2/hv/O_2$ (photocatalysis)
- O_3/H_2O_2 (PEROXON-process)
- O_3/UV (UVOX-method)
- H_2O_2/UV (UV-PEROX-method) [16]
- electrochemical •OH production   (electrochemical oxidation)

Another important aspect concerning the opportunity of AOPs' application is chemical oxygen demands. Only wastes with relatively small COD contents (≤ 5.0 g/l) can be suitably treated since higher concentrations would require the consumption of too large amounts of expensive reactants. [16], [25]

Next chapters include more detailed description of some existing AOPs.

4.1.   Photo – induced oxidation reactions

Oxidation processes driven by UV/VIS radiation are called photooxidation reactions. Photo-induced oxidations, such as photoionization of molecules M are induced by absorption of electromagnetic radiation. Ejection of an electron from the electronically excited substrate molecule M* into the surrounding medium leads to the formation of radical cation ($M^{\bullet+}$), which is presented in Eq. 4.1

Eq. 4.1: $M + h\nu \rightarrow M^* \rightarrow M^{\bullet+} + e^-$

Usually, photo-induced oxidation reactions include reactions of a substance M with oxygen under the influence of UV/VIS radiation. In this case, the photooxidation is induced by electronic excitation of the substrate M, from which the electron transfer to ground state molecular oxygen takes place.[3] This reaction could be described as following:

$$O_2 \searrow$$

Eq. 4.2: $M + h\nu \rightarrow M^* \rightarrow Products$
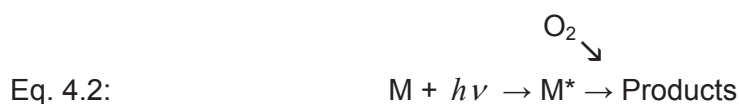
4.2.   Photolysis of aqueous hydrogen peroxide

Photolysis of aqueous hydrogen peroxide in the UV-C range represents one of the easiest ways of producing a sufficient amount of hydroxyl radicals. The general photochemical reaction is described by Eq. 4.3:

Eq. 4.3: $H_2O_2 + h\nu \rightarrow H_2O_2^* \rightarrow 2\ ^\bullet OH$

The major drawback of this process is the small molar extinction coefficient of H_2O_2 which is only 18.6 M^{-1} cm^{-1} at 254 nm. This means that only a relative small fraction of incident light is therefore exploited in particular in the cases where organic substrates will act as inner filters. The rate of photolysis of aqueous H_2O_2 depends on pH-value and increases when more alkaline conditions are used [1]. This could be caused by higher molar absorption coefficient of the peroxide anion HO^{2-} which at 254 nm is 240 M^{-1} cm^{-1}. [1], [16]

Hydroxyl radicals can oxidise organic and inorganic substrates by different types of reactions like those presented in Eq. 4.4 - Eq. 4.6. [1]

Eq. 4.4: $^\bullet OH + M^n \rightarrow M^{n+1} + (OH^-)_{aq}$ (electron transfer)

Eq. 4.5: $^\bullet OH + R\text{-}H \rightarrow R + H_2O$ (hydrogen abstraction)

Eq. 4.6: $^\bullet OH + R_2C{=}CR_2 \rightarrow CR_2{=}C(OH)R_2$ (electrophilic addition)
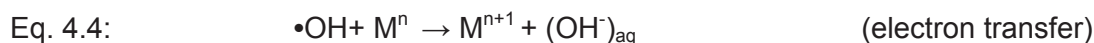
4.3.   AEOPs

Advanced Electrochemical Oxidation Processes are based on the production of hydroxyl radicals (•OH) from water oxidation on the surface of a high O_2-overvoltage anode and/or from Fenton's reaction between added Fe^{2+} and hydrogen peroxide electrogenerated at the cathode. There are two possibilities of AEOP reactions:

- direct oxidation on the anode

- indirect process with application of strong oxidation compounds [5], [16]

4.3.1. Direct oxidation

The aim of direct oxidation is total mineralisation of the organic molecules to CO_2 and H_2O. This is possible because of the reaction of organics with adsorbed hydroxyl radical $(•OH)_{ads}$, which is formed at the anode from water oxidation. The adsorbed radicals react with organic compounds R and result in CO_2 and H_2O formation. The whole reaction process could be described as follows:

Eq. 4.7: $2H_2O \rightarrow •OH_{ads} + H_3O^+ + e^-$

Eq. 4.8: $M + •OH_{ads} \rightarrow M(•OH)_{ads}$

Eq. 4.9: $R + M(•OH)_{ads} \rightarrow M + mCO_2 + nH_2O$

The whole oxidation reaction is described with following general scheme:

Eq. 4.10: $C_mH_nO_l + (2m - 1) H_2O \rightarrow m\ CO2 + (4m + n - 2l)\ H^+ + (4m + n - 2l)e^-$
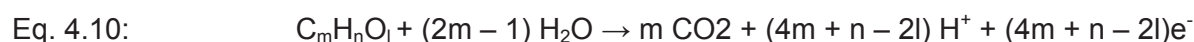
According to Eq. 4.10 the theoretical amount of needed electrons could be calculated with following equation:

Eq. 4.11: $z_{theor} = 4m + n - 2l$

The mechanism of oxidative decomposition is in fact much more complicated. The reaction sequence leading to the formation of CO_2 rests upon gradual charge of electrons to the electrode runs in many elementary reactions and formation of adsorbed intetrmediates.

Direct oxidation can be run only at high anodic potentials, when •OH radicals are generated with simultaneous oxygen evolution, thus producing regeneration of the anode surface.

The oxidation processes are usually held in acid electrolytes as the solubility of CO_2 is in that case much lower than in basic range and CO_2 could be removed as a gas from the electrolyte. [5], [16]

4.3.2. Indirect electrooxidation methods

In the last years potent indirect electrooxidation methods have been developed. They involve continuous supply of hydrogen peroxide to the contaminated solutions. The oxidant is generated in acid medium from the two-electron reduction of O_2 (see Chapter 2.2).

The oxidation power of hydrogen peroxide is often enhanced by addition of Fe^{2+} what allows to formation of •OH radicals (so-called Fenton's reaction).

Eq. 4.12: $Fe^{2+} + H_2O_2 \rightarrow Fe^{3+} + •OH + OH^-$
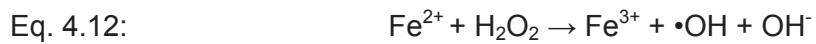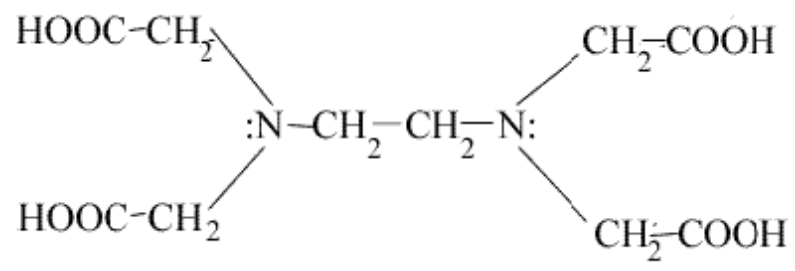
In a photoelectro-Fenton reaction, the solution is also irradiated with UV light of λ_{max} = 360 nm to try to accelerate the mineralisation process by the photolysis of the complex of Fe^{3+} with some intermediates and/or by the enhancement of the rate of Fe^{2+} regeneration from additional photoreduction of Fe^{3+} species, such as $Fe(OH)^{2+}$, via photo-Fenton reaction [16]:

Eq. 4.13: $Fe(OH)^{2+} + hv \rightarrow Fe^{2+} + •OH$

5. AOPs as an instrument of EDTA degradation

5.1.   EDTA

Table 4: Chemical and physical characteristic of EDTA [17]

Structural form	
Structural form	HOOC-CH$_2$ $\N-CH_2-CH_2-N:$ CH$_2$-COOH HOOC-CH$_2$ CH$_2$-COOH
Other names	Ethylene diamine tetraacetic acid, Edetic acid, Edetate, Versene, Ethylene diamine tetraacetic acid, Titriplex® II, Idranal® II, Chelaplex II
Molecular formula	$C_{10}H_{16}N_2O_8$
Appearance	colorless cristalline solide
CAS number	60-00-4
Molar mass	292,25 [g/mol]
Density	0,86 g/cm³
Melting point	237-245 °C (decay)
Solubility in water	1 g/l (20 °C)
R- and S-phrases	R: 36-52/53 S: 61
Hazardous criteria	irritant
LD50	30 mg/kg (rat, oral)

5.1.1. General description

EDTA refers to the chelating agent, which is widely used to sequester di- and trivalent metal ions (for example Ca^{2+} and Mg^{2+}). Those metals ions are bound via four carboxylate and two amine groups. Examples of especially strong EDTA complexes are: with Mn(II), Cu(II), Fe(III), Pb (II) and Co(III). EDTA strongly chelates also radioactive plutonium and radioisotopes of Am^{3+}, Cm^{3+} and TH^{4+}, which are then vastly more mobile than the unchelated metal ions.

EDTA is the most abundant anthropogenic compound in many European surface waters because of its widespread use in many industries and its slow removal - EDTA is not degraded or removed during conventional wastewater treatment. EDTA concentration in European rivers is reported between 10-100 µg/l, and in lakes between 1-10 µg/l.

Complexing agents in wastewater are of great concern in last times, because of their ability to solubilize heavy metals from plumbing, deposits containing heavy metals or other waste disposal sites. What is more, chelating agents may be a factor in determining algal growth.

A further problem is, that chelating agents are nontoxic to many forms of life on acute exposure; however the effects of longer-term low-level exposure are unknown. In laboratory tests on animals EDTA has been found to be both cytotoxic and weakly genotoxic. [17], [18], [19]

5.1.2. Common application

The most important uses of EDTA are:

- **Industrial cleaning** -complexation of Ca^{2+} and Mg^{2+} ions, binding of heavy metals

- **Detergents** - complexation of Ca^{2+} and Mg^{2+}: reduction of water hardness

- **Photography** - use of Fe(III)-EDTA as oxidizing agent.

- **Pulp and paper industry** - complexation of heavy metal ions during chlorine-free bleaching, stabilization of hydrogen peroxide.

- **Textile industry** - complexation of heavy metal ions, bleach stabilizer.

- **Agrochemicals** - Fe, Zn and Cu fertilizer, especially in calcareous soils.

- **Hydroponics** - iron-EDTA is used to solubilize iron in nutrient solutions.

More specialised uses of EDTA:

- **Food** - added as preservative to prevent catalytic oxidation by metal ions or stabilizer and for iron fortification.

- **Personal care** - added to cosmetics to improve product stability.[6]

- **Flue gas cleaning** - removal of NO_x.

- **Recycling** - recovery of lead from used lead acid batteries.

- **Medicin:** chelation therapy, an anticoagulant for blood samples, in dentistry as a root canal irrigant, iron removal from the body in the disease thalassemia

- **Laboratory science:** EDTA as a scavenging of metal ions, complexometric titrations, buffer solutions, determination of water hardness, EDTA used as masking agent to remove metal ions, a titrant used to determine the nickel concentration [17][19]

5.2.   Direct anodic EDTA oxidation

Direct anodic oxidation is a well-known method of EDTA mineralisation. A lot of investigations were done according to this subject, especially with application of diamond electrodes. [20],[21] Some experiments done by Zelenka were carried out also with the use of titan electrode laminated with iridium oxide as an anode and glassy carbon as cathode material. [22] The best results were achieved at a current density of 20 A/m^2 at the anode, pH = 4,9 and temperature of 25 ^{o}C.

The EDTA has four different dissociation levels, which influence the dissociation grades. The selection of the optimal pH range is very important for the direct EDTA oxidation process. According to the pH–value the EDTA follows one of the dissociation level curves, which are presented at Figure 5.1.
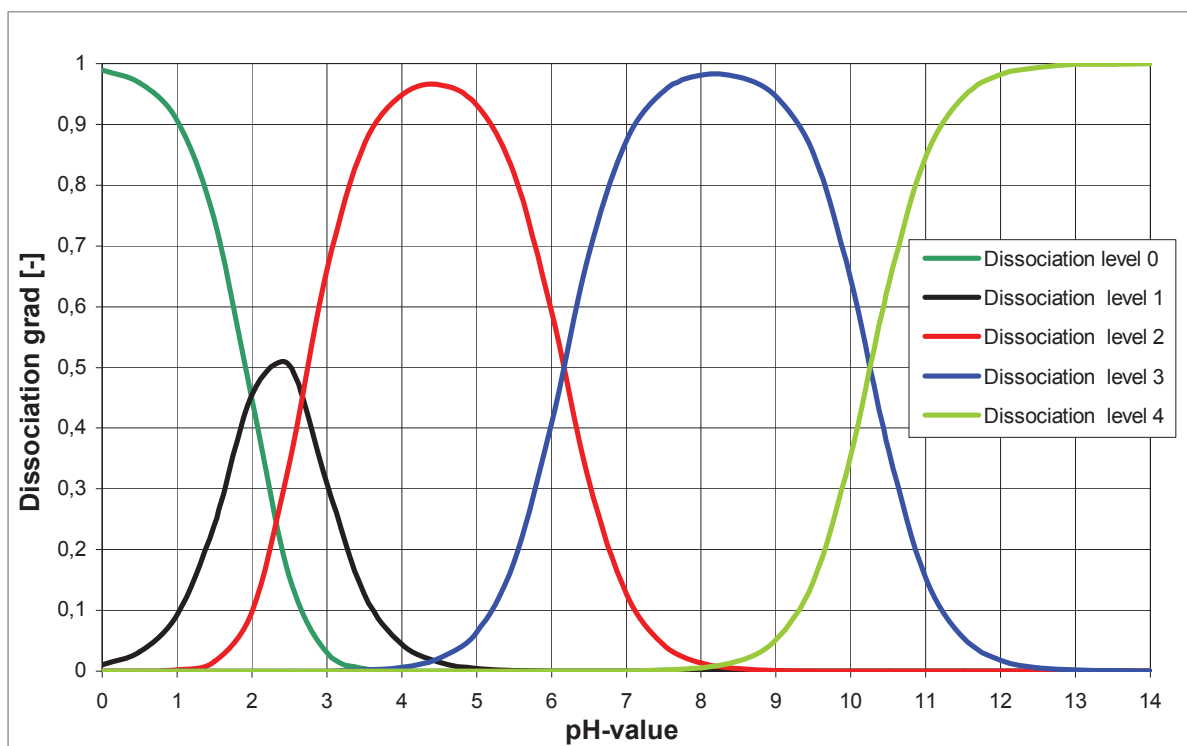
Figure 5.1: Dissociation of EDTA [22]

5.3.   Photochemistry of the Fe(III)–EDTA complexes

As it was mentioned in Chapter 5.1, EDTA builds a very stable complex with many metal ions. The Fe(III)-EDTA-complex is stable in the range of pH-value between 1...8,5 and Fe(III)-EDTA-complex between 2...12,5. The stable constant of FE(III) is equal to $K_{Fe(III)EDTA}$ = 1,3 x 10^{25}. [26]

The decomposition of Fe(III)-EDTA or EDTA under UV radiation was investigated and the degradation scheme presents Figure 5.2.
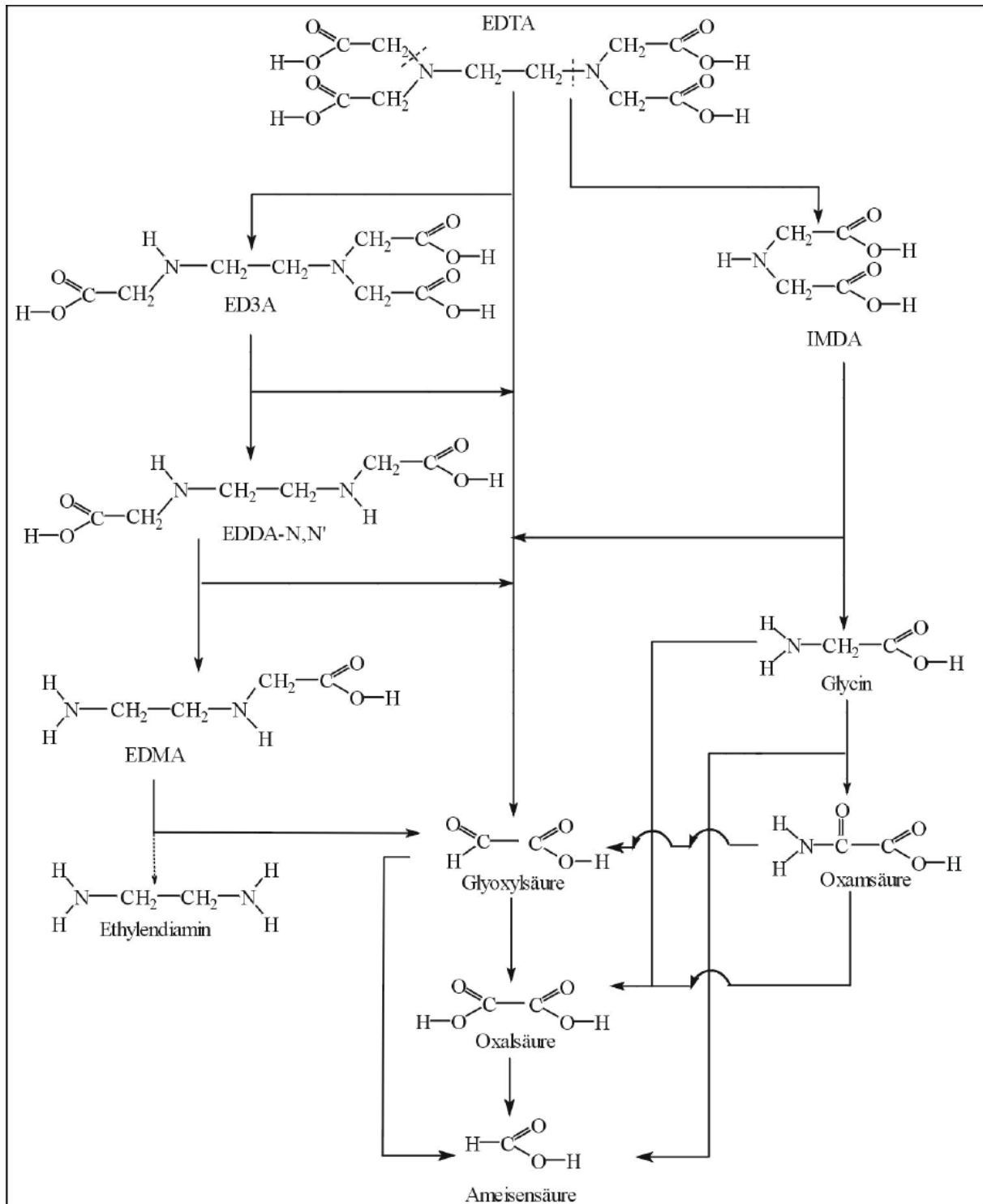
Figure 5.2: Degradation scheme for the oxidation of EDTA in the UV oxidation process in presence (left) and absence of Fe^{2+}, Fe^{3+} (right).The arrows represent the reaction paths to identified (–►c) and to not identified (---►c) degradation products. [23]

During the decomposition reaction of Fe(III)-EDTA complex, it is reduced to the dimer intermediate Fe(II)-ED3A. This reaction could be explained with Ligand to Metal Charge

Transfer Reaction (LMCT), where the electron from Ligands (Acetatgroup) is transferred to Fe(III) and reduced it to Fe(II).

According to the laboratory conditions:

a) in deoxygenated media the innersphere electron is transferred to the Fe(III) centre yields Fe(II) species and EDTA oxidation products, or

b) in aerated or oxygenated media the outersphere two-electron are transferred to O_2, what results in fast oxidation of the dangling $CH_2COO\bullet$ group to CO_2 and HCHO, with the concerted regeneration of the Fe(III) in form of Fe(III)-ED3A and the parent complex [24]

The whole process presents Figure 5.3.
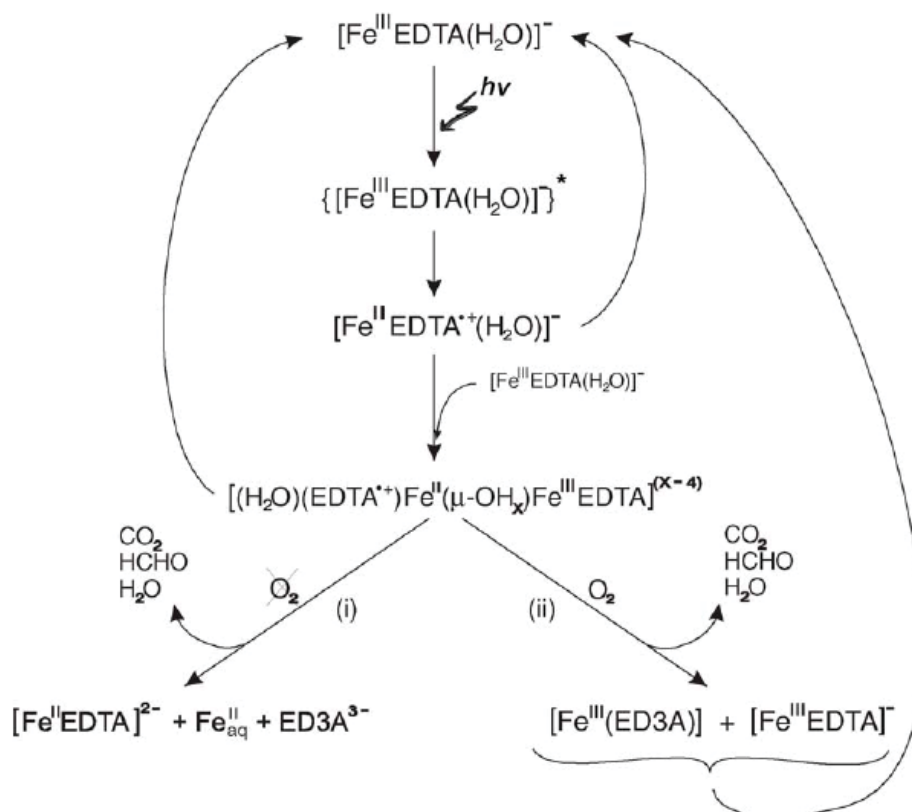
Figure 5.3: Mechanistic pathways of the secondary thermal reactions proceeding in deoxygenated (i) and oxygenated (ii) solutions of Fe(III)-EDTA(H_2O). [24]

According to the investigation done by Gangl [26] with a low pressure lamp (λ = 254 nm) the best results of Fe(III)-EDTA mineralisation could be achieved while using Fe(II)-EDTA as an output solution instead of Fe(III)-EDTA at the ratio of $c_{Fe(III)}:c_{EDTA}$ = 1:2, start pH-value under 3 and aeration with 8,3 mg/l. The reaction rate constant k at those circumstances was equal to 0,061 M-min.

5.4.   Anox/$H_2O_2^{cath}$/UV

AEOPs in EDTA mineralization were investigated in many combination forms by Gangl [26] and by Zelenka [22]. One of them was the conjunction of direct anodic oxidation of EDTA with hydrogen peroxide generation on the cathode and its irradiation with ultraviolet radiation. This method is therefore particular, that usually extra dosed H_2O_2 is in this case produced *in situ* from the exceed oxygen amount from anode reaction and it is built on the glassy coal. In this case EDTA will decompose according to three processes: direct anodic oxidation, EDTA- photolysis and H_2O_2/UV processes.

Both Gangl and Zelenka studied EDTA decomposition with application of 15 W low pressure lamp and the Na_2EDTA solution with concentration of 1,34 mM but with different output pH-values and current densities. The results achieved by Gangl at pH_{start} = 3, j_{an} = 85 A/m^2 and j_{cath} = 64 A/m^2 have shown almost completely degradation of EDTA (95%) after 180 minutes. In case of investigation done by Zelenka with pH_{start} = 5, j_{an} = 20 A/m^2 and j_{cath} = 0,49 A/m^2 this effect was achieved after 350 minutes.

6. Reactor characteristic

6.1.   The residence time distribution

In ideal flow patterns, the average time needed by a particle to pass through the reactor is called mean residence time and is equal to the space-time.

Eq. 6.1: $$\bar{t} = \tau = \frac{V_R}{\overset{\bullet}{V}}$$

Deviation from the ideal flow patterns could be caused by:

- channeling of fluid
- recycling of fluid
- short-circuit
- stagnant regions in the vessel [27],[28]

Because of all disruptions mentioned above, elements of fluid in non-ideal flows take different routes through the reactor and different lengths of time to pass through the vessel. The distribution of these times for the stream of fluid leaving the reactor is called the residence time distribution (RTD) and could be described with the exit age distribution curve E with units of time $^{-1}$. However one restriction on the E curve has to be taken into account, which concerns closed vessel boundary condition. This means that the fluid enters and leaves the vessel only one time. [27] The exit age distribution E could be defined as a probability of the volume element, which entered the reactor in the moment $t = 0$, to leave the vessel in time interval between t and $t+dt$. After endless long time the probability is equal to 1 as all of particles have left the reactor.

Eq. 6.2: $$\int_{0}^{\infty} E(t)dt = 1$$

To obtain a non-dimensional residence time, *E(t)* curve is represented in such a way that the area under the curve is unity and the residence time is normalised into the form of *θ*. [28]

Eq. 6.3 $$\theta = \frac{t}{\tau}$$

According to Figure 6.1 the fraction of exit stream of age between *t* and *t+dt* is *Edt*, the fraction younger than age t_1 is $\int_{0}^{t_1} Edt$, whereas the fraction older than t_1 is

Eq. 6.4 $$\int_{t_1}^{\infty} Edt = 1 - \int_{0}^{t_1} Edt$$
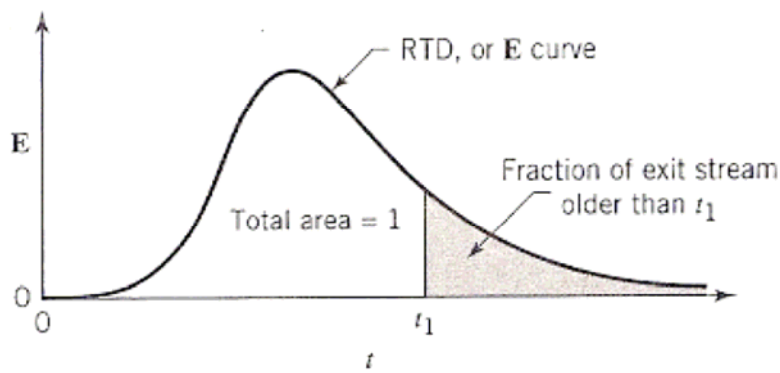
Figure 6.1 The exit age distribution curve E also called the residence time distribution (RTD) [27]

The residence time cumulative curve *F(t)* in continuous flow systems describes, which volume fraction at the exiting fluid flow has the residence time between 0 and t. In other words *F(t)* relates to the probability of the volume element, which in the moment $t = 0$ entered the reactor and left it in a period between 0 and *t*. If at the moment $t = 0$ there are no particles in the reactor and after endless long time none of the particles remain in the reactor following equations is true:

Eq. 6.5:
$$\begin{cases} F(0) = (0) \\ F(\infty) = 1 \end{cases}$$

The differential of the residence time cumulative curve gives the fraction of the fluid, which leaves reactor between *t* and *t+dt*, what relate exactly to residence distribution function *E(t)*.

Eq. 6.6:
$$E(t) = \frac{dF(t)}{dt}$$

and according to basic conditions (Eq. 6.5) relation between *F(t)* and *E(t)* could be described with Eq. 6.7:

Eq. 6.7:
$$F(t) = \int_0^t E(t)dt$$

The mean residence time is calculated with following equation:

Eq. 6.8:
$$\bar{t} = \int tdF(t)$$

In case of discrete values approximation could be used:

Eq. 6.9:
$$\bar{t} \approx \sum_i t_i \Delta F_i$$

Figure 6.2 presents a graphical illustration of Eq. 6.9.
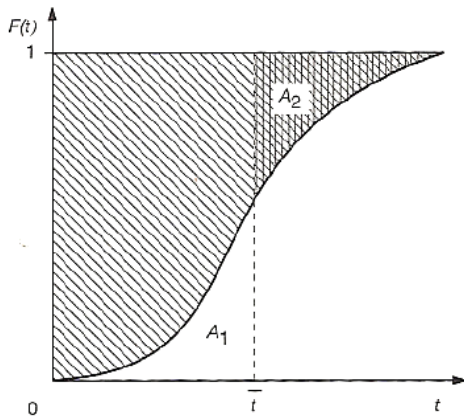
Figure 6.2 Determining the mean residence time from cumulative curve *F(t)* [29]

The integral from equation Eq. 6.8 relates to hatched area in Figure 6.2 and also to mean residence time *t*. Both of the areas: A_1 and A_2 have to be equal size.

6.1.1. Experimental determination of RTD

The simplest and most direct way of determining the residence time distribution in non-ideal reactors is to use a physical non-reactive tracer, which is inert into the fluid flowing through the reactor. The concentration of the tracer is measured at the reactor's exit and compared with its entering value. The examples of tracers are: a colour tracer, acid, leach or a salt solution. The measured attributes except the concentration of the trace could also be conductivity, absorption or radiation. [27],[28]

The most common methods to characterise RTD of a reactor are the pulse or the step experiment. Below the step input method is described as it was applied in RTD investigation.

Step input methode

At a time *t* = 0 ordinary fluid with known flow rate passing through the reactor is switched into fluid with tracer with given concentration c_{max}. With the time *t* > 0 the tracer concentration measured at the reactor's exit c_{Step} will be becoming closer to the value of c_{max} and after endless time c_S will be equal to c_{max}.

Figure 6.3 Step input experiment [27]

Figure 6.3 presents the step input experiment with input and output reading of the tracer concentration curves. The dimensionless form of the c_S curve is called *F(t)* curve and is described with following function:

Eq. 6.10:
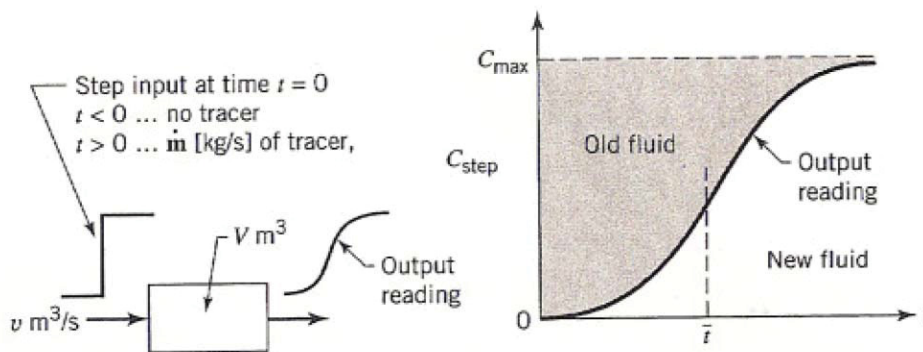$$F(t) = \frac{c_S}{c_{max}} \quad \text{with} \quad F(0) = 0, F(\infty) = 1$$

The mean residence time distribution in step input method is equal to hatched area and could be calculated with following equation:

Eq. 6.11:
$$\bar{t} = \frac{\int_0^{C_{max}} t\,dc_S}{\int_0^{C_{max}} dc_S} = \frac{1}{c_{max}} \int_0^{C_{max}} t\,dc_S$$

6.2. Iodite/iodate actinometer

The chemical actinometer is the most common method in radiation measurements. By means of various chemical substances it could be applied in wavelength range of 130-770 nm. To describe the photon flow in reactors a method from Rahn was applied, where an iodide/iodate solution was used as a chemical actinometer. [30]

The iodide/iodate chemical actinometer is intended for low-pressure mercury lamp that puts out more than 85% of its energy at wavelength of 254 nm. The solution is made of 0,6 M iodide (KI) and 0,1 M calium iodate (KIO_3) and 0,01 M borate buffer (Dinatriumtetraborat, $Na_2B_4O_7* 10H_2O$). Iodate acts as an electron scavanger and borate as a buffer which holds pH-value at the level of 9,25. Irradiation results in the formation of triiodate, which is than quantified by measuring its absorbance at 352 nm.

6.2.1. Absorption spectra

At Figure 6.4 the absorption spectra of potassium iodide (a), potassium iodate (b) and the mixture of both (c) are compared before (–UV) and after (+UV) irradiation with a germicidal lamp.
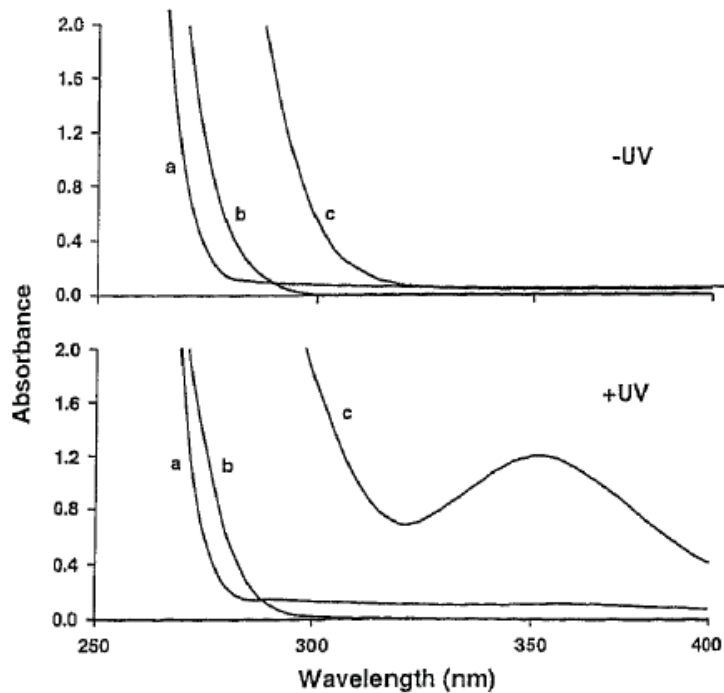
Figure 6.4: Absorption spectras [30]

The chemical actinometer solution is optically opaque at the wavelength of $\lambda = 254$ nm and shows neglible/very low absorbance value over $\lambda = 330$. In other words, iodide/iodate mixture should absorb all light below 290 nm and none above 330 nm. Such a spectra is very favorable for actinometer experiment's run as the solution is very stable at day light.

After irradiation the absorption spectra of the mixture shows its maximum at $\lambda = 352$ nm, what causes the formation of triiodide. This wavelength was used in further experiments to define triiodide concentration.

6.2.2. Reaction mechanism

After irradiation of actinometer solution with UV-light the charge transfer [I⁻H$_2$O*] would be formed.

Eq. 6.12: $I^- + H_2O + h\nu \rightarrow I^-H_2O^*$

The charge transfer state relaxes to a caged complex containing an iodine atom and an electron.

Eq. 6.13: $I^-H_2O^* \rightarrow (I^{\bullet}, e^-) + H_2O$

From the caged complex [I$^{\bullet}$,e⁻] two different processes can take place. The first one is a back reaction to reform iodide. The second possibility is a breakdown of the caged complex and the migration of the electron out of the cage and into the bulk solution where it is free to react as an aqueous electron. So after photon absorption iodine atoms and a solvated electron are formed.

Eq. 6.14: $I^- + h\nu = \overset{\bullet}{I} + e_{aq}^-$

The total reaction is given by Eq. 6.15:

Eq. 6.15 : $8I^- + IO_3^- + H_2O + h\cdot\nu \rightarrow 3I_3^- + 6OH^-$
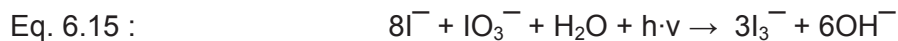
6.2.3. Quantum yield

According to investigation done by Rahn [30], the quantum yield depends on the temperature of the solution, the radiation wavelength and the concentration of potassium iodide. At the temperature of T = 20,7 ^oC, a wavelength of $\lambda = 254$ and a potassium concentration of c_{KI} = 0,6 M the quantum yield is equal to Φ_{254nm} = 0,75 ± 0,02. A precise expression, considering dependence of temperature and concentration is given by Eq. 6.16 :

Eq. 6.16: Φ_λ = 0,75 [1 + 0,02 (T − 20,7)]*[1 + 0,23 (C − 0,577)]

Evaluation of triiodide concentration

The concentration of triiodide could be evaluated from the absorbance measurement in a spectrophotometer at the wavelength of 352 nm. Using the Lambert-Beer law, the calculation follows Eq. 6.17, where A is the absorbance value, d [cm] is the irradiative cuvette length, ε_{352} is the molar extinction coefficient and S is the dilution factor.

Eq. 6.17: $c_{I_3^-} = \dfrac{A \cdot S}{\varepsilon_{352} \cdot d}$,   with $\varepsilon_{352}\left(I_3^-\right) = 27400 \left[\dfrac{1}{mol \cdot cm}\right]$

Evaluation of the photon flow and the radiant power

The photo irradiance could be described in other words as a ratio of created triiodide moles at the certain reactor volume and within a certain time to its quantum yield. The evaluation in batch reactors is given by Eq. 3.8 and in PFRs by Eq. 3.9. The radiant power could be calculated with Planck's law equation Eq. 3.11.

6.3. Electrochemical hydrogen peroxide generation

Usually hydrogen peroxide is produced by electrochemical methods, such as electrolysis of inorganic chemicals and autooxidation of organic compounds. However, for those processes non-aqueous solvents for catalysts cycle are required.

H_2O_2 can also be generated directly from water, hydrogen and oxygen using thermal, photochemical or electrical discharge processes. Most of the hydrogen peroxide electro-generation processes are conducted in alkaline solutions with a high electrolyte concentration. Considering further using of H_2O_2 in *electro-Fenton processes* (see Chapter 4) the optimal pH range would be found between 2,5...3,5. There are reports, which prove, that hydrogen peroxide can be electrochemically produced by reduction of dissolved oxygen at

the cathode. In acidic solutions, the dissolved oxygen is electrochemically reduced with two electrons to hydrogen peroxide at the cathode. [31]

Eq. 6.18: $\qquad O_2 + 2H^+ + 2e^- \rightarrow H_2O_2, \qquad E^0 = 0,44$ V vs SCE
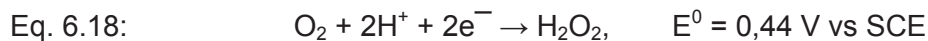
At the anode, the oxidation of water leads to formation of oxygen gas and protons.

Eq. 6.19: $\qquad 2H_2O \rightarrow 4H^+ + O_2 + 4e^-, \qquad E^0 = 0,987$ V vs SCE
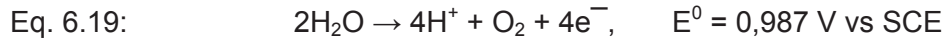
The protons will be driven to the catholyt electrostatically and partially supply the protons consumption during the synthesis of H_2O_2.

Except Eq. 6.18 two other reactions can occur simultaneously at the cathode. One of them is the reduction of H_2O_2 to H_2O according to Eq. 6.20:

Eq. 6.20: $\qquad H_2O_2 + 2H^+ + 2e \rightarrow 2\ H_2O, E^0 = 1,534$ V vs SCE

The second reaction could be the hydrogen gas evolution.

Eq. 6.21: $\qquad 2H^+ + 2e \rightarrow H_2, \qquad E^0 = -0,242$ V vs SCE
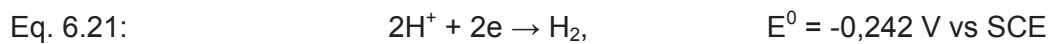
According to the investigation done by Qiang, Chang and Huang [31], the optimal conditions for hydrogen peroxide generation are at cathodic potential of –0,5 V (vs. SCE), oxygen mass flow rate of 8,2 x10-2 mol/min, pH 2 and average current efficiency of 6,4 A/m^2. In case of using air instead of oxygen, the average current density decreases to 2,1 A/m^2. H_2O_2 production is favoured at low temperatures in range of 10...20 ^{0}C, as with higher temperature and also pH value the self-decomposition rate is growing. [31] On the other hand, experiments run by Gangl gave the best results in alkaline solutions.[26]

7. Experimental part

7.1. Analytics

7.1.1. UV-VIS spectrometry

UV-VIS spectrometry measures the intensity of an absorption of a monochromatic radiation across a range of wavelengths passing through a solution. The absorbance is proportional to the number of absorbing species in the illuminated sample and is described with Lambert-Beer law (see: Chapter 3.3)

A spectrometer is composed of polychromatic broad spectrum sources, dispersive units, sample cells, detectors and a computer for data manipulation and storage.

In the laboratory test a double beam *Thermo Scientific Helios*[TM] *Zeta (Omega)* spectrophotometer with the dual-source tungsten and deuterium lamp system was used. Such a light source allows maximum performance over the wavelength range of 190...1100 nm with accuracy of ± 1.0 nm. The photometric range of absorption expands between –0,3...3,0 A and the measurement accuracy at 1 A is equal to 0,005 A. Measurements of absorbance could have been read from an integrated active display or transferred through a built-in USB interface and stored on the PC and controlled via the VISION*lite*[TM] software. [32],[33],[34]
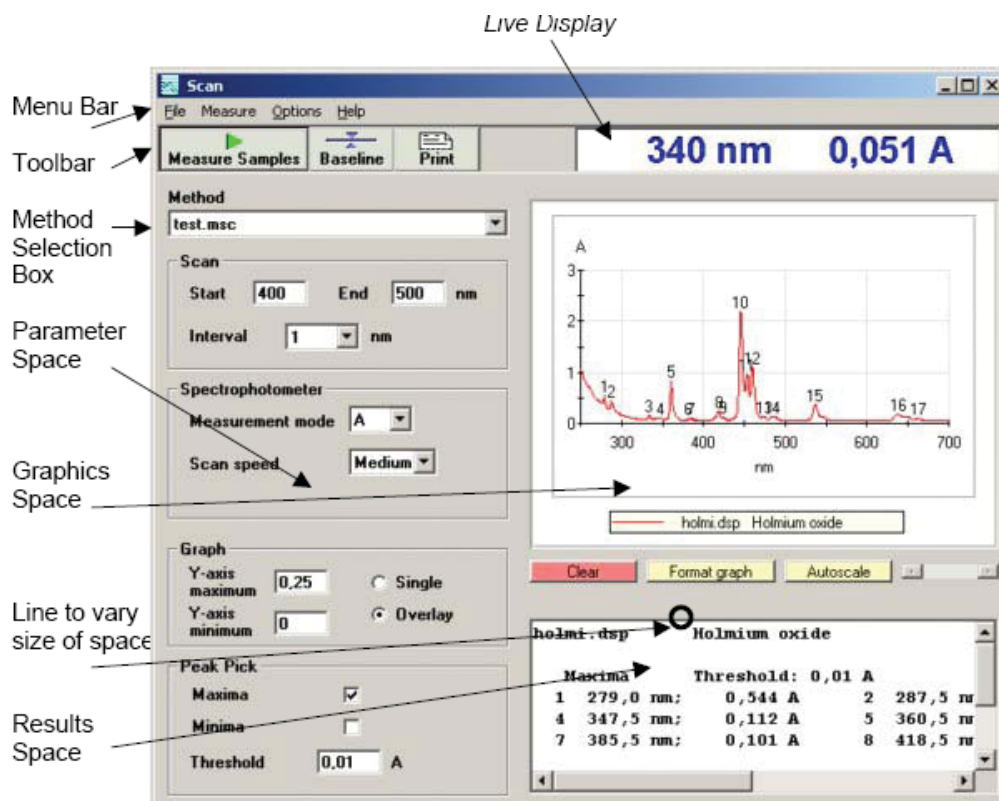

Figure 7.1: Example of UV/VIS spectrometry data collection using VISION*lite*[TM] software [34]

7.1.2. Hydrogen peroxide analytical determination

In acid solution hydrogen peroxide reacts with potassium iodide according to the equation:

Eq. 7.1: $$H_2O_2 + 2\,I^- + 2\,H^+ \rightarrow I_2 + 2\,H_2O$$

To determinate hydrogen peroxide concentration 10 ml potassium iodide with concentration of 0,2 M was added to the sample bottles, acidulated with 2 ml of 1 M sulphuric acid and weighed. After that, a 10 ml sample with unknown hydrogen peroxide content was dosed into the probe under continuous mixing of potassium iodide solution and after that scaled again. Thus prepared probes were put away for one hour until the whole reaction had been completed: the solution's colour had changed to deep yellow. Finally, the samples were titrated with 0,01 M sodium thiosulphate until the solution became colourless again. According to the reaction:

Eq. 7.2: $$I_2 + Na_2S_2O_3 \rightarrow 2\,NaI + Na_2S_4O_6$$
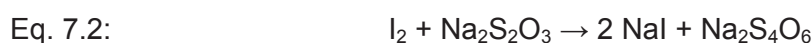
and knowing that 1 ml of 0,01 M $Na_2S_4O_6$ = 0,17007 mg H_2O_2, the hydrogen peroxide concentration could be calculated from titrated amount of sodium thiosulphate. [35]

7.2.   HPLC analysis

The EDTA concentration was determined using a HPLC analysis, which was curried out an external department. The result were achieved in a form of reports, like the one presented in Figure 7.1. The data from the reports was used for further calculations.

High-performance liquid chromatography (HPLC) is a form of column chromatography used frequently in analytical chemistry to separate, identify, and quantify compounds. The principle of liquid chromatography is based on the passage of the constituents to be separated between two immiscible phases. For this, the sample is dissolved in a liquid mobile phase and moved across stationary phase – column. Due to the interactions of the constituents with stationary phase they separate after sufficient running time.

Main principles of the separation are:

- adsorption
- distribution
- ion exchange
- exclusion

The components of a classical unit for liquid chromatography are:

- an elution medium reservoir containing the solvent for the mobile phase
- a separation column made of glass tube typically with an inner diameter of 1 cm and a length of 30 cm
- a syringe or an injection valve to feed in the sample solution
- a fraction collector with which a few millimetres of the eluate are collected manually or automatically [36]

In EDTA analyse *HP 1100 Series HPLC Systems* was used with built-in UV/VIS detector. The whole instrument was controlled through *Agilent ChemStation* software. A *Lichrospher 100RP18* produced by *Agilent Technologies* was applied as a separating column. Figure 7.2 presents the whole HPLC station.

Figure 7.2: *HP 1100 Series* HPLC instrument used to EDTA concentration determination

EDTA concentration was determined according to: *German standard methods for the examination water, waste water and sludge – Single components (group P) – Part 8: determination of NTA, EDTA and DPTA by liquid chromatography*, norm: DIN 38413-8: 2000-09. Possible application range for EDTA determination is a concentration of 0,1...20 mg/l. A solution consisting of 0,6 mmol/l nitric acid, 7,4 mmol tetrabutylammoniumhydrogensulphate, 2,6 tetrabutylammonium hydroxide was used as an eluent. The derivatisation solution had following composition: 37 mmol/l iron (III) ions and 130 mmol/l tetrabutylammoniumhydrogensulphate. HPLC analysis gave two peaks at the chromatogram: the first one was from not fully-converted iron, the second one from EDTA. Sometimes also third peak appeared: it was one of EDTA degradation products, probably ED3A. Figure 7.3 presents example of HPLC analyse chromatogram.
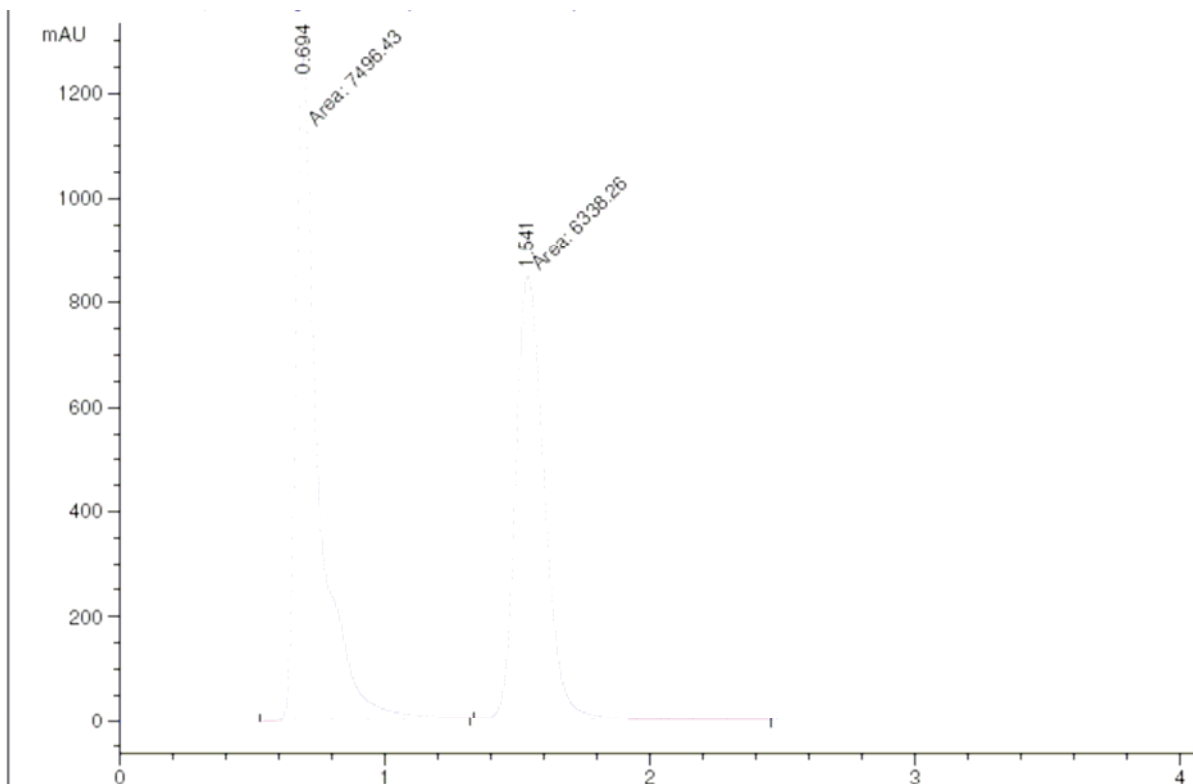
Figure 7.3: Example of chromatogram printout from HPLC analyse of EDTA.

EDTA concentration was calculated from ratio of peaks area: the sample's area with known concentration (of starting solution) was used as a reference for next samples. Calculations were done with following equation:

Eq. 7.3:
$$c_{EDTA} = \frac{A_{EDTA}}{A_{EDTA0}} \cdot c_{EDTA0}$$

7.3. Chemicals

7.3.1. Borax

Table 5: Chemical and physical characteristic of borax [17]

Molecular formula	$Na_2B_4O_7 \cdot 10H_2O$ or $Na_2[B_4O_5(OH)_4] \cdot 8H_2O$	
Molar mass	381,37 g/mol	
Appearance	white solid	
Density	1,73 g/cm^3, solid	
Producent		
Hazardous criteria		harmful

7.3.2. Iron (II) sulfate (heptahydrate)

Table 6: Chemical and physical characteristic of of iron (II) sulfate (heptahydrate) [17]

Molecular formula	$FeSO_4 \cdot 7H_2O$ (heptahydrate)	
Molar mass	278,05 g/mol (heptahydrate)	
Appearance	blue/green crystals	
Density	1,898 g/ cm^3	
Solubility in water	Soluble	
Producent	Carl Roth P015.2	
Hazardous criteria		harmful

7.3.3. Potassium iodide

Table 7: Chemical and physical characteristic of potassium iodide [17]

Molecular formula	KI
Molar mass	166,00 g/mol
Appearance	white crystalline solid
Density	3,13 g/ cm^3, solid
Solubility in water	128 g/100 ml (6 °C)
Producent	Roth 6750.3
Hazardous criteria	None

7.3.4. Potassium iodate

Table 8: Chemical and physical characteristic of potassium iodade [17]

Molecular formula	KIO_3		
Molar mass	214,00 g/mol		
Appearance	white crystalline powder		
Density	3,89 g/ cm^3, solid		
Solubility in water	32 g/100 ml (100 °C)		
Producent			
Hazardous criteria		oxidizing	harmful

7.3.5. Sodium sulphat

Table 9: Chemical and physical characteristic of sodium sulphat [17]

Molecular formula	Na_2SO_4
Molar mass	142,04 g/mol
Appearance	White crystalline solid,hygroscopic
Density	2,68 g/cm³
Solubility in water	42,7 g/100 ml (100 °C)
Producent	Carl Roth 8631.2
Hazardous criteria	None

7.3.6. Sodium thiosulfate

Table 10: Chemical and physical characteristic of sodium thiosulfate [17]

Molecular formula	$Na_2S_2O_3$
Molar mass	158,097 g/mol
Appearance	White crystalline solid,hygroscopic
Density	1,667 g/ cm^3, (20 °C)
Solubility in water	Very soluble
Producent	Carl Roth HN25.4
Hazardous criteria	None

7.3.7. Sulphuric acid

Table 11: Chemical and physical characteristic of sulphuric acid [17]

Molecular formula	H_2SO_4	
Molar mass	98,078 g/mol	
Appearance	clear, colorless, odorless liquid	
Density	1,84 g/cm^3, liquid	
Solubility in water	fully miscible (exothermic)	
Producent	Carl Roth 4623.5	
Hazardous criteria		acridly

7.4.   Experimental setup

7.4.1. UV-radiation source

As an UV-radiation source a low pressure mercury lamp from *Heraeus* was used with power output of 35 W and maximum emission at λ = 254 nm. Irradiance at that wavelength achieves 0,06 mW/cm^2 at the distance of 100 cm and a typical UV-radiation efficiency is located at about 40%. An ambient temperature of working UV radiator should not extend range of 10...30 ^{o}C, that is why during the experiments the lamp was kept in glass cooling coat filled with water, which was held by thermostat at a constant temperature of 25 ^{o}C. As a power supply for low pressure mercury lamp *EPS 1/1.2/2/4* device was used. [37],[38]

(a)   (b)
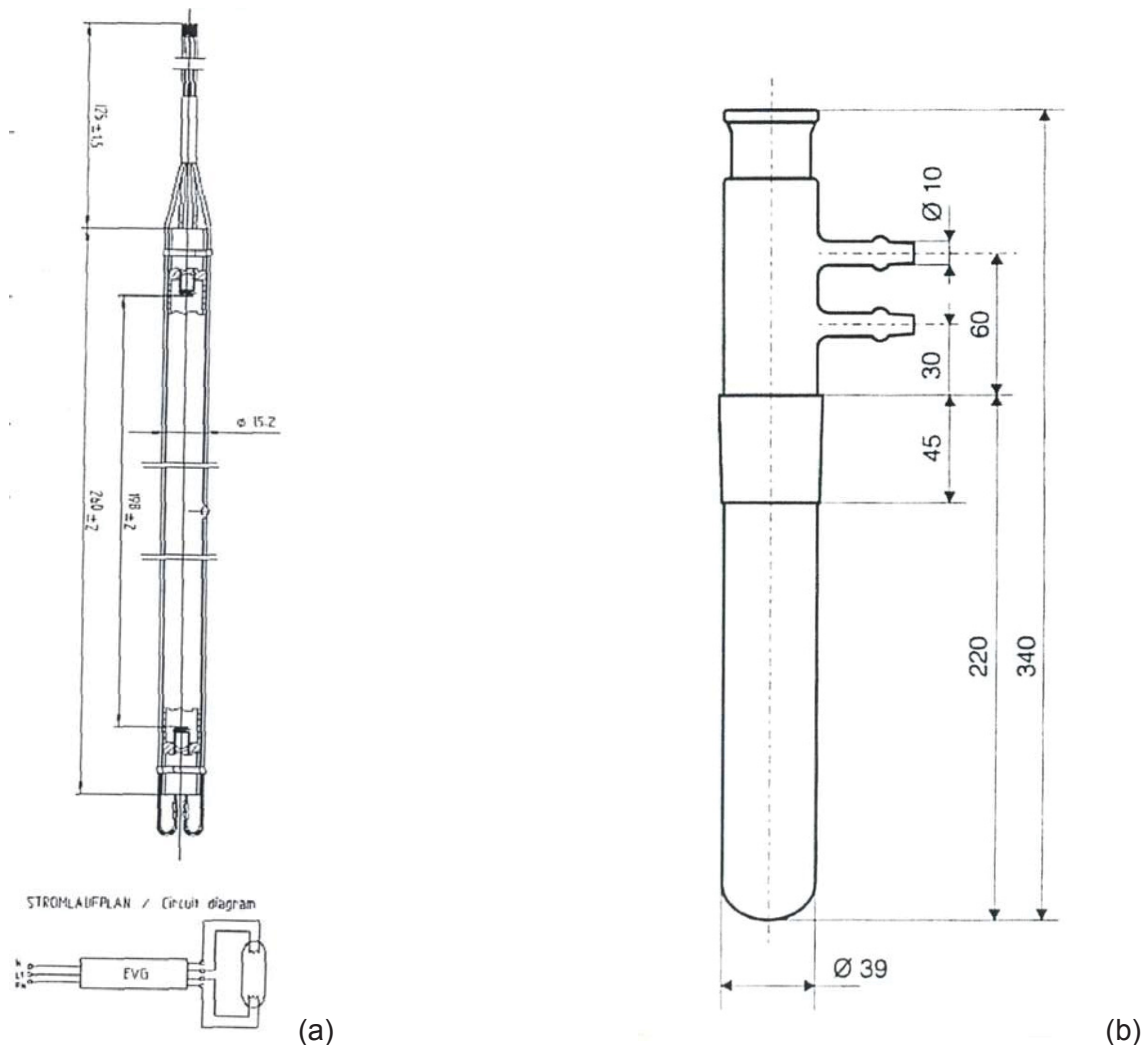
Figure 7.4: 35 W -Low pressure mercury lamp schema with circuit diagram (a) and glass cooling coat side view (b)

7.4.2. Chemical reactors

In laboratory tests four different reactors were used. All of them were fabricated from borosilicate according to VTU drawings. Three of those reactors were plug flow reactors and one of them was a continuous stirredt-tank reactor, sometimes used also as a batch reactor. Figure 7.5 presents the scheme of two plug flow reactors, which had namely the same shape, but different reactor volume. During experiments an UV lamp was immersed in the reactors from the upper side, the rear side was capped with a gas frit plug.
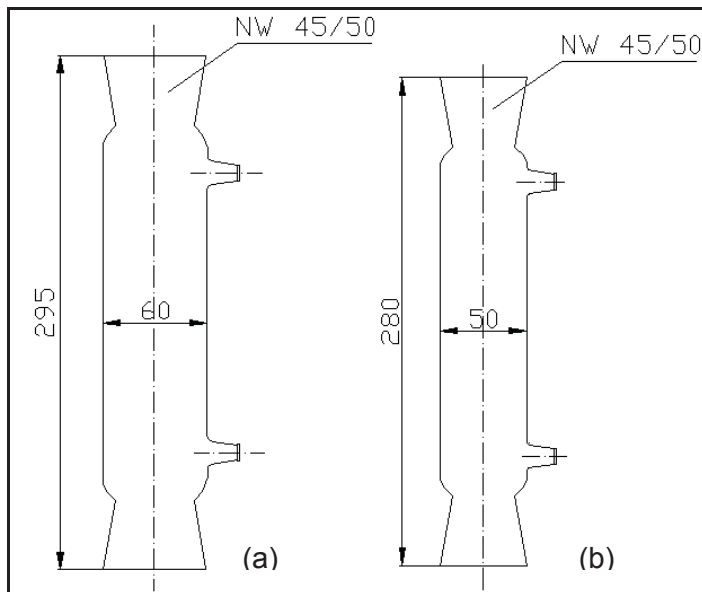
Figure 7.5: Plug flow reactors: large one (a) and small one (b)

At Figure 7.6 the coil reactor is presented. It consisted of 3 parts, combined togehther with PVC tubes. During experiments the UV-lamp was attached inside the coil reactor, up to the cooling coat inlets.
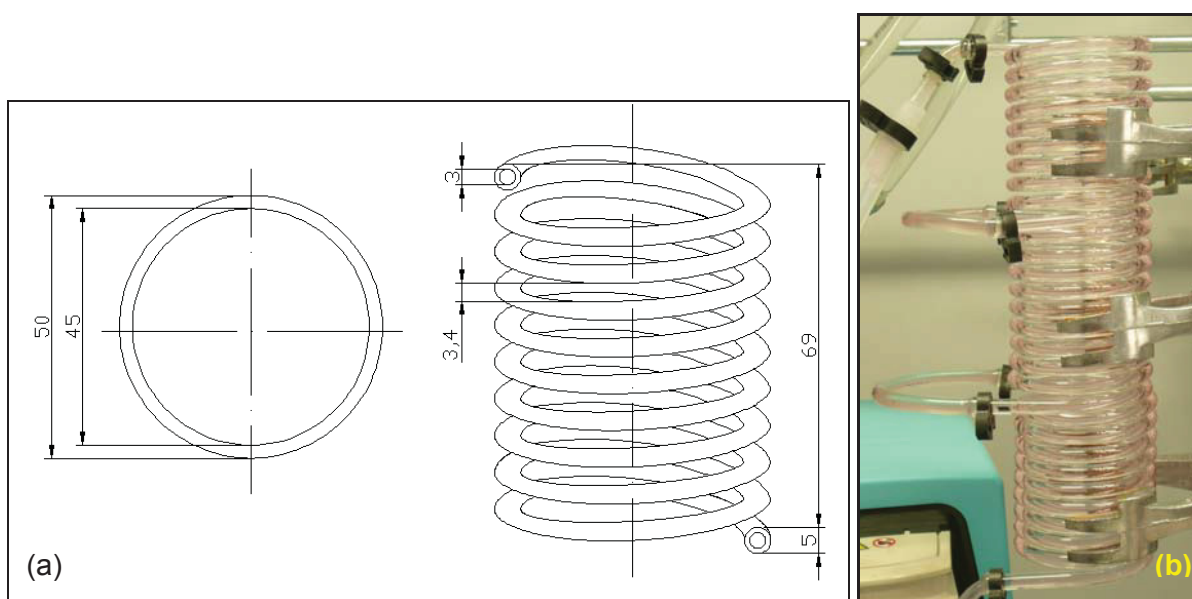
Figure 7.6 Coil reactor: scheme (a) and (b) in attached in laboratory unit

At Figure 7.7 the continuous stirred-tank reactor (CSTR) scheme and photo are displayed. What is not visible at the drawing, but only on the photo, are the three inlets located in the lower part of the reactor and one placed in the middle. In those inlets the measuring instruments could have been fixed, enabling using the CSTR not only as an UV-reactor, but also as a tank for outlet solutions. During the experiments the solution entered through upper inlet and left out through the lower inlet. The solution in the reactor was mixed with a stirrer, usually with the speed of 250 rmp (descritption of the mixing device: Chapter 7.4.8). In the experiments with photochemical Fe(II)-EDTA degradation (see Chapter 9.2) and during the determination of photon flow (see Chapter 1.1.1) the reactor was applied as a batch reactor.
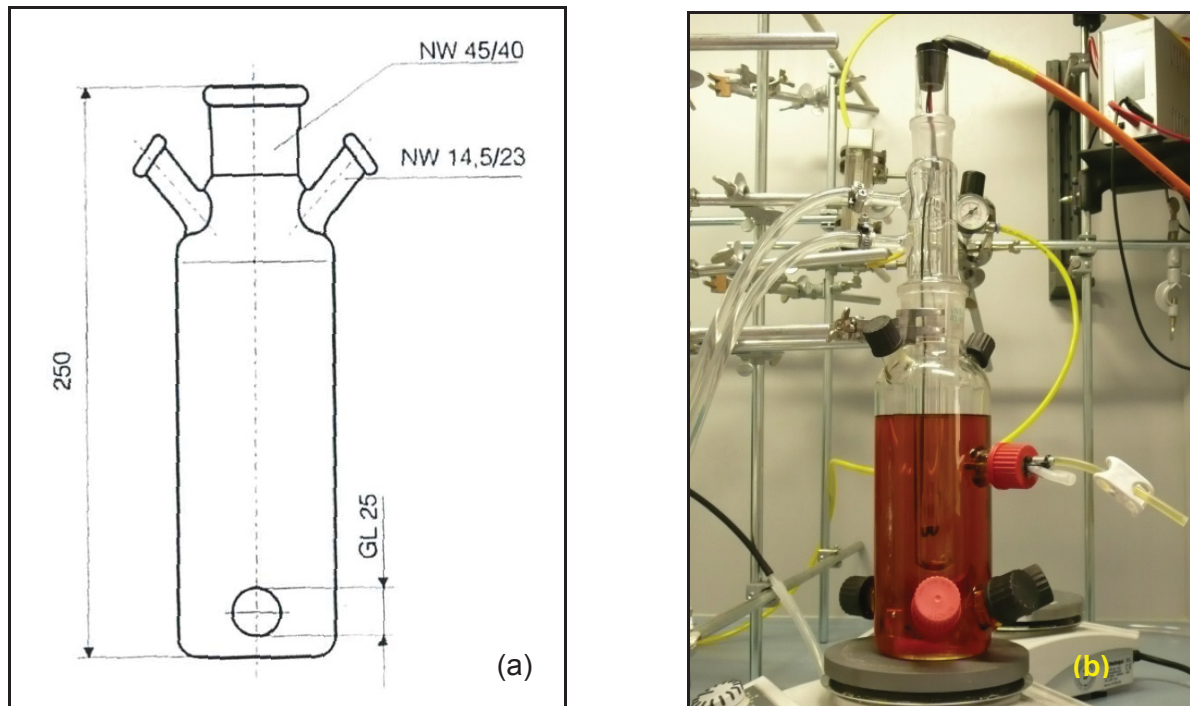
Figure 7.7: Continuous stirred-tank reactor (CSTR): scheme (a) and with immersed UV-lamp in laboratory setup (b).

7.4.3. Electrolysis cell

A specially designed *EC Electro MP-Cell* was tested as an electrolysis cell. *Electro MP-Cell* is a small multipurpose plate-and-frame cell, the general scheme of it is shown below.
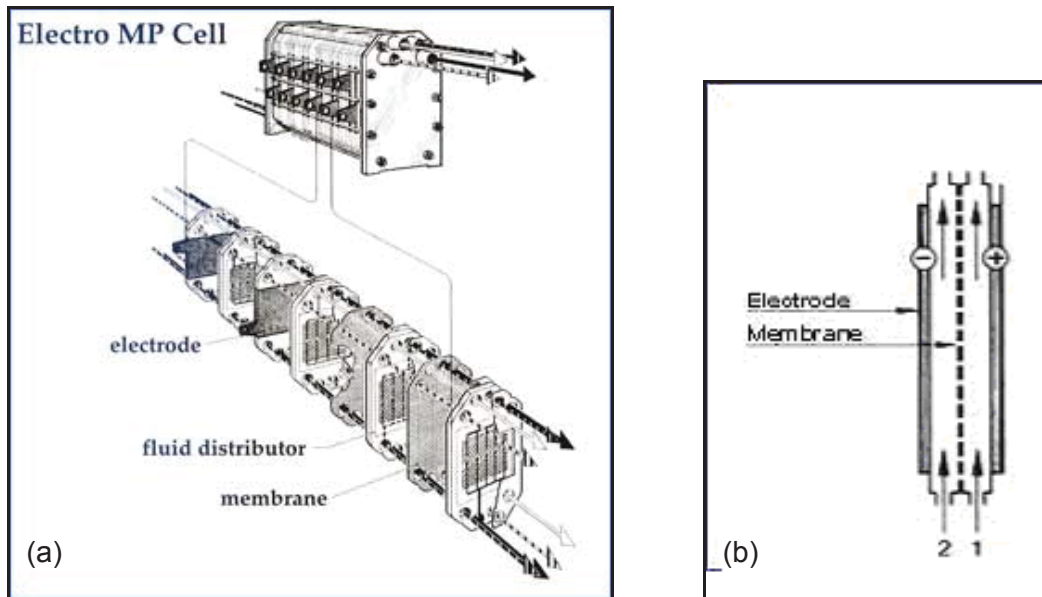
Figure 7.8: *EC Electro MP-Cell*: general setup scheme (a) and inner diameter (b) [39]

An iridium oxide plate with an active area of 0,096 m^2 was used as an anode and as a cathode - glassy carbon *SIGRADUR® K,* located before a high quality steel plate which served as an electric current connector. The space between the plates with the dimensions of: 6 x 16 x 2,5 cm was filled with 147 g of glassy carbon with a diameter of 3150...4000 μm and density of 1,54 g/cm^2. Taking average diameter of the particle into calculations, the active area of the cathode was equal to 0,147 m^2. The original ion selective membrane was replaced with granulate backing fence, which allowed a free flow of electrolyte between the electrodes. [39],[40]
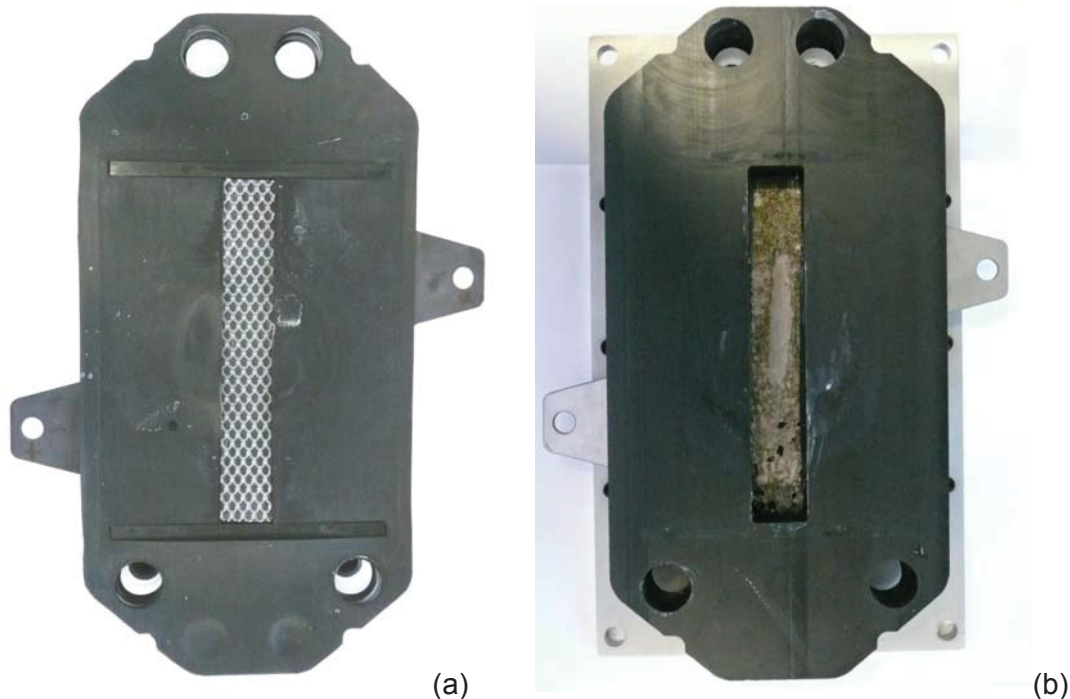
Figure 7.9: *EC Electro MP-Cell*: anode electrode with granulate backing fence (a) and stainless steel plate without glassy carbon filling (b).

7.4.4. Elelectrolysis cell power supply unit

As an electrolysis cell current source a *Bolz electronic TG30-2T* power supply unit was applied. The instrument could work at a constant output voltage with a range between 0...30 V or with a constant output current between 0...2 A. [41]

7.4.5. Circulation flow in bench scale unit

In the laboratory tests a *WASON-MARLOW Bredel 323Du/D* tube pump with 3 roller pump-head was used to distribute solution in the bench scale unit. The possible speed range of the pump expanded between 3...400 rpm what responded to solution's flow rate of 0,3...24 l/h. In the pump-head a rubber tube was installed, the rest of the tubes used in the bench scale unit were PVC hose. [42]

7.4.6. pH- and conductivity measurement

The pH-value, the conductivity and the temperature in the solution were measured by a *Thermo Scientific Orion 5-Star Plus* portable multi-parameter. A gel-filled (Ag/AgCl) *pH/ATC Triode* ^{TM} with an built-in thermostat for Automatic Temperature Compensation (ATC) was used as the pH electrode. The pH-value range extended between 1...14 and the temperature range between 0...90 ^{o}C. For a conductivity electrode a *DuraProbe*^{TM} *4-Electrode Conductivity Cells (013010MD)* was chosen with recommended application range of 1µS/cm...200 mS/cm and a cell constant of 0,475 cm^{-1}. [43]

7.4.7. Temperature monitoring

To ensure comprehensible laboratory conditions the temperature in the solution was kept at the same level with use of a thermostatic circulator *LAUDA Ecoline Staredition E 206* with a working temperature range of 20...100 °C and a temperature control of ± 0,01 °C. The heater power was working with 2,25 kW and the pressure pump could achieve a maximal pressure of 0,4 bar and a flow of 17 l/min. [44]

7.4.8. Mixing device

To mix the solution in the CTSR a *Heidolph*® *MR Hei-Standard Magnetic Hot Plate Stirrer* was used, with the plate diameter equal to 145 mm. The possible speed range was situated between 100...1400 rotation per minute, an excellent stirring results could have been achieved with volumes up to 20 liters of water. [45]

8. Experimental results – reactors' characterisation

8.1.   Residence time distribution in reactors

Residence time distribution in the reactors was measured with a step input method as it carried fewer technical problems. A colour medium was used as a mark tracer fluid and the residence time distribution was shown as a change of its concentration in the solution. The colour medium content in flowing solution was determined with absorbance value, which measured in a spectrophotometer at the exit of the reactor.

8.1.1. RTD investigation characteristic

Diluted food colouring produced by *Schimek*[®] was used as a fluid tracer. Its density was equal to 0,1 g/l and the mean absorbance varied between 0,18...0,2 A at the wavelength of 500 nm. The absorbance of the fluid was defined with a *Thermo Scientific Helios*[TM] *Zeta* spectrophotometer. A glass flow cuvette fixed with tubes coming from the reactor enabled continuous measurement of fluid absorbance. The data were automatically record on a PC and controlled from the VISION*lite*[TM] software at 4 seconds interval. The minimal interval of 4 seconds was the program's limit and could not be changed. Because of the small volume of the coil reactor and its RTD situated below 60 seconds the data had to be recorded manually from main device display which was able to show diagrams with minimal 1 second interval. These limitations could interfere with the accuracy of the RTD measurement data. Another problem related to the measurements' registration were air bubbles that sometimes changed the real value of fluid absorbance in the cuvette, especially at very low flow rates like 3 l/h.

As the construction of the experiment enabled a continuous measurement only at the exit from the reactor, the tracer absorbance value was checked before every start of the experiment to identify the tracer concentration. After that, the reactor was filled up with water coming from a 2-liter storage tank with a specific flow rate. As the reactor filled up, the water flow turned into the tracer flow coming from the second storage tank. Both tanks were connected with a cock, which allowed an easy regulation of the water and tracer flow.
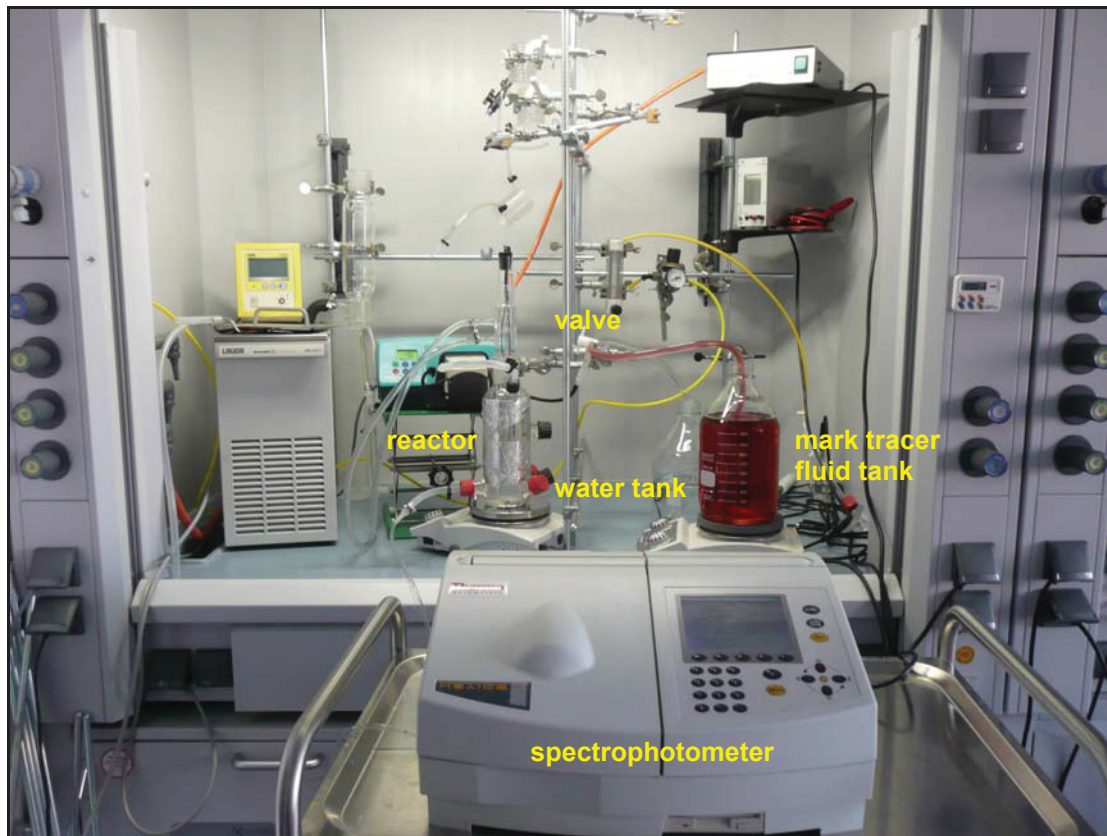
Figure 8.1: Experimental setup at residence time distribution tests in the CSTR

The residence time distribution was measured in all reactors and also in the electrolysis cell with different flow rates: 3l/h; 6 l/h; 10 l/h; 15 l/h; 20 l/h. As a cathod a glassy carbon was used, which was located before steel plate. It caused considerable pressure losses and made a solution flow under value of 10 l/h not possible. Lower flow rates passed only through the anode tube system, the cathode tube system was filled with water and remained in balance. That was the reason to measure RTD of electrolysis cell at the 10 l/h, till the maximal possible pump flow rate of 24 l/h.

To prove reproducibility of the investigations all measurements of every reactor and every flow rate were done twice. The obtained values in both experimental runs were nearly the same, what confirms comparability of the tests.

In the investigation all four reactors, described in 7.4.2, were used. The electrolysis cell was also analysed, however it cannot be considered as a type of reactor because of its specific construction.

8.1.2. RTD in the coil reactor

The RTD in the coil reactor showed the smallest variation from an ideal step tracer F curve. Figure 8.1 presents the RTD in the coil reactor at different flow rates. At 15 l/h the $F(t)$ curve grew rapidly, reaching the value of $F(t)$ = 0,98 after 7 seconds. The mean RTD, calculated using Eq. 6.11 was equal to 3,7 seconds. At a flow rate of 10 l/h, the $F(t)$ value of 0,97 was reached after 11 seconds and the mean RTD was equal to 5,4 seconds. At the other two flow

rates the F curve started to bend. The value of *F(t)*=0,97 was reached after 20 seconds at the flow of 6 l/h and at 3 l/h after 46 seconds. The mean RTD was accordingly equal to 11,0 and 23,2 seconds. The *F(t)* curve run showed no irregularities at any of the flow rates.
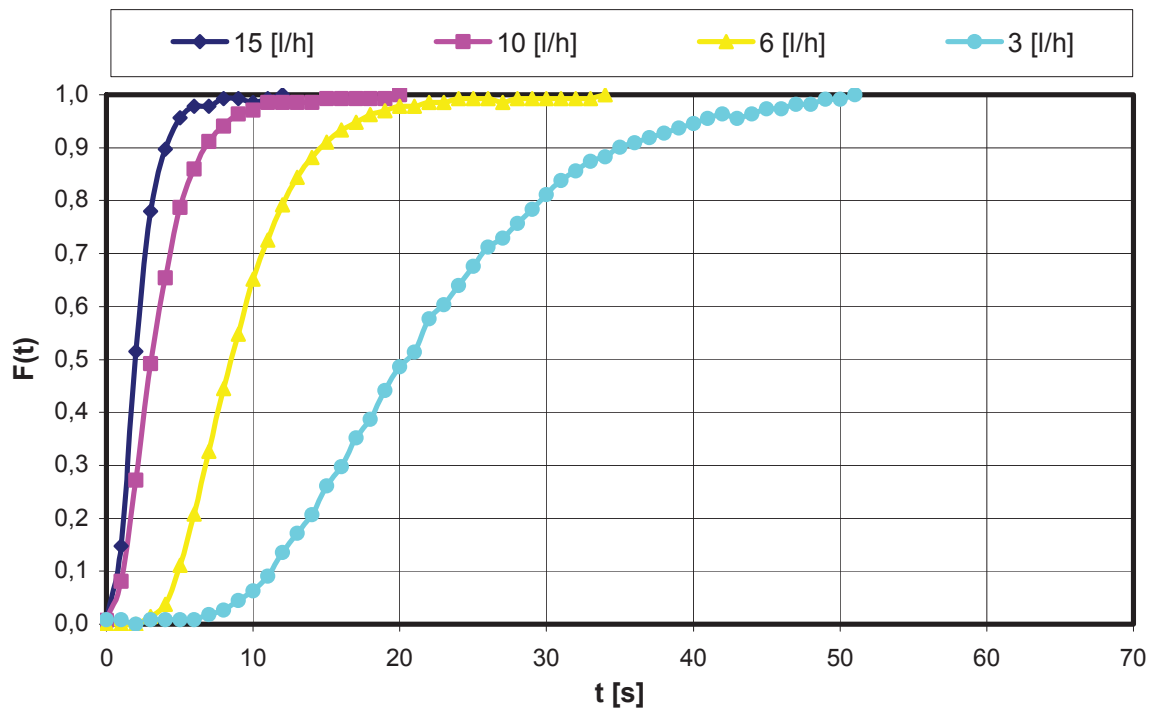
Figure 8.2: *F(t)* curves obtained from step tracer experiments done in coil reactor at different flow rates

8.1.3. RTD in PFRs

The RTD measurement of the PFRs were carried out with an immersed UV lamp to reflect the same laboratory conditions as those held by EDTA degradation test. The trace solution was pumped from the storage tank into the bottom inlet of the PFRs and the outlet took place through upper inlet. The volume of water to fill the small PFR was equal to 113 ml and by the large one 345 ml.

Figure 8.2 presents the results from the RTD tests in the small PFR. As the volume of the reactor is small also the RTD is short: the *F(t)* curve reached 0,97 value after 57 second at a flow rate of 20 l/h, at 15 l/h after 80 seconds. The same amount of *F(t)* = 0,97 was recorded after 108 second at 10 l/h and 184 seconds at 6 l/h. The flow rate of 3l/h needed 340 seconds to achieve the same level.
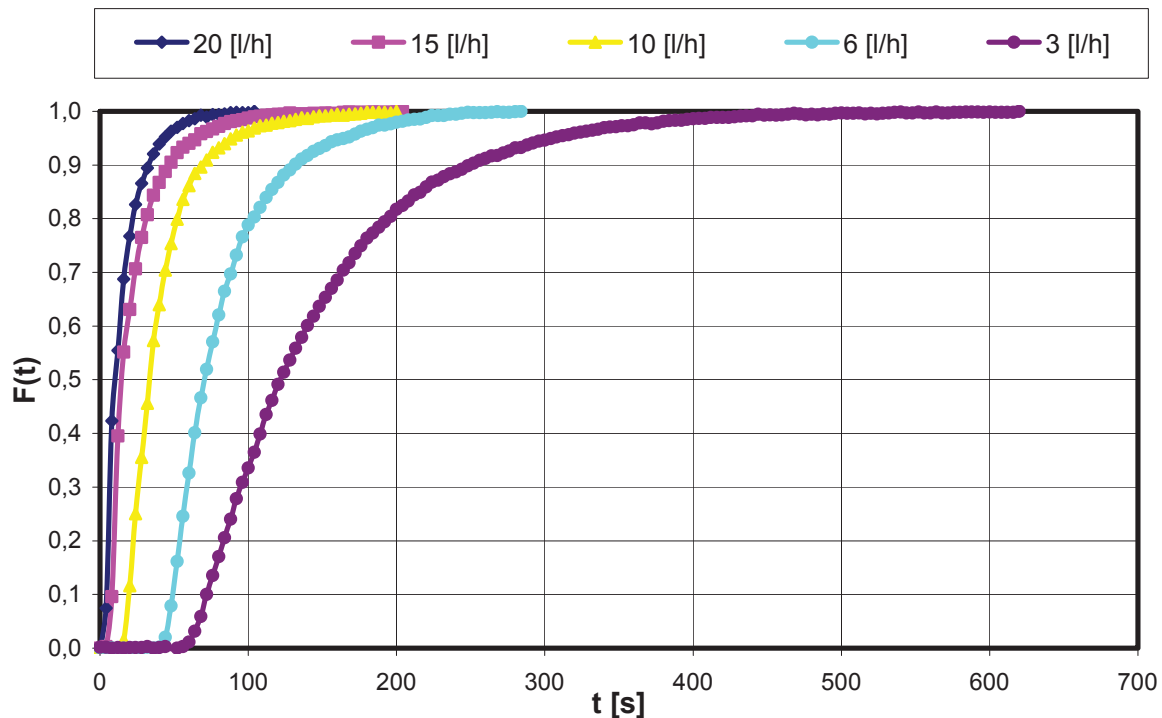
Figure 8.3: *F(t)* curves obtained from step tracer experiments done in small PFR at different flow rates

The mean RTD numbers are much greater than those from coil reactor. The highest flow rate brought a value equal to 17,3 seconds, the lowest a value of 148,1 seconds. The tracer moving with 15 l/h yield to a value of 24,7 seconds and a flow rate of 10 l/h 44,1 seconds. At 6 l/h the mean RTD was equal to 84,2 seconds. No irregularities in the *F(t)* curves run were noticed.

The volume of the large PFR was twice greater than the small one and as a consequence the mean RTD values had also higher values. At the flow rate of 20 l/h the mean RTD was equal to 52,6 seconds, at 15 l/h – 70,3 seconds. The run of the *F(t)* curve at those flow rates was relatively similar and up to a value of *F(t)* = 0,9 it raised rapidly. The value of 0,9 was reached in 92 seconds at the greatest flow rate, at 15 l/h it needed 124 seconds. The *F(t)* curve at the flow rate of 10 l/h was no more steep and approached the point of 0,9 in 196 seconds. At 6 l/h the tracer concentration was growing gently to reach *F(t)* = 0,9 after 380 seconds. The mean RTD values of those flow rates were accordingly: 115,5 and 199,3 seconds. As Figure 8.4 presents, the run of the *F(t)* curve at the lowest flow rate showed some irregularities, which were partly a consequence of air bubbles in the solution flow. After the first tracer answer (100 seconds) the curve raised rapidly up to the value of 0,52 (152 seconds) and after that fell down a little bit under *F(t)*=0,5 and started raising again up till maximum, but in a very gentle way. The mean RTD of that flow was equal to 344 seconds.
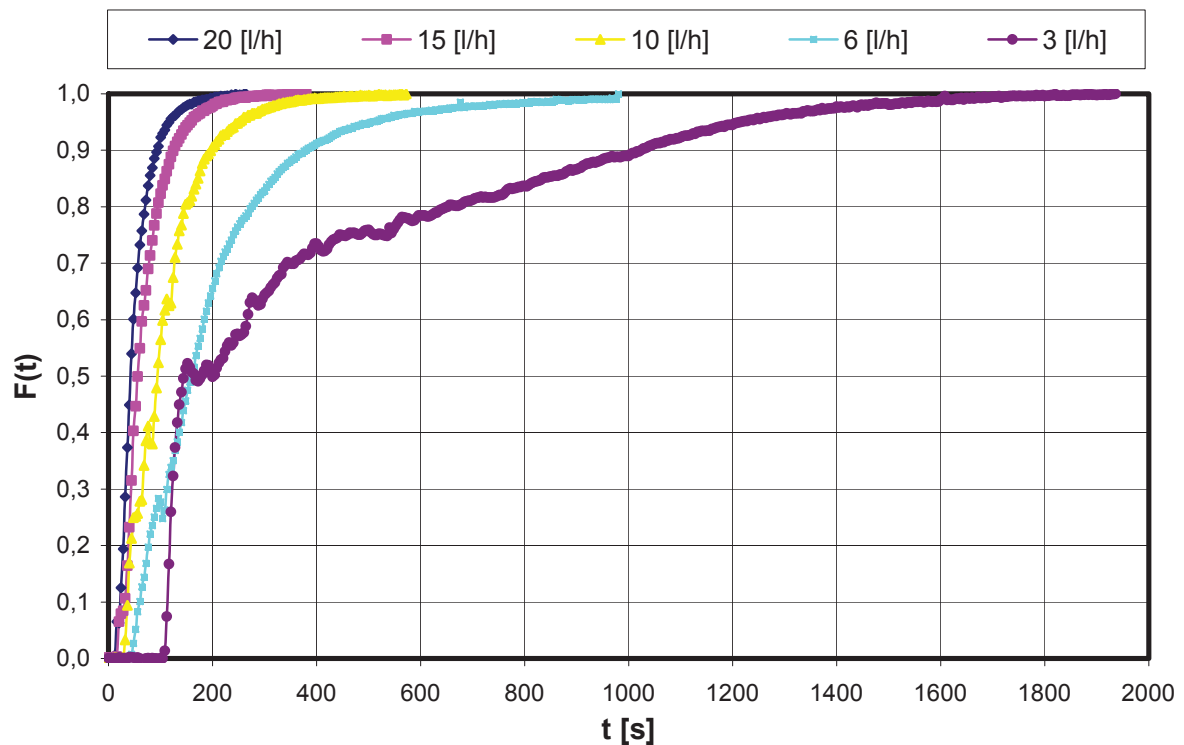
Figure 8.4: F(t) curves obtained from step tracer experiments done in large PFR at different flow rates

A flow rate of 6 l/h with its *F(t)* curve was more alike RTD run in the CSTR rather than in PFR. This situation could be explained by extremely small flow rate in comparison to large reactor volume.

8.1.4. RTD in the CSTR

RTD measurements in the CSTR caused some problems. Because of the UV lamp, immersed in the reactor during the tests, an adequate tightness between those two elements could not be assured. That led to the fluctuation of the fluid level in the CSTR at the flow rate of 20 l/h and enabled to run the experiment at this rate. On the other hand at the speed of 3 l/h, air bubbles disturbed the spectrophotometer measurement, causing abrupt jumps of the absorbance value.

The solution was pumped from the storage tank into the CSTR through the upper inlet, than it was mixed in the reactor with a speed of 250 rpm and left the reactor through the lower inlet (for the reactor setup see Chapter 7.4.2). Figure 8.5 shows the *F(t)* curves recorded at the RTD tests in the CSTR.
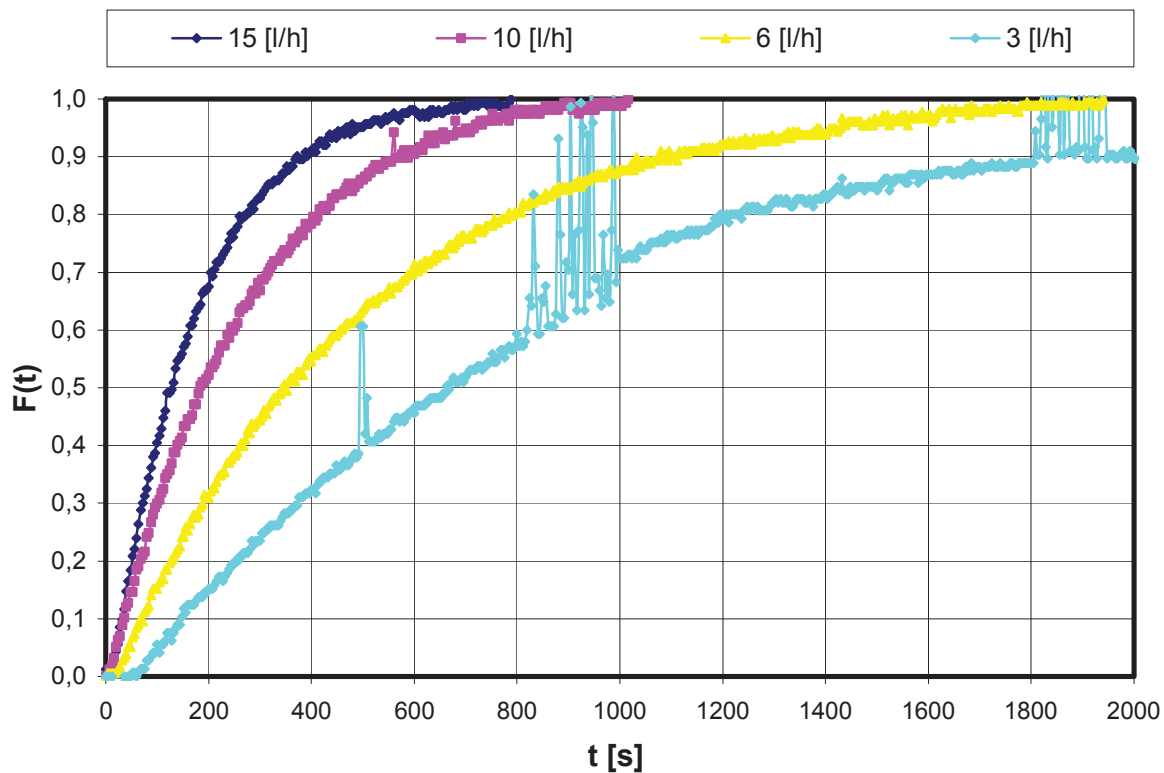
Figure 8.5: *F(t)* curves obtained from step tracer experiments done in CSTR at different flow rates

In this case the mean RTD at the flow rate of 15 l/h was equal to 176, 5 seconds and the value of *F(t)* = 0,97 was reached after 76 second. The mean RTD of the rest of the investigated flow rates were growing nearly linear: at 10 l/h it had the value of 263 second, at 6 l/h flow rate 485,7 seconds and at the minimal speed 612,8 seconds. To reach the point of *F(t)* = 0,97 at the speed of 10 l/h nearly 13 minutes were required, at the 6 l/h almost 26 minutes. The minimal flow rate achieved the value of *F(t)* = 0,92 after 38 minutes and then the experiment was disrupted by too intensive fluid's level fluctuations.

8.1.5. RTD in the electrolysis cell

The RTD of the electrolysis cell was difficult to compare with theoretical existing reactor models because of its specific setup. Two inner flows through the micro tubes and the glassy carbon filling made the classification of the electrolysis cell as a one of the known RTD models impossible. The experiment gave important information about the cathode flow: it allowed to identify the minimal flow rate through the cathode tube system, which had to be equal or greater than 10 l/h. At the flow rate of 9,5 l/h the outlet tube from cathode stayed filled with water and the whole flow passes through anode tubes. The experimental results are presented at Figure 8.6.
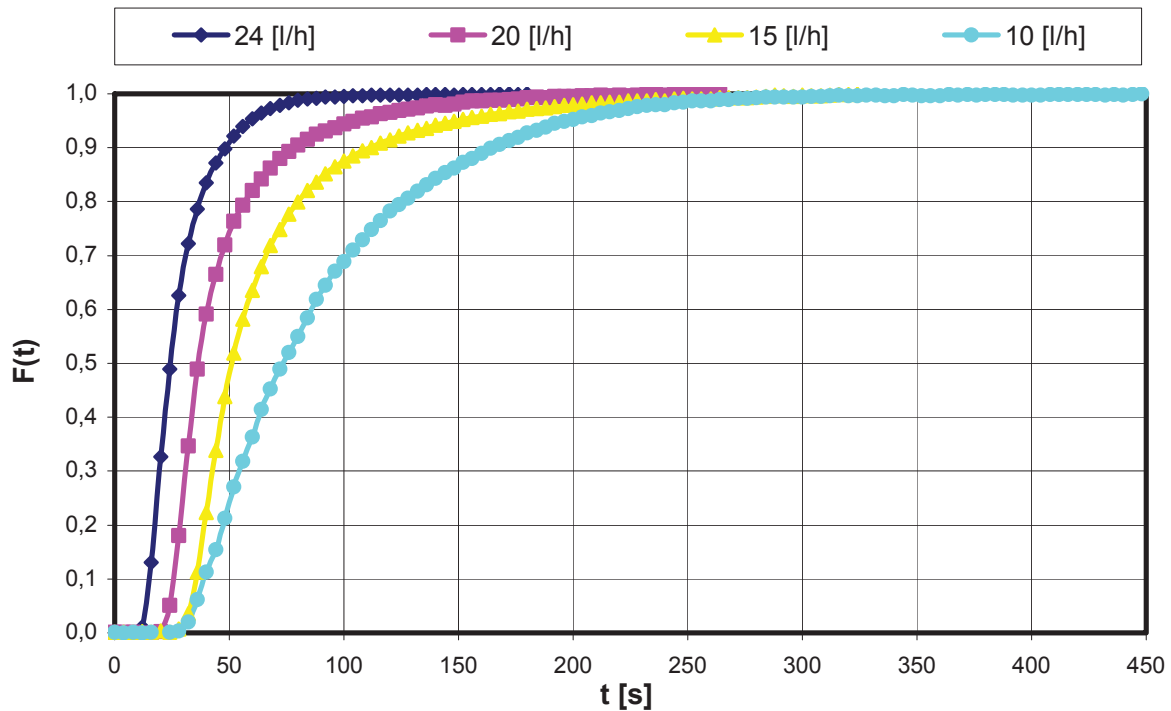
Figure 8.6: *F(t)* curves obtained from step tracer experiments done in electrolysis cell at different flow rates

The *F(t)* curve at the minimal flow rate was growing gently, showing similarities to the CSTR curve. The mean RTD was equal to 90,6 seconds and the point of *F(t)* = 0,9 was reached after 104 seconds. The flow rate of 15 l/h also did not result in a rapid rise of the curve. Its mean RTD was the same as 67,3 seconds and *F(t)* = 0,9 was achieved after 72 seconds. Prompt increases of the *F(t)* values could only be noticed at 20 l/h and 24 l/h. The mean RTD at the greatest flow rate was equal to 31,2 seconds, the value of *F(t)*=0,9 was reached after 48 seconds. At the flow rate of 20 l/h the rapid growth ended after *F(t)* = 0,8 after 56 second. The mean RTD at that flow was only a bit lower and equal to 48,1 seconds.

8.1.6. Hydraulic residence time vs. mean residence time

Experimentally established mean residence time values in different reactor types should be close to the one calculated from Eq. 6.1. Table 12 shows that data achieved in RTD investigation had higher or smaller variations from the hydraulic residence time values. In that comparison electrolysis cell was not considered.

Table 12: Hydraulic- and mean residence time in different reactor types

Flow rate	Hydraulic and mean residence time [s]							
	Coil reactor		Small PFR		Large PFR		CSTR	
[l/h]	HRT	MRT	HRT	MRT	HRT	MRT	HRT	MRT
3	33,6	23,2	135,6	148,1	414,0	344,6	984	612,8
6	16,8	11,0	67,8	68,2	207,0	199,3	492	485,7
10	10,1	5,4	40,7	44,1	124,2	115,5	295,2	263,0
15	6,7	3,7	27,1	24,7	82,8	70,3	196,8	176,5
20	-	-	20,3	17,3	62,1	52,6	147,6	

The greatest differences were noticed in the coil reactor tests, the effective values determined about 50 – 60 % of the hydraulic residence time values. That fact could be explained with existence of dead zones (see Chapter 6.1). The other deviation was observed in the PFRs, at the lowest and highest flow rates. In this case we can speak about two different flows. As the fluid flow was easier to observe when the colour solution was replaced with water, one of the test was done in that way. Figure 8.7 clearly shows two various fluid flows: the one is located just next to the UV lamp area (deeper rose colour) and the other one (light rose colour) is running with higher speed in some distance from the lamp.

Figure 8.7: Step tracer test in large PFR: two flows in fluid visible (deep and light rose)

The fact, that the mean residence time values were lower than the hydraulic residence time ones, could also be explained with persistence of dead zones in the reactor, for example under the UV lamp in PFRs. Higher than theoretically values could be considered as a consequence of pressure lost, especially at low flow rates.

As the effective mean residence time was not always identical as the hydraulic one, there was also a difference between the mean residence time estimating. This inequality shows Figure 8.8, where two *F(t)* curves of the small PFR at a flow rate of 20 l/h are presented, as well as *F(t)* of the ideal PFR. MTD was established according to Eq. 6.9 twice: once using the hydraulic residence time and the second time using the mean residence time.
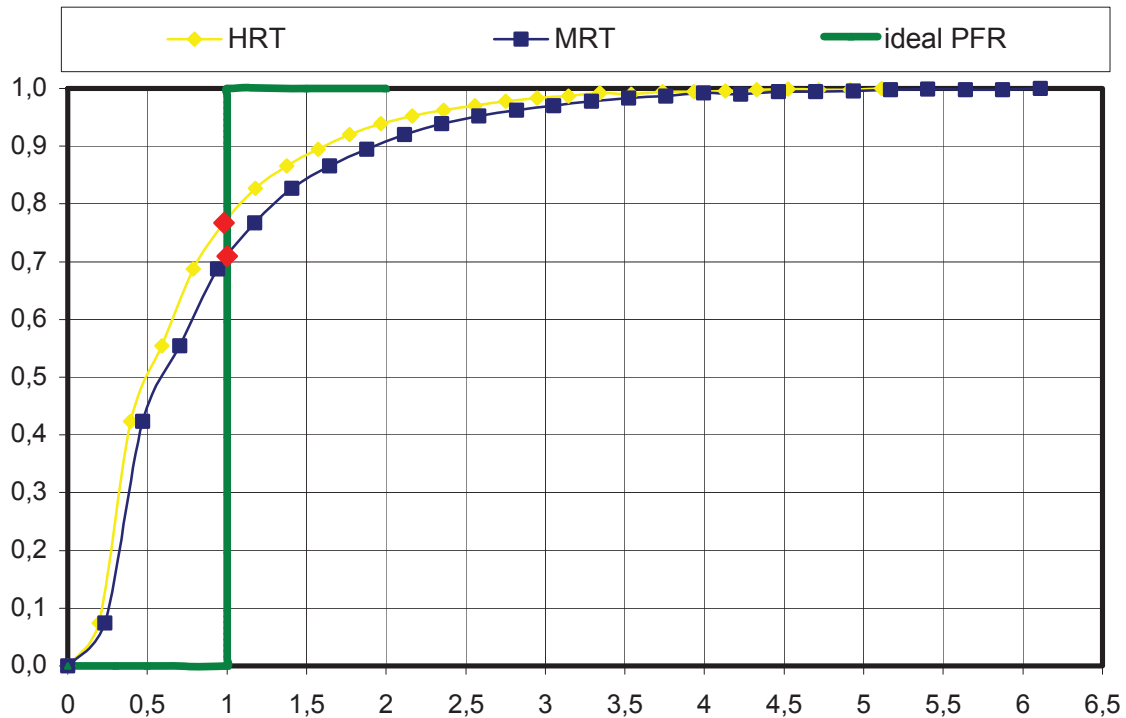
Figure 8.8: *F(t)* curve in small PFR according to HTR, MRT and ideal PFR

Because the differences between the hydraulic and the effective MTD were sometimes significant, further comparisons of various reactors will be carried out using the real data and effective MTD.
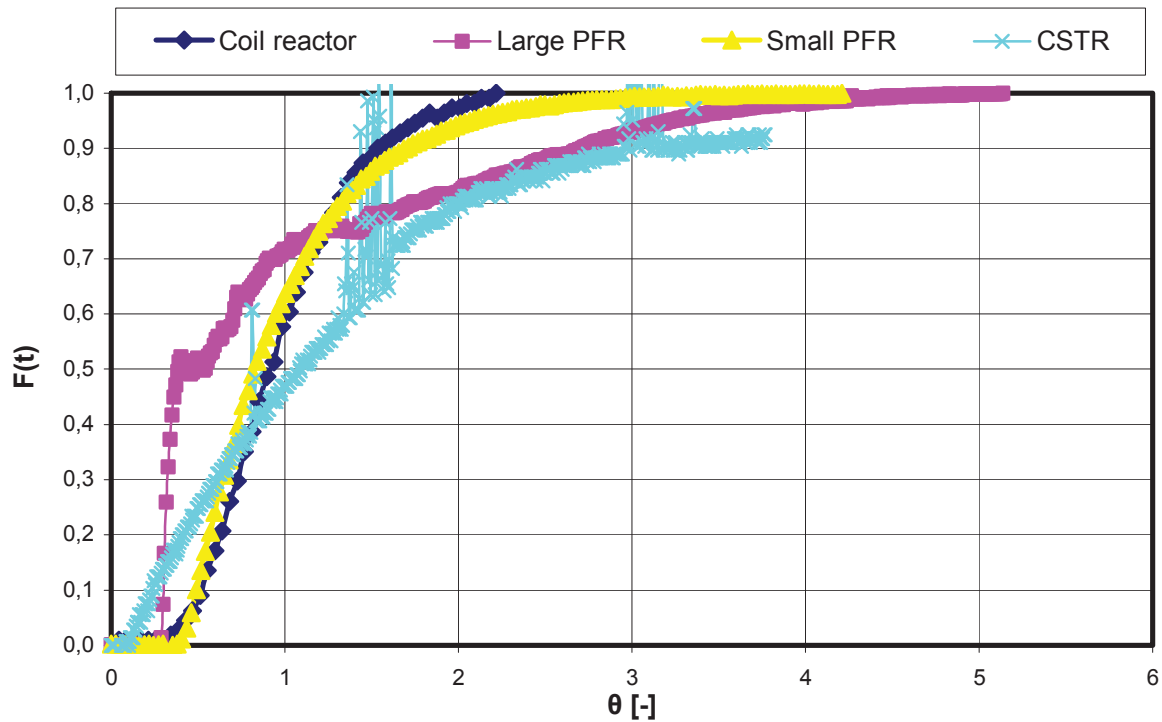
Figure 8.9: Comparison of *F(t)* curves in different reactors at the flow rate of 3 l/h

Figure 8.9 displays different reactors at the flow rate of 3 l/h over time (θ). The coil reactor had the shortest RTD and a very steep run of the *F(t)* curve, which means, that its flow was the closest to the ideal one. The *F(t)* curve of the small PFR was very similar to that of the coil reactor, only its RTD was longer. The value of *F(t)* = 0,7 was first reached by the large PFR, however its later RTD curve run did not increase as fast as the small PFR. The RTD curve of the CSTR was the most gently growing one and achieved only *F(t)* = 0,47 at θ = 1.
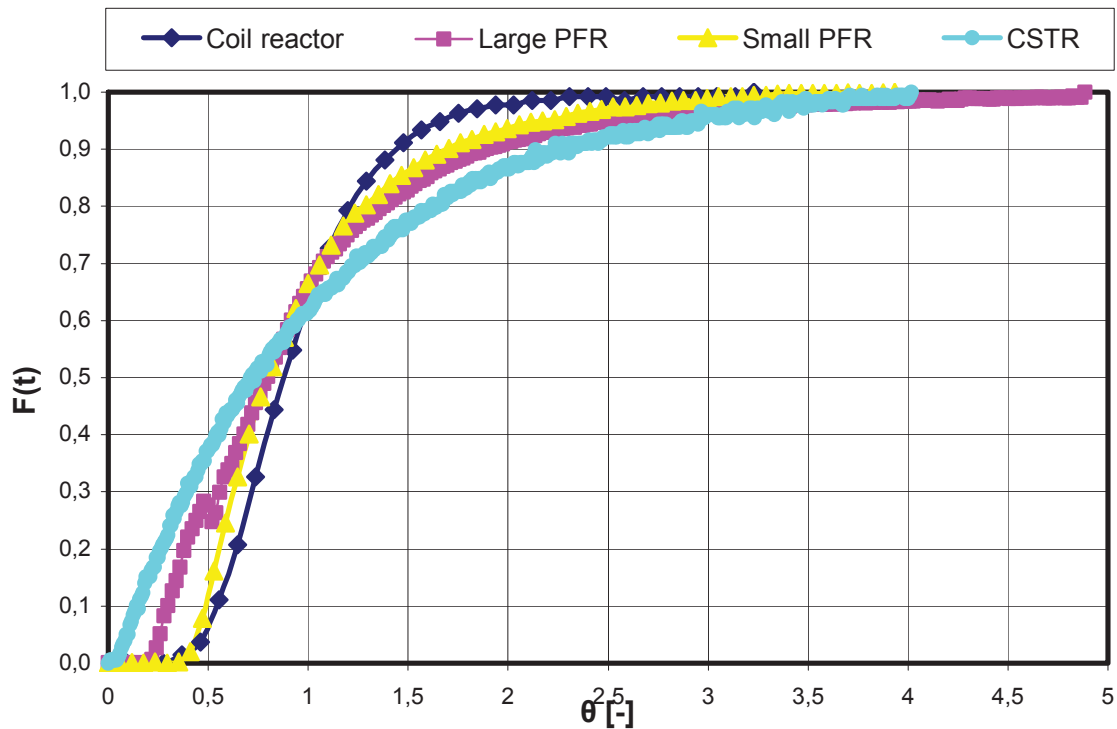
Figure 8.10: Comparison of *F(t)* curves in different reactors at the flow rate of 6 [l/h]

Figure 8.10 confirms the tendency of Figure 8.9: the *F(t)* curve of the coil reactor grew rapidly and reached its maximum after 3,2 θ, while the large pipe reactor needed almost 5 θ. The RTD curve of the small PFR still remained an ideal one, but the curve of the larger one was more like the RTD curve of the CSTR. All of the reactor types had the θ value of 1 in the range of *F(t)* = 0,65, only the CSTR curve came to that point at *F(t)* = 0,62.

At the comparison of flow rates of 10 l/h, presented at Figure 8.11, the coil reactor flow was again a very near example of the ideal one. The RTD curve of the small PFR was very similar to that of the coil reactor. It had the same value for θ = 1, which was *F(t)* = 0,67, only the maximum was reached much later: after θ = 4,7. The large PFR curve was in that case very irregular. It has the same *F(t)* value equal to 0,64 for θ = 1 as the CSTR, however its run was much steeper.
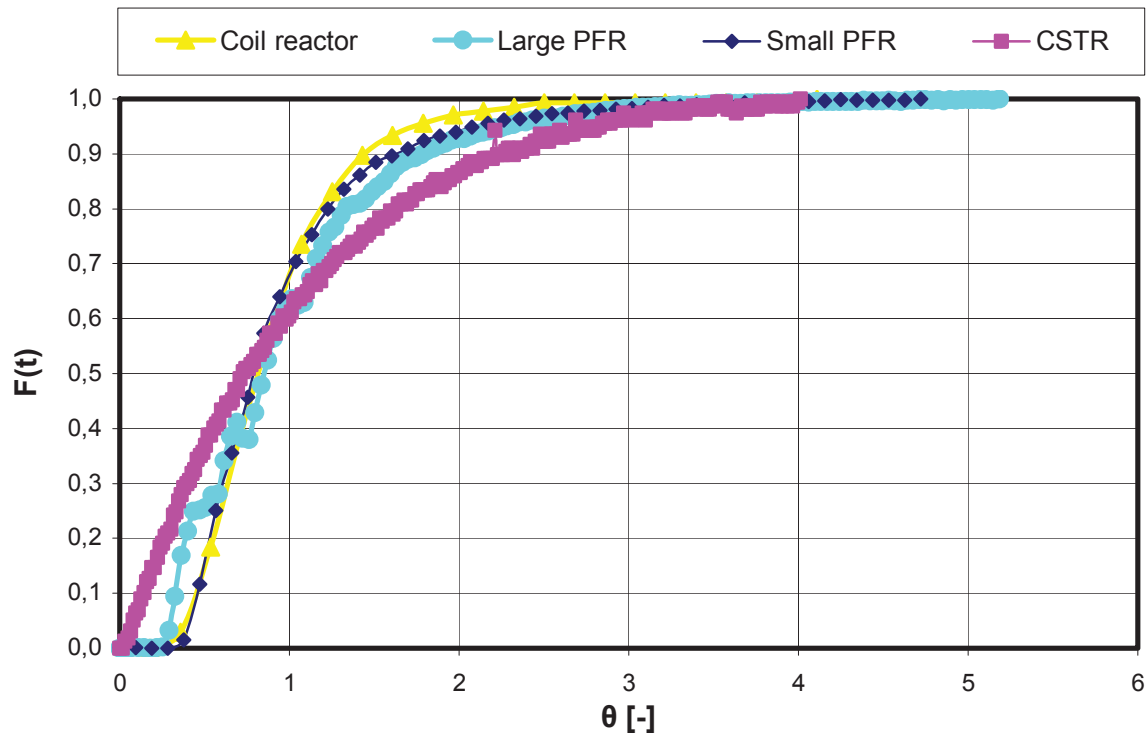
Figure 8.11: Comparison of *F(t)* curves in different reactors at the flow rate of 10 [l/h]

Figure 8.11 shows that with higher flow rate the RTD curves of the reactors became much steeper. It was again the coil reactor, which reached $F(t) = 0,97$ after $\theta = 1,4$ as the first one. The large PFR needed 2,5 θ to achieve that point, the small one 3,3 θ and the CSTR 3,4 θ. However the run of the small PFR's *F(t)* curve was growing rapidly at the beginning and matched the large reactor curve until the $\theta = 0,8$, afterwards it required a long time to reach the maximum. The coil and the small PFR had the same *F(t)* value for $\theta = 1$ which was equal to 0,7. The large PFR and the CSTR had at that point the value $F(t) = 0,63$.

At Figure 8.12 *F(t)* curves of various reactors at 15 l/h are presented. The small PFR and the coil reactor reached the mean time $\theta = 1$ at *F(t)* value equal to 0,7. The large PFR and the CSTR at that time had a value of 0,62. The coil reactor *F(t)* curve was again the steepest one. Although the small PFR curve run was at the beginning very steep, after $\theta = 1$ it increased at a much slower rate.
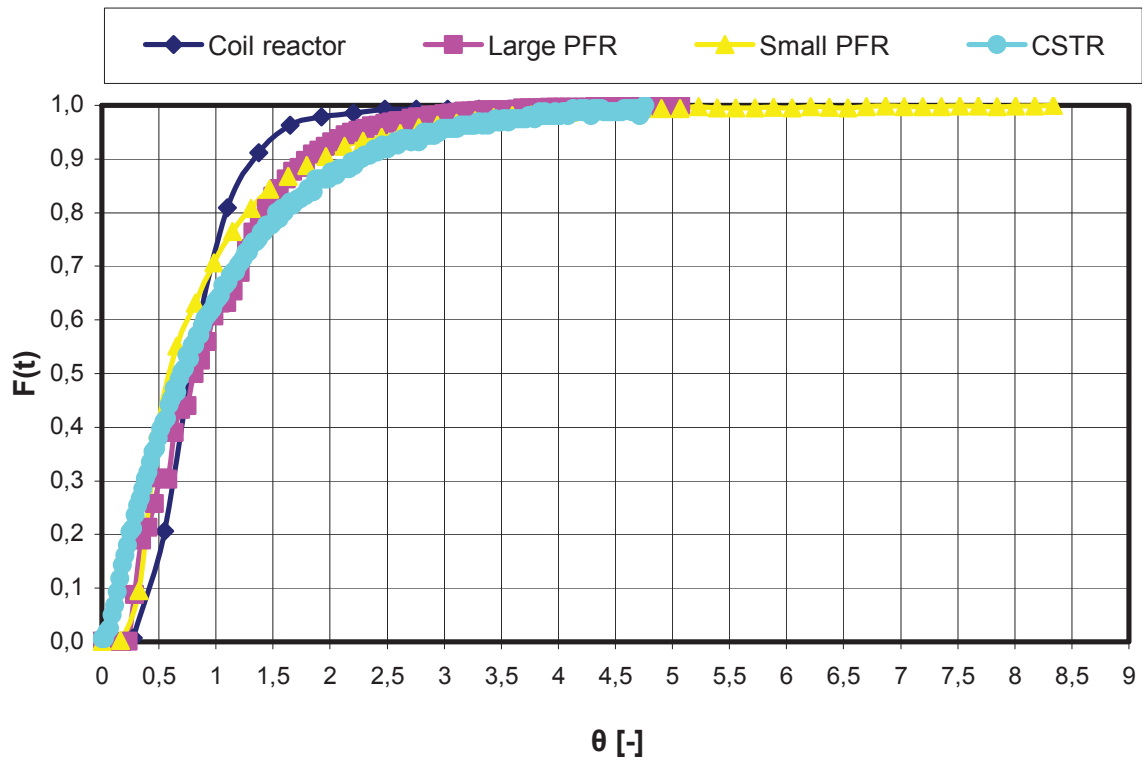
Figure 8.12: Comparison of *F(t)* curves in different reactors at the flow rate of 15 [l/h]

8.2.   Radiant power in various reactors

Photon irradiance with UV radiation in various reactors was determined using chemical actinometer, which in this case was potassium iodide/iodate solution. According to Rahn [30] it has a very good ability to measure photon flow from a low-pressure mercury lamp with a wave length of 254 nm. Using Eq. 3.11 the radiant power recovery could have been calculated.

The actinometer experiments were run in all reactor types with various flow rates as a continuous process (no circulation of fluid). The batch reactor was tested in discontinuous conditions with mixing at 250 rpm.

8.2.1. Experimental run

The experimental setup consisted of a 3 liter tank T1 with a potassium iodide/iodate solution, which was pumped into the reactor and gathered in the second tank T2. Both of the tanks were covered with aluminum foil to prevent the solution from visible light influence. The reactors with an immersed UV lamp were also wrapped with foil to protect the user from harmful radiation. Samples were taken just behind reactor's outlet, using a special cock, at time intervals estimated from RTD measurements. In the reactors with larger volume, like the large PFR, it was necessary to mix gathered solution from T2 with that what remained in T1 after every flow rate change. The zero sample was collected before every run, which enabled to estimated the real value of photon irradiance for each experiment.

Quantum yield in PFRs was examined at flow rates of 3; 6; 10; 15 l/h. In the coil reactor there were also extra tests at the minimal speeds of 0,3; 0,75; 1; 1,5 l/h. At every flow at least three samples were taken. In the batch reactor eight samples were taken in a time interval of 3 minutes.

To warm up the UV lamp, it was switched on a few minutes before starting the experiments. In an investigation with the batch reactor, potassium iodide/iodate solution was inserted through one of the upper inlets and the first sample was taken directly after finish of this action.

During the experiment the UV-lamp was placed in cooling cover connected to the heat exchanger with provided stable temperature of 25 $^{\circ}$C.

The outlet solution was prepared according to Rahn [30]. Potassium iodide, potassium iodate and Borax ($Na_2B_4O_7$) where mixed together with 3 liter of deionized water with concentration c_{KI} = 0,6 M, c_{KIO3} = 0,1 M and c_{Borax} = 0,01 M. The pH-value of the outlet solution varied between 9,22...9,3 and at the end of the measurements increased a little bit – about 0,05.

8.2.2. Experimental results

The effective UV-lamp radiant power was calculated basing on the triiodide concentration measurements. Before starting the photons flow calculations, it had to be specified whether all the radiation at the wavelength of 254 nm was absorbed in the reactors. The path length of reacting zone could be estimated with the Lambert-Beer law using Eq. 3.6. The molar absorptivity of potassium iodide at concentration of 0,6 M was equal to 27400 M^{-1}cm^{-1} and assuming radiation capability of I/I_0 = 90% we get the value of path length d = 0,6 *10^{-4} cm. The result gave the information, that 90 % of the whole radiation was absorbed just at the boundary layer of actinometer solution and reactor's quartz glass wall.

The absorbance of the samples was checked at the wave length of 352 nm and using Eq. 6.17 amount of triiodide, which was built through photochemical reaction, could have been calculated. Table 13 shows an example of actinometer data evaluation for coil reactor at flow rate of 10 l/h.

Table 13: Example of actinometer measurement data report with the evaluation

Sample	Time	Abs$_{352nm}$	Delution 1:x	$c_{Triiodid}$	$\Delta c_{Triiodid}$	V_{BR}	Φ_P	$P_{eff.}$
[Nr]	[min:sec]	[-]	[-]	[mol/l]	[mol/l]	[mol/h]	[einstein/s]	[W]
AKT-I-00		0,970	10	3,540E-04				
AKT-I-01	00:00	1,205	10	4,398E-04	8,577E-05	0,0013	4,574E-07	0,22
AKT-I-02	01:30	1,204	10	4,394E-04	8,540E-05	0,0013	4,554E-07	0,21
AKT-I-03	03:00	1,178	10	4,299E-04	7,591E-05	0,0011	4,048E-07	0,19
AKT-I-04	04:30	1,172	10	4,277E-04	7,372E-05	0,0011	3,931E-07	0,19

Mean value   **0,20**

8.2.3. Effective radiant power in reactors

The UV-lamp was described in details in Chapter 7.4.1. The efficient radiator power of a 20 cm long arc is equal to 10 W. In fact, the real value in the reactors was much lower as the cooling cover construction did not allow immersing the whole lamp in the reactors.

In case of the coil reactor only 13,5 cm of the arc length was surrounded with the coil. What is more, in the middle of the lamp cooling coal, a grinding was situated, causing further loss of UV radiation. Another source of radiation loss were space gaps between reactor's coils as well as the coils' glass walls. These reasons gave 3,5 mm of losses between two coils and the final value was equal to 2,9 W. The whole calculation of real UV-lamp radiation could be found in Table 14.

Table 14: Coil reactor technical data and effective radiation evaluation

Technical Data		Arc length [cm]	Radiant power [W]
Low Pressure UV lamp		20	10,00
Arc length in coil reactor		13,5	6,75
	Grinding	3,5	
	Rest	10	
Arc length without space gaps		6,85	3,43
	Grinding	2,1	
	Rest	4,75	
Real radiant power			**2,90**

Only 36 % of the arc length of the UV lamp could have been immersed in the large PFR which resulted in radiant power of 3,6 W. In the small PFR that value was equal to 3,75 W. In the batch reactor filled with 0,82 liter of actinometer solution 7 cm of the arc was effectively used. After every sampling the solution volume in the reactor was slightly changing and at the end of the experiment the liquid surface was 1,3 cm below its starting level. Because of the reactor's construction, the most remarkable drop took place at the first sampling (about 0,5 cm), after that the differences were minimal and their influence on reliability could been neglected.

8.2.4. Radiant power in the coil reactor and PFRs

The coil reactor and PFRs would be compared together as all of them had continuous flow as opposed to discontinuous batch reactor. Figure 8.13 presents the effective power radiation achieved during the experiments at various rate flows.
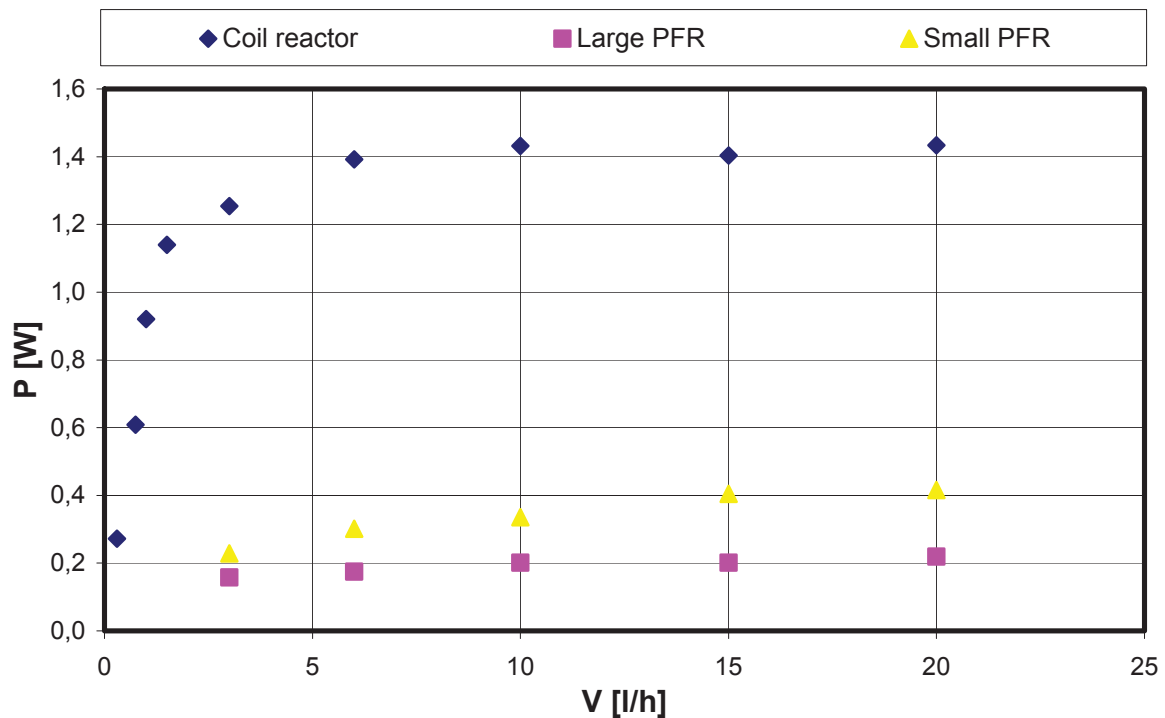
Figure 8.13: Radiant power in the coil reactor and the PFRs. Actinometer solution: c_{KI} = 0,6 M (small PFR: c_{KI} = 0,4 M), c_{KIO3} = 0,1 M, c_{Borat} = 0,01, pH_{start} = 9,2 ± 0,2, T = 25°C, Low-pressure lamp (35 W), λ = 254 nm.

Clearly, the highest values were reached in the coil reactor. A relative small radiant power value at minimal speeds was increasing together with the growing flow rate up to 6 l/h, when it became constant at P = 1,4 W.

In case of PFRs a little growth of power during flow rate escalation can be noticed. The minimal value of small reactor was equal to 0,23 W and the maximal to 0,42 W. The power radiation at the flow rate of 3 l/h in the large reactor was the same as 0,16 W and at the highest speed 0,22 W.

According to the theoretical power, which should be achieved in reactors the recovery of radiant power was analysed and its results can be seen at the Figure 8.14.
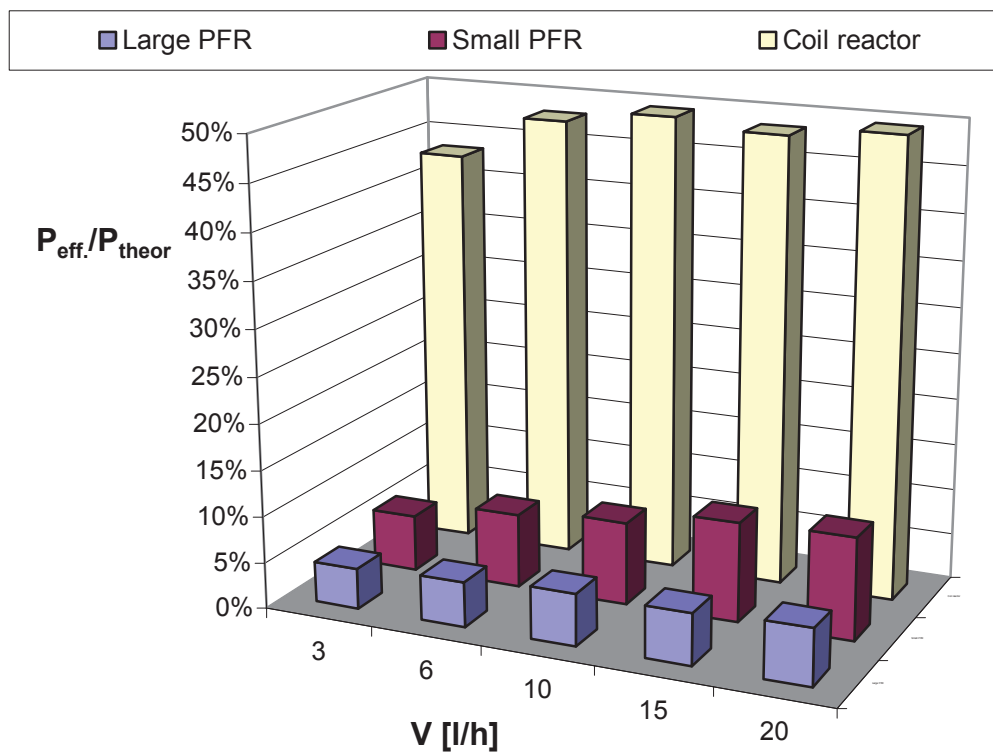
Figure 8.14: Effective radiant power achieved in actinometer measurements in the coil reactor and PFRs vs theoretical power. Actinometer solution: c_{KI} = 0,6 M (small PFR: c_{KI} = 0,4 M), c_{KIO3} = 0,1 M, c_{Borat} = 0,01, pH_{start} = 9,2 ± 0,2, T = 25°C, Low-pressure lamp (35 W), λ = 254 nm.

With the recovery reaching nearly 50 %, it is obvious, that the coil reactor is the most efficient one. The small PFR exceeds the value of P_{eff}/P_{theor} = 11 % at the highest flow rates, while the large PFR's efficiency is situated at 6 %.

8.2.5. Radiant power in batch reactor

As the actinometer measurement in the batch reactor was a discontinuous process, concentration of triiodide increased as the time elapsed. Figure 8.15 shows how the yellow colour would be intensified in every next taken sample.

Figure 8.15: Samples taken from actinometer measurement in the batch reactor: AKT-S test

The actinometer experiment in the batch reactor was carried out twice. At the first time a small stirrer was used with 250 rpm. Maximal photon flow at those conditions reached the value of $1*10^{-6}$ einstein/s. In comparison with tests done by Gangl [26] in the similar laboratory conditions, the results were not satisfying. In the second run a larger stirrer was used at the 500 rpm. As a result, the photon flow was equal to $2,2*10^{-6}$. Up to 30 minutes the concentration of triiodide was growing linearly, after that time its increase slowed down. As after some time the amount of triiodide achieved the point of saturation, in the reactor characterisation only the first seven values would be taken into consideration. At Figure 8.16 triiodide concentration against time is presented during the run of both experiments.
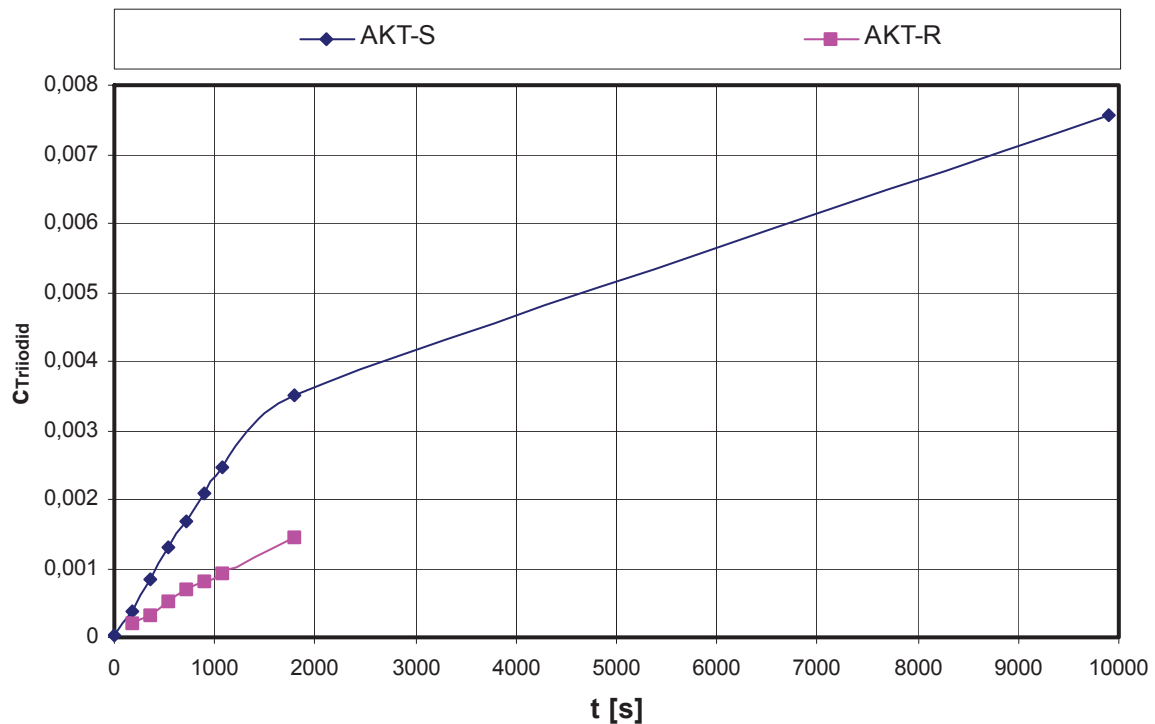
Figure 8.16: Triiodide concentration in the batch reactor. Actinometer solution: c_{KI} = 0,6 M (AKT-R), c_{KI} = 0,4 M (AKT-S), c_{KIO3} = 0,1 M, c_{Borat} = 0,01, pH_{start} = 9,2 ± 0,1, T = 25°C, Low-pressure lamp (35 W), λ = 254 nm, f_{small} = 250 rpm (AKT-S), f_{large} = 500 rpm (AKT-R)

As it comes to the radiant power and its recovery in the batch reactor it has to be mentioned, that the sample drawing could have influenced solution's level in the reactor and reduced the arc length immersed in it, however this fact had not such a big impact on the radiant power determination. The radiant power, calculated from first seven samples, brought the mean value of 1,08 W. There was a problem with defining the recovery of the photon flow. The estimated value was situated in the range of 38 – 47 %.

8.3. Cathodic hydrogen peroxide generation

As it was mentioned in Chapter 1 H_2O_2/UV combination is one of the better known AOPs method. Further laboratory test with combined EDTA anodic oxidation and photochemical degradation had also the purpose to generate hydrogen peroxide on the cathode, which should improve synthetic water decomposition. To characterise possibility of cathodic generation of hydrogen peroxide some laboratory tests were done applying various output currents, solution flow rates and pH-values. The used electrolyte solution was 0,5 M Na_2SO_4.

8.3.1. Electrolysis cell resistance and cathodic potential

According to Qiang, Chang and Huang [31], the best cathodic potential for hydrogen peroxide production is located at U_c = -0,5 V. To find out an optimal output current value, scanning tests were done to obtain desirable cathodic potential value. Anodic potential calibration tests on iridium oxide anode done by Zelenka [22] allowed to calculate the electrolysis cell resistance and the cathodic potential.
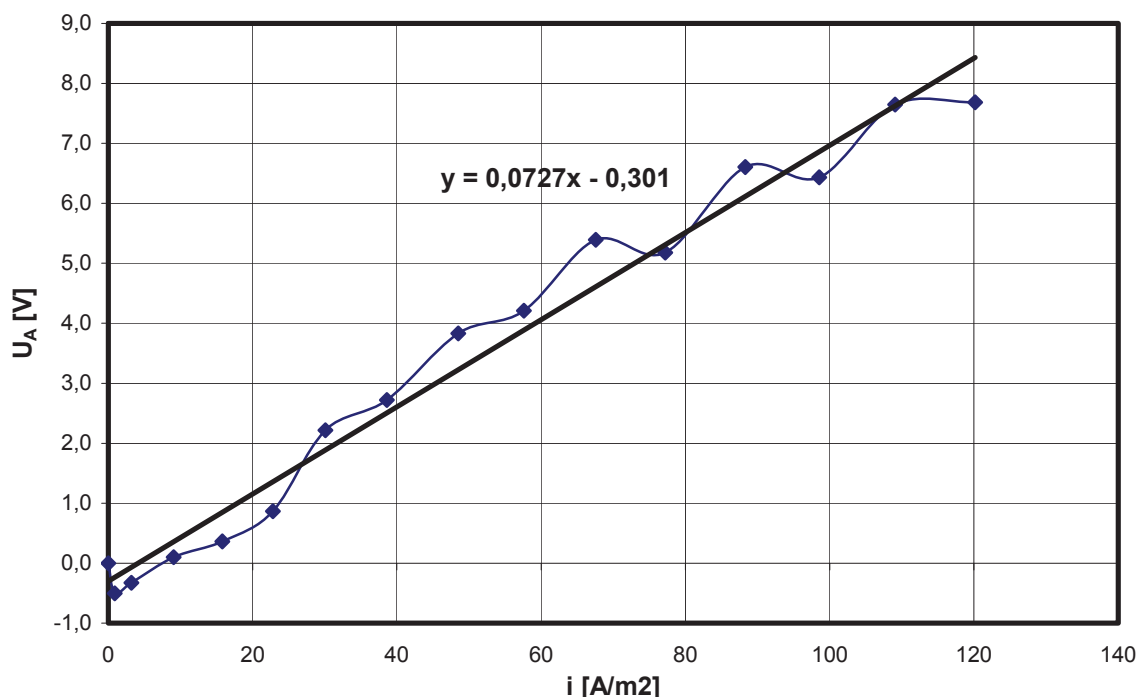
Figure 8.17: Anode potential against current density - results of tests done by Zelenka [22] on electrolysis cell with iridium oxide as anode and glassy carbon as cathode material

At Figure 8.17 data from anode potential calibration against current density done by Zelenka [22] is presented. Setting a trend line and using Eq. 8.1

Eq. 8.1   y = 0,0727x - 0,301

a dependence between anode potential and current density could have been determined.

Figure 8.18 represents scanning results in *EC Electro MP-Cell* with 0,5 Na$_2$SO$_4$ electrolyte and pH = 2.
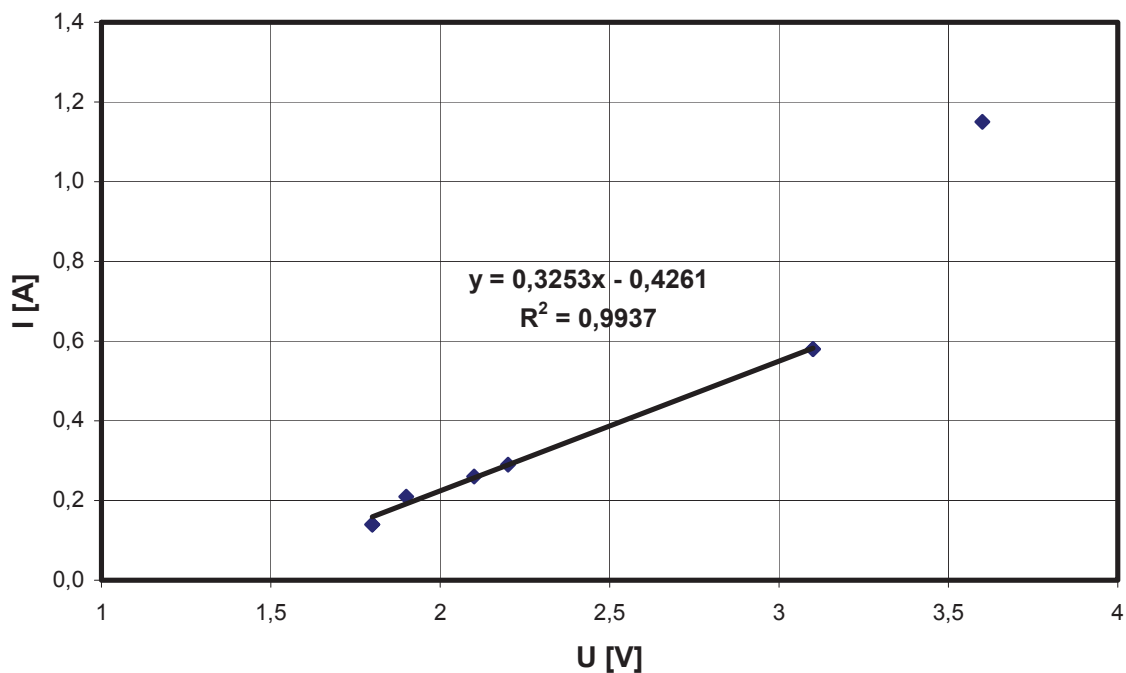
Figure 8.18: Electrolysis cell voltage vs electric current: establishing electric resistance in *EC Electro MP-Cell*. Anode: IrO$_2$ (A$_{specific}$ = 0,096m^2), Cathode: Stainless steel (A$_{specific}$ = 0,096m^2) with glassy carbon filling (A$_{specific}$ = 0,147m^2). Electrolyte solution: V$_{total}$ = 1l, c$_{Na2SO4}$ = 0,05 M.

The measured values allowed to establish the current-voltage trend line, which is described with Eq. 8.2. The trend line does not take the last noticed value into consideration.

Eq. 8.2   y = 0,3253x – 0,4261

Using Eq. 8.2 the electrolysis cell resistance was determined as R = 0,325 V/A. The Table 15 consists whole cathode potential evaluation. The values more desired for hydrogen peroxide production could be achieved at output current of 0,26...0,29 A.

Table 15: Data and calculation from electrolysis cell scanning using 0,5 M Na$_2$SO$_4$ electrolyte, pH = 2

I	U	R	U-(R*I)	j$_{Anod}$	Anode potential	Cathode potential
[A]	[V]	[V/A]	[V]	[A/m2]	[V]	[V]
0	0	0	0	0	0	
0,140	1,8	3,074	1,370	14,583	0,759	0,610
0,210	1,9	3,074	1,254	21,875	1,289	-0,035
0,260	2,1	3,074	1,301	27,083	1,668	-0,367
0,290	2,2	3,074	1,309	30,208	1,895	-0,587
0,580	3,1	3,074	1,317	60,417	4,091	-2,774
1,150	3,6	3,074	0,065	119,792	8,408	-8,343

8.3.2. Current density and solution rate flow variation

To describe the possible hydrogen peroxide production on the cathode three test series were done with various solution rate flows and different output current. All the taken samples were analysed with potassium iodide titration, described in Chapter 7.1.2.

During the first test run: OM_10, the electrolyte was circulating at a flow rate of 10 l/h and a start pH = 3 ± 0,2. Hydrogen peroxide production was checked at three current densities: 1,1 A/m^2; 2,2 A/m^2 – both within 45 minutes and 4,4 A/m^2 within 165 minutes. Blank samples were taken from the solution tank before starting the experiment and their analysis showed no presence of hydrogen peroxide. Figure 8.19 presents the achieved values. After every test the electrolyte was pumped out of the laboratory unit, which was then filled again with a new solution.
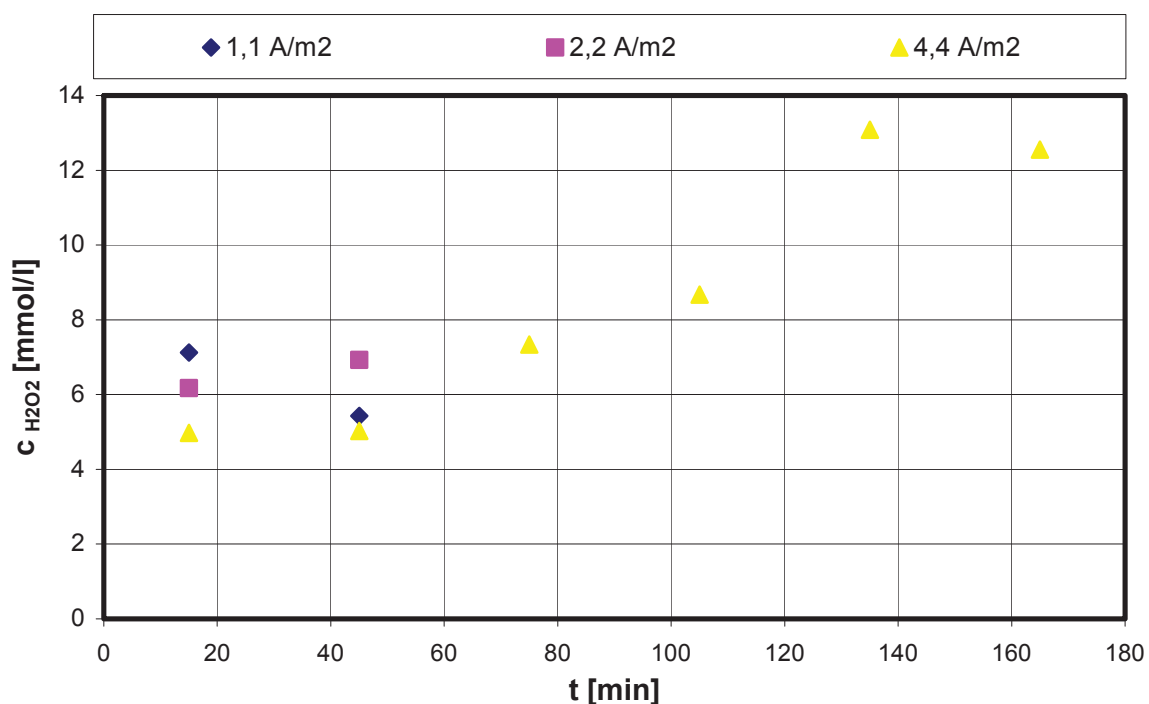
Figure 8.19: Hydrogen peroxide generation at different current densities (related to anode) at a flow rate of 10 l/h, pH = 3. Anode: IrO_2 ($A_{specific}$ = 0,096m^2), Cathode: Stainless steel ($A_{specific}$ = 0,096m^2) with glassy carbon filling ($A_{specific}$ = 0,147m^2). Electrolyte solution: V_{total} = 1,2 l, c_{Na2SO4} = 0,05 M.

The result of the experiment revealed very little cathode ability to product hydrogen peroxide at these laboratory conditions. In the first two tests hydrogen peroxide concentration was much below expected value and the experiments were interrupted. Only OM_10c test with a current density of 4,4 A/m^2 was carried out longer. In 135 minutes hydrogen peroxide concentration reached maximum c_{H2O2} = 13,08 mg/l and after that fell down again. Obtained values represent less than 10 % recovery in comparison with theoretical ones, calculated from Eq. 2.19.

OM_24 test serie was done without electrolyte exchange between the switching of the current density. The solution circulated at a maximal possible flow rate of 24 l/h and pH = 2.

Blank sample was taken from the tank before laboratory test begun. OM_24c test at the current density of 8,8 A/m^2 was done after 12-hour break from the previous one. Obtained values are presented at Figure 8.20.

Figure 8.20: Hydrogen peroxide generation in OM_24 serie at flow rate of 24 l/h, pH = 2. Anode: IrO$_2$ (A$_{specific}$ = 0,096m^2), Cathode: Stainless steel (A$_{specific}$ = 0,096m^2) with glassy carbon filling (A$_{specific}$ = 0,147m^2). Electrolyte solution: V$_{total}$ = 1,15 l, c$_{Na2SO4}$ = 0,05 M.

The maximum hydrogen peroxide concentration value was achieved in 315 minutes at the current density of 4,4 A/m^2 and after that dropped slightly. However, in this test run only absolute values change had to be taken into account. As it can be easily noticed, the highest concentration increase Δc_{H2O2} = 16,8 mg/l had occurred during current density of 2,2 A/m^2. At 1,1 A/m^2 hydrogen peroxide amount was oscillating between 5 and 10 mg/l without any visible growing tendency and at 4,4 A/m^2 and 8,8 A/m^2 concentration growth was about 5 mg/l. After a 12-hour break the hydrogen peroxide level dropped down nearly to its start value of c_{H2O2} = 9 mg/l. That fact was a clue that although hydrogen peroxide was degraded, some part of it always remained in the electrolysis cell.

The next run consisted of three tests done at current density of 2 A/m^2: OMd24, OMh24 and OMi24; and one done at 1,76 A/m^2: OMe24. Output current was chosen according to cathode potential calculations in Chapter 8.3.1. The electrolyte was changed after every test, but this time blank samples were taken after few minutes of current-less solution circulation in the laboratory unit. The electrolyte was distributed with a rate flow of 24 l/h and pH = 2.
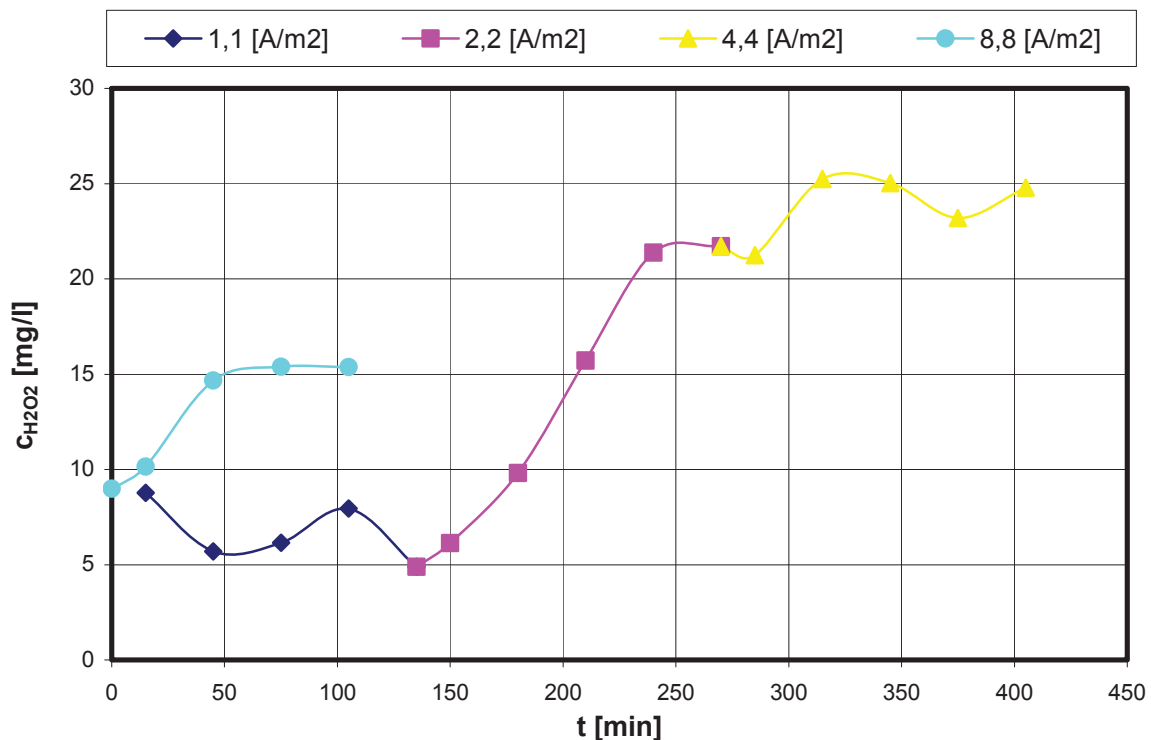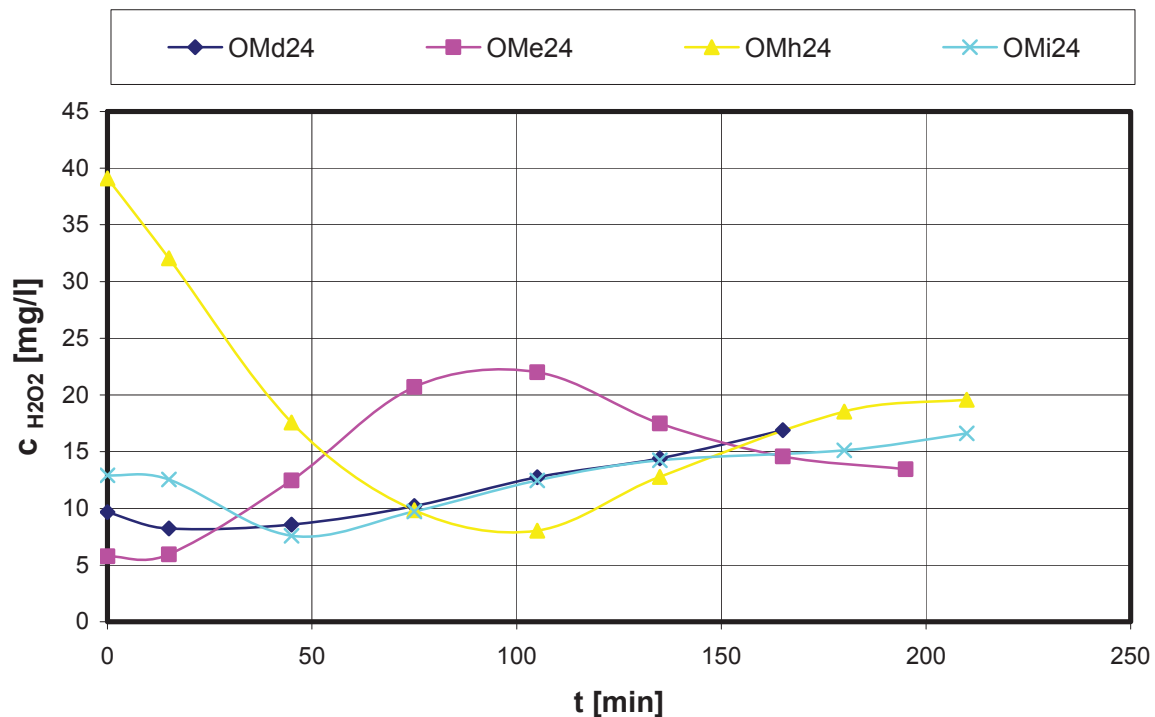
Figure 8.21: Hydrogen peroxide generation at flow rate of 24 l/h, pH = 2. Anode: IrO_2 ($A_{specific}$ = 0,096m^2), Cathode: Stainless steel ($A_{specific}$ = 0,096m^2) with glassy carbon filling ($A_{specific}$ = 0,147m^2). Electrolyte solution: V_{total} = 1 l, c_{Na2SO4} = 0,05 M.

As Figure 8.21 presents, hydrogen peroxide concentration in the blank samples was surprisingly high, located between 5 and 15 mg/l and in the case of OMh24 reaching even the value of 40 mg/l. The maximal hydrogen peroxide amount during the experimental run was achieved in the OMe24 test with the value of c_{H2O2} = 22 mg/l. However, after reaching top value the hydrogen peroxide content in the electrolyte began to decrease. In the OMd24 and OMi24 test runs the hydrogen peroxide amount was growing continuously to achieve a concentration level between 15 and 20 mg/l. The OMh24 experimental curve, after abrupt fall from the starting value, at 105 minute began to increase and in 210 minutes reached the point of c_{H2O2} = 20 mg/l.

According to performed tests, cathodic hydrogen peroxide generation in *EC Electro MP-Cell* would have to be further optimised to result in more predictable values. What could be determined is, that using the 0,5 M Na_2SO_4 electrolyte at a flow rate of 24 l/h and current density between 1,8 – 2,2 A/m^2 a hydrogen peroxide concentration of c_{H2O2} = 20 ± 5 mg/l in *EC Electro MP-Cell* could be achieved.

9. Experimental results – EDTA degradation

9.1. Anodic oxidation

The laboratory investigation of the anodic oxidation of EDTA was carried out according to the optimised experiments done by Zelenka [22]. Taking laboratory conditions from the best results achieved by Zelenka, in tests with *EC Electro MP-Cell* the current density of 20,2 A/m^2 was selected and an electrolyte 0,05 M Na$_2$SO$_4$ and 1,34 mM EDTA solution. To confirm reproducibility of the investigation, two tests were done in the same laboratory conditions. The EDTA concentration in the samples was measured by HPLC analysis, described in Chapter 7.2.

The laboratory unit consisted of a mixing tank from which the solution was pumped through the thermostat into the electrolysis cell and after that back again into the tank. The pH-control was installed in the mixing tank. The laboratory unit scheme is presented at Figure 9.1.
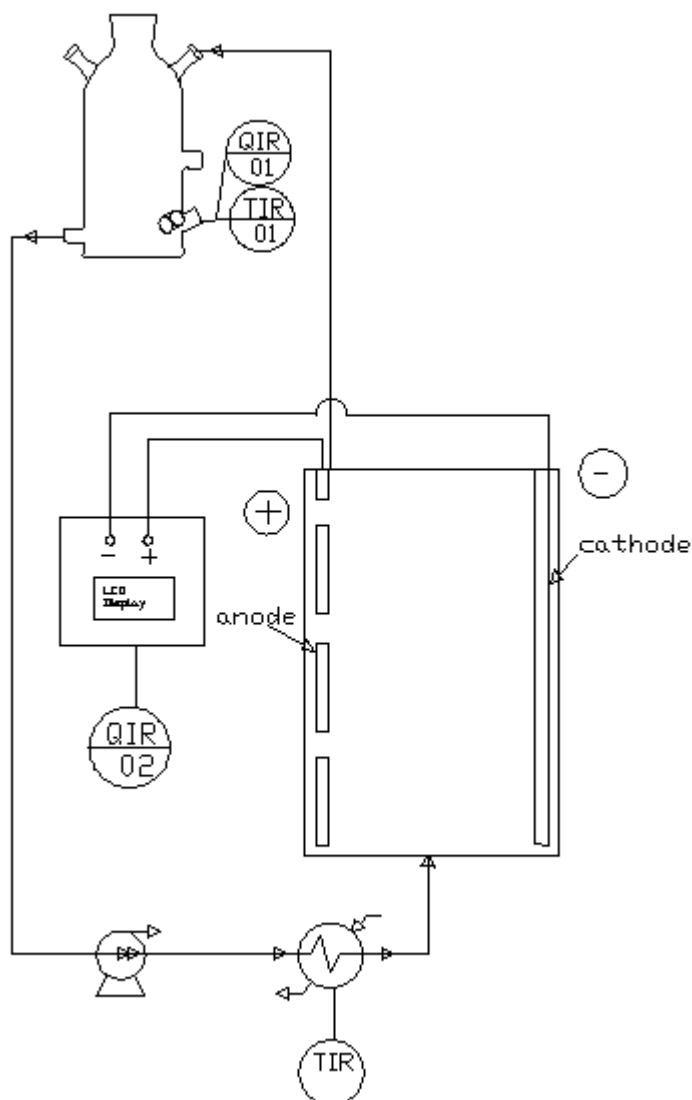
Figure 9.1: Anodic oxidation of EDTA: laboratory unit scheme

Figure 9.2 represents both tests' results: AOP-6 and AOP-9.
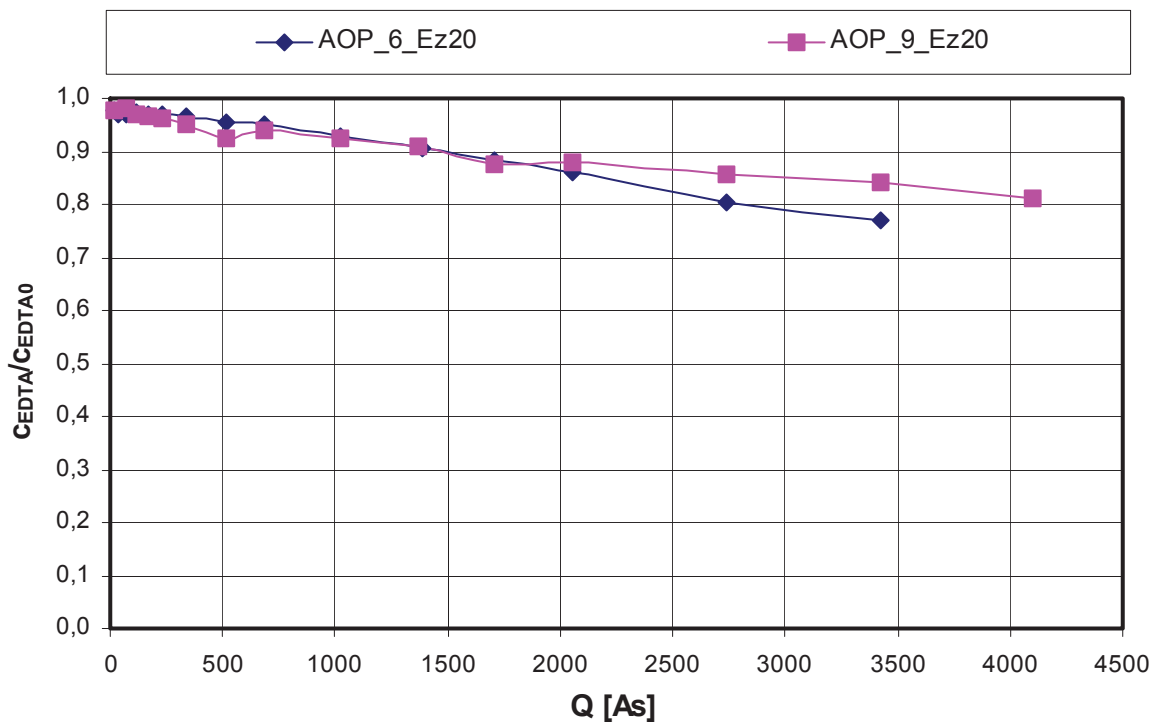
Figure 9.2: EDTA degradation vs Faraday charge. Anode: IrO_2 ($A_{specific}$ = 0,096m^2), Cathode: Stainless steel ($A_{specific}$ = 0,096m^2) with glassy carbon filling ($A_{specific}$ = 0,147m^2), I = 0,19 A, j_{anode} = 20,2 A/m^2, Electrolyte solution: c_{Na2SO4} = 0,05 M, c_{EDTA} = 1,34 mM EDTA, V_{total} = 1,1 l, $\dot{V}$ = 15 l/h, T = 25 ^{o}C.

The degradation curves of AOP-6 and AOP-9 show some differences in their run. By the first experiment, after 300 minutes EDTA was decomposed in 77 % and in the second one after 360 minutes only in 81%. The reaction rate constants calculated according to 1st order reaction run were equal to 0,0009 ¯min in the first experiment and 0,0006 ¯min in the second one. According to Eq. 2.22 EDTA-degradation grade achieved after 300 constituted only 53% of the expected value in AOP-6 experiment and 36% in case of AOP-9.

The fact of the various EDTA degradation run could be explained with unequal pH-value run in both experiments, what can be observed at Figure 9.3.
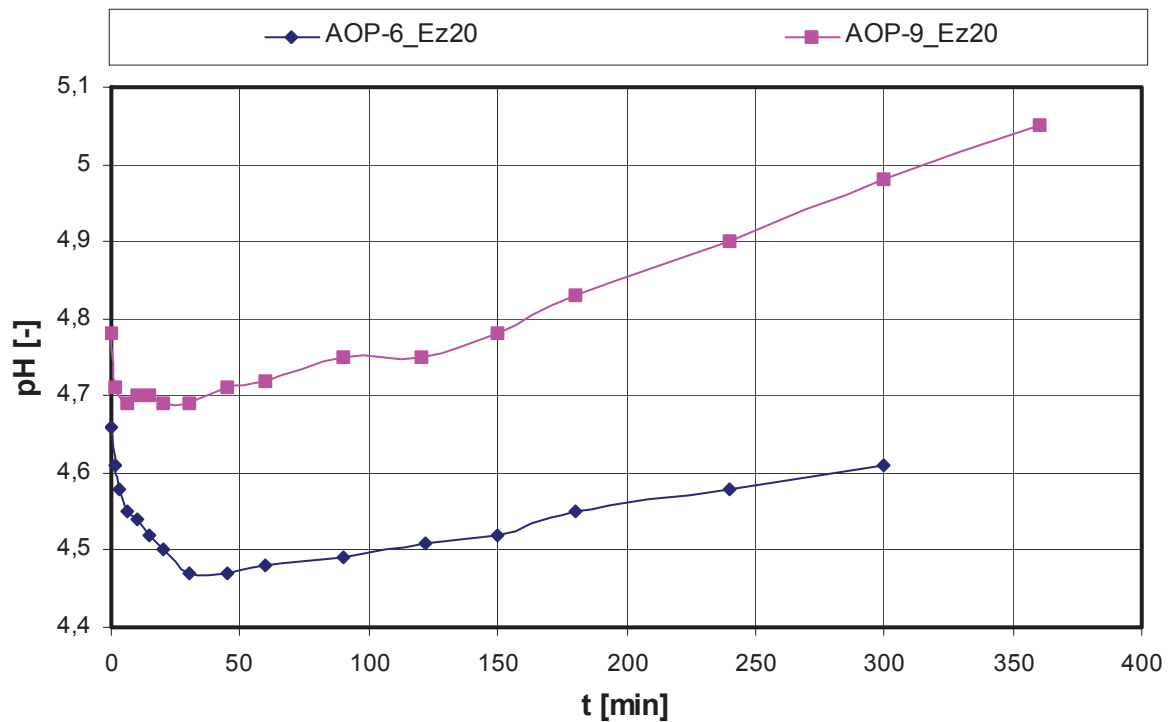
Figure 9.3: pH-value run during anode oxidation of EDTA. Anode: IrO_2 ($A_{specific}$ = 0,096m^2), Cathode: Stainless steel ($A_{specific}$ = 0,096m^2) with glassy carbon filling ($A_{specific}$ = 0,147m^2),   I = 0,19 A, j_{anode} = 20,2 A/m^2, Electrolyte solution: c_{Na2SO4} = 0,05 M, c_{EDTA} = 1,34 mM EDTA, V_{total} = 1,1 l, $\dot{V}$ = 15 l/h, T = 25 ^{o}C.

Although the starting pH-value was nearly the same: pH_{EAOP6} = 4,66 and pH_{EAOP9} = 4,78, in the first case much greater pH-value drop could be observed and later growth is not so fast as in case of AOP-9. The end pH-value of AOP-6 test was nearly the same as at the beginning, however during AOP-9 run the end value reached pH_{EAOP9} = 5,05.

According to Chapter 1.1 and Figure 5.1 the EDTA has various dissociation grades with various reaction constant rates, which strongly depends on the pH-value. Even small differences of 0,1 [-] could influence the whole degradation process.

9.2.   Photochemical degradation of Fe(II)-EDTA

Laboratory tests with photochemical degradation of Fe(III)-EDTA complex were investigated in the coil reactor, the small PFR and the batch reactor. Additionally the coil reactor was tested in a closed system, where defined volume of solution was circulating in the laboratory unit during 30 minutes.

Based on investigations carried out by Gangl [26], the ratio between Fe(II) and EDTA in the solution was the same as 2:1, because of the best EDTA degradation rate constant achieved at those proportions. The outlet solution used in all tests consisted of 1,34 mM EDTA and 0,67 mM $Fe_2SO_4*7H_2O$ mixture.

Fe(III)-EDTA complex has a quite high value of extinction coefficient, which at a wavelength of λ = 254 nm and pH = 3,5 is equal to 8350 ± 150 $M^{-1}cm^{-1}$. Using Eq. 3.5 it could be calculated, that 90 % of the whole radiation will be absorbed within the path length of d = 1,7 mm.

As the degradation process requires a pH value between 3…5 all of the experiments had a starting pH-value of 3 ± 0.1. In the case of the PFRs the pH limit at the reactor outlet was not exceeded. The batch reactor represented the only problem, as the experimental setup did not allow to retain the pH-value at the same level and after 30 minutes it exceeded pH = 5. This fact did not considerably influence the whole test, as the main degradation process was finished in 20 minutes.

During the experiments the temperature was equal to 25 ± 1 ^{o}C and the Fe(II)-EDTA solution was aerated with the air flow rate of 20 l/h (STP). The volume of the solution used in tests with the batch reactor and the coil reactor as a closed system was the same as 0,82 l. All the samples were analysed with a HPLC instrument, following instructions described in Chapter 7.2.

9.2.1. Photochemical Fe(II)-EDTA degradation in coil reactor

Fe(II)-EDTA degradation in the coil reactor was examined in two cases: as a plug flow and also as a closed circulation process. In the first case, the experimental setup consisted of a container C1 with 1 litre output solution, the coil reactor with the immeresed UV lamp, the cock and the collecting basin. Container C1 and the reactor with fixed UV lamp were wrapped in aluminium foil to prevent from UV radiation and day light influence. The solution passed through reactor only once and samples were taken just behind reactor outlet using the cock closure and kept in darkness until analysis.

Various flow rates were tested starting at a very low speed rate of 0,3 l/h through 0,75; 1,0; 1,5; 3,0; 6,0 up to 10 l/h. Time interval of sample drawing was calculated from mean residence time. To prove reproducibility of the experiment two samples were taken from each flow rate. To better compare the effectiveness of different flow rates, Figure 9.4 presents the test results as constant rates.
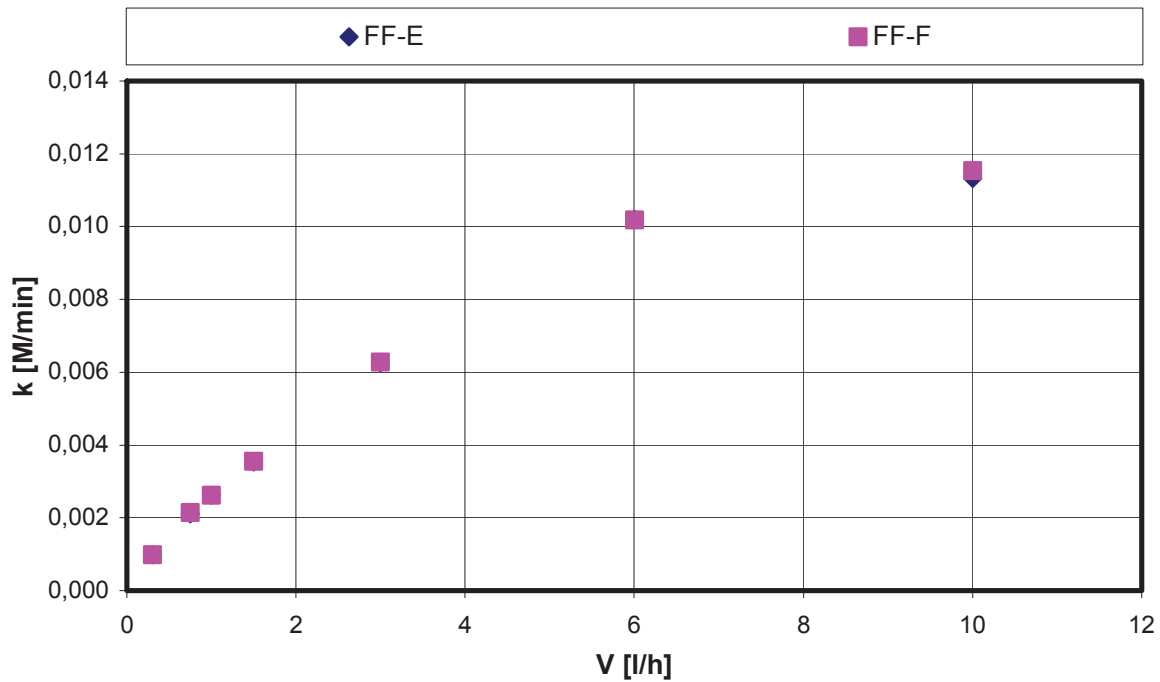
Figure 9.4: Flow rate vs constant rate of Fe(II)-EDTA degradation in the coil reactor. Low-pressure lamp (35 W), λ = 254 nm, V_R = 0,028 l, solution: c_{EDTA} = 1,34 mM, $c_{Fe2SO4*7H2O}$ = 0,67 mM, pH_{start} = 3 ± 0.1, T = 25°C, $\dot{V}_{Air}$ = 20 l/h (STP)

Although at the flow rate of 0,3 l/h Fe(II)-EDTA was degraded in 99% and at 10 l/h in only 35% it did not really describe the real radiation effect. The residence time of the solution in the reactor had to be taken into consider. As Figure 9.4 shows: with a growing flow rate in reactor the constant rate value was also increasing. The maximum was achieved at $\dot{V}$ = 10 l/h and its value was k = 0,011 M/min. At the minimal speed the constant rate was the same as k = 0,001 M/min. Those results could be easily explained with the character of the flow in the reactor. With growing speed of the fluid, the reactor turbulence was higher. Considerable turbulence of the fluid particles enables to radiate more of them, what could not be achieved at a laminar flow.

According to Chapter 8.2, where the photon flow for every flow rate was determined and using Eq. 3.9 the quantum yield of Fe(III)-EDTA could be calculated. The value of the quantum yield varied depending on the flow rate. Up till 1,5 l/h it was smaller than Φ_λ < 0,2. At the maximal flow rate it was equal to Φ_λ = 0,43. Explanation of that fact is the same as the one given to the rate constant differences at various flows. Exact values of the experiments could be found in the annex.

The second experiment with the coil reactor was run as a closed system, where Fe(III)-EDTA solution of volume V = 0,82 l was circulated in the laboratory unit until it was completely degraded. Experimental setup consisted of the mixing tank, in that case the CSTR, from which the solution was pumped into the coil reactor with an immersed lamp and led back into the tank. Samples were drawn just behind the reactor with following time intervals: 0,5; 1; 2;

4; 6; 8; 10; 15; 20; 30 minutes. To achieve maximal turbulence, the highest possible flow rate was chosen, which meant 20 l/h. The pH-value at the beginning of the experiment was equal to 3,05 and at the end had came over to pH = 5. Figure 9.5 represents the degradation run of Fe(III)-EDTA.
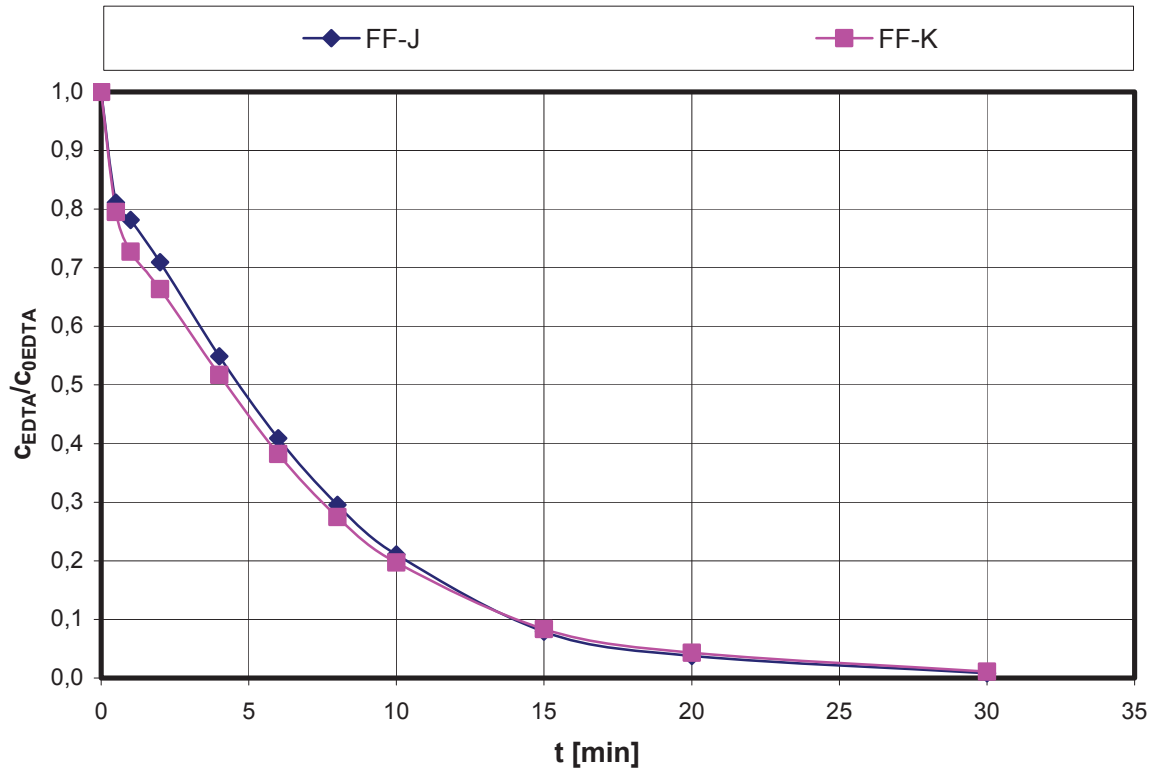
Figure 9.5: Fe(II)-EDTA decomposition in coil reactor as a circulatory system. Low-pressure lamp (35 W), λ = 254 nm, Φ_P = $3*10^{-6}$ einstein/s, V_R = 0,028 l, solution: V_{total} = 0,82 l, c_{EDTA} = 1,34 mM, $c_{Fe2SO4*7H2O}$ = 0,67 mM, pH_{start} = 3,05, T = 25^oC, $\dot{V}$ = 20 l/h, $\dot{V}_{Air}$ = 20 l/h (STP)

The most apparent remark from Figure 9.5 is the abrupt and steep fall of the degradation curve in the first 30 seconds to the value c_{EDTA}/c_{EDTA0} = 0,8. This fact could be explained with sample taking. The first one was taken just as the solution passed through the coil reactor for the first time. The next ones were drawn after the irradiated fluid was mixed in the tank with not yet irradiated solution, which led to a later non-linear degradation of the solution. After 15 minutes less than 90 % of Fe(II)-EDTA was left, after 30 minutes it was completely removed.

9.2.2. Photochemical Fe(II)-EDTA degradation in the small PFR

Experimental setup for degradation of the Fe(II)-EDTA complex in the small PFR was almost the same as the one used in the coil reactor: the prepared outlet solution was kept in the mixing tank T1 from which it was led into the reactor with an immersed lamp at various flow rates and gathered in the storage tank T2. The difference concerned the way of aeration:

in the experiments FF-G and FF-H air bubbles were let direct into the reactor with a flow of 10 l/h (STP) and FF-I was used as a control run, where the aeration with the same flow took place in batch reactor. The point was to investigate if the air bubbles did not absorb too much of the UV-radiation as they covered about 30 % of the reactor surface.

Figure 9.6: Air bubbles in small pipe reactor

Following flow rates were tested in the small PFR: 0,3; 0,75; 1,0; 1,5; 3,0; 6,0; 10,0; 15,0 l/h. The outlet pH-value was equal to pH = 3±0.1 and in series FF-G and FF-H at the end exceeded the value of pH = 5 at the minimal speeds. The temperature was constant and equal to 25 °C. Figure 9.7 displays experimental results presented as constant rates.
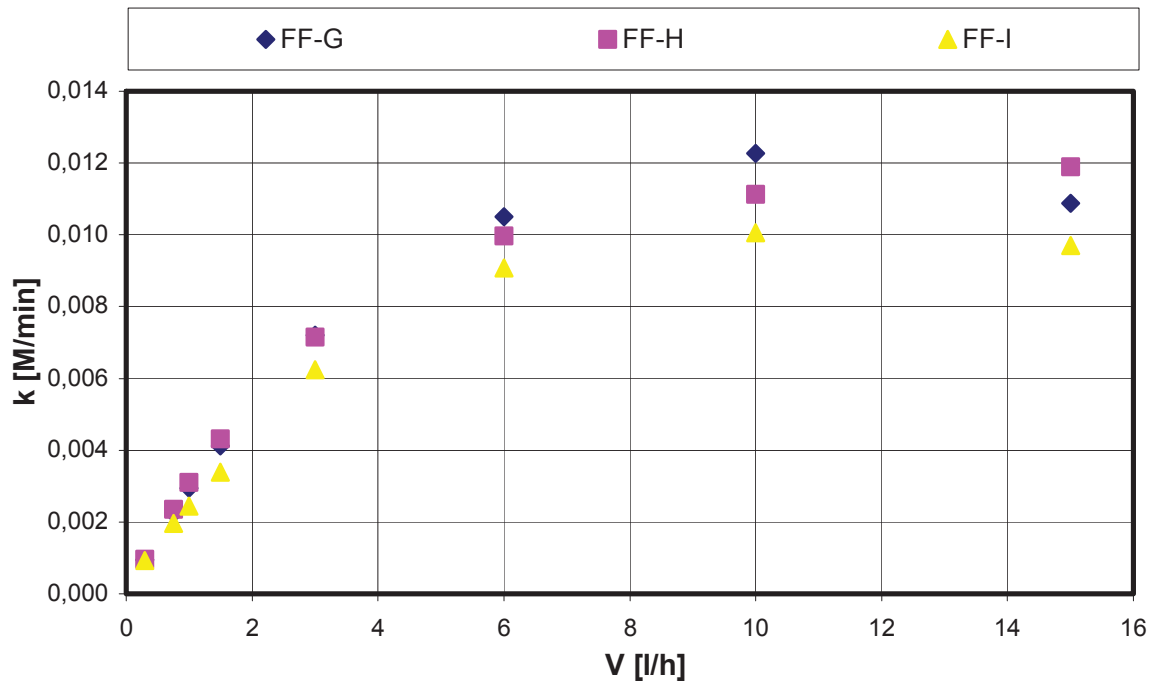
Figure 9.7 Flow rate vs constant rate of Fe(II) EDTA degradation in small PFR. Low-pressure lamp (35 W), λ = 254 nm, $\Phi_{P(\text{value from batch reactor})}$ = 2,29*10^{-6} einstein/s, V_R = 0,113 l, solution: c_{EDTA} = 1,34 mM, $c_{Fe2SO4*7H2O}$ = 0,67 mM, pH_{start} = 3 ± 0,1, T = 25°C, $\dot{V}_{Air}$ = 20 l/h (STP)

Although test series FF-G and FF-H were run in the same laboratory conditions, slight differences between achieved constant rate values could be noticed, especially at higher solution flow rates. With greater turbulence of the fluid in the reactor, particle and air bubbles distribution in the solution were different in every test, which could cause various radiation absorbance. The maximum value of the constant rate was reached in FF-G test at the flow rate of 10 l/h and overstepped a bit 0,012 M/min. At the highest speed it was slightly smaller, equal to k = 0,011 M/min. The constant rate in FF-H run was increasing with the growing flow rate of the solution in the reactor and at 15 l/h had the value of 0,012 M/min. On the contrary to what was expected, the control run FF-I brought worse results than FF-G and FF-H. The constant rate in that case reached the peak in k = 0,01 M/min. Apparently, the aeration directly in the reactor improves the degradation of the Fe(II)-EDTA complex.

As it comes to the quantum yield in the small PTR, the situation was slightly complicated. Using the data obtained through the chemical actinometer measurements done in Chapter 8.2.4, the calculation of the quantum yield in the small PFR gave the value greater than 1, what is technically impossible. The fact was, that the actinometer experiments where done without aeration and the extinction coefficient of iodide was much greater than that of Fe(II)-EDTA, which means, that the pathway of the irradiated solution was much smaller. The conclusion is simple: at the actinometer experiments only boundary layer of d = 0,6 *10^{-4} cm was irradiated, while in Fe(II)-EDTA it was equal to d = 0,17 cm. That means, that in the case of Fe (II)-EDTA degradation much more of the solution particles had to be irradiated. That was the reason to assume the same photon flow in the small PFR

as the one achieved in the batch reactor experiment. In that case it was equal to Φ_P = 2,29*10^{-6} einstein/s. The calculations done with that value, gave a quantum yield of the small PFR, which varied depending on ithe solution flow rate. Up till 1,5 l/h it was smaller or equal than 0,2. At higher flow rates it was situated over Φ_λ > 0,5 in series FF-G and FF-H and in case of F-I Φ_λ < 0,5.

9.2.3. Photochemical Fe(II)-EDTA degradation in the batch reactor

Tests in the batch reactor were run as a closed process, where defined volume of Fe(II)-EDTA solution was mixed and irradiated with UV-radiation until it would be completely degraded. The whole experimental setup consisted of the batch reactor with immersed lamp and a stirrer moving with 300 rpm, a pH electrode, an aeration frit and a sampling outlet attached to the reactor.

The UV-lamp was turned on for few minutes to warm up before starting the experiment and after that 0,82 l of the solution was quickly added into the reactor and the first sample was taken. Next samples were drawn after 3; 6; 10; 15; 20; 30; 45 minutes and in the FF-D run also after 60 minutes. The pH-value was not regulated during the experiment. Its start value was pH = 3 ± 0.1 and after 30 minutes exceeded the limit of 5. The temperature was held constant at T = 25 ^{o}C and the aeration flow rate was the same at 20 l/h (STP).

Figure 9.8 describes the Fe(II)-EDTA decomposition in the batch reactor. FC run shows experiment's results done by Gangl [26] in the same type of a reactor, but with the pH-value of pH = 3 kept all the time at that level.
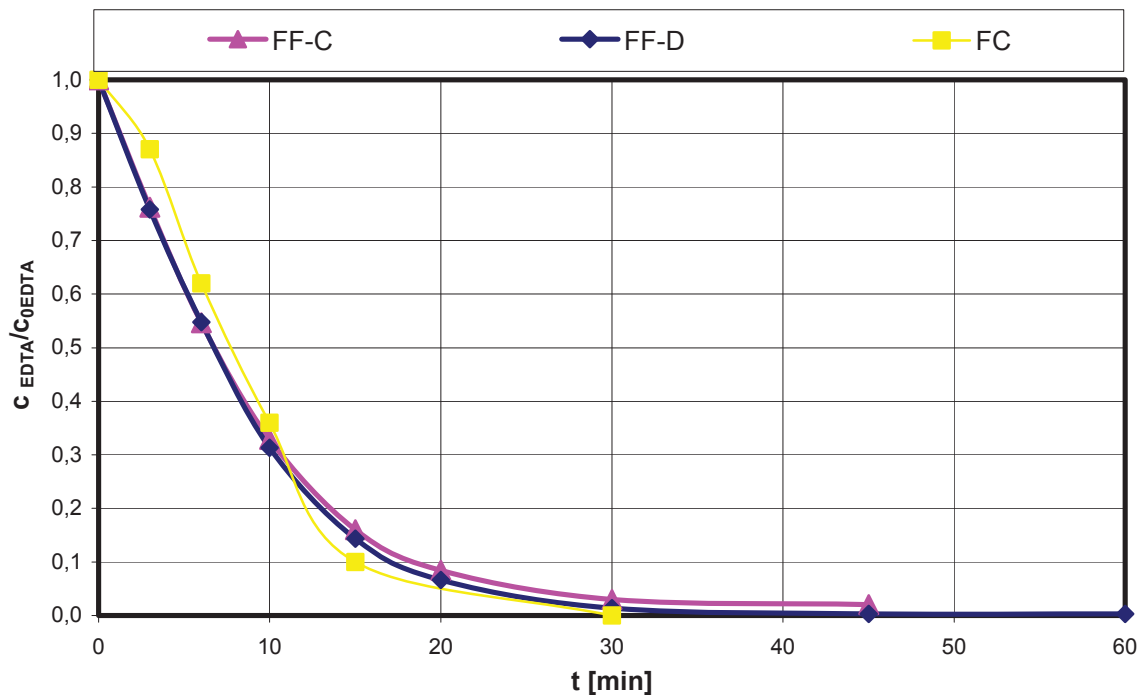
Figure 9.8: Fe(II)EDTA degradation in the batch reactor. Low-pressure lamp (35 W), λ = 254 nm, Φ_P = 2,34*10^{-6} einstein/s, solution: V_{total} = 0,82 l, c_{EDTA} = 1,34 mM, $c_{Fe2SO4*7H2O}$ = 0,67 mM, pH_{start} = 3 ± 0,1, T = 25 ^{o}C, $\dot{V}$ = 20 l/h, $\dot{V}_{Air}$ = 20 l/h (STP), f = 300 rpm

The degradation curves do not differ from each other, only the FC run is slightly steeper and achieved 90 % of FE(III)-EDTA degradation after 15 minutes, while FF-C and FF-D series reached about 85 % at that time. Photochemical reactions are in principle 0. order reactions. First four points of the FF-C and FF-D series created almost a perfectly linear line, the next ones made it more similar to a 1st order reaction run. This fact could be explained with the Fe(III)-ED3A formation as one of the decomposition products, which absorbed part of the UV-radiation, and the photon amount available for Fe(III)-EDTA complex degradation would be smaller. Another possible explanation of that exponential trend of the curve was that 90 % of the irradiation was absorbed within 0,17 cm so the most remote particles, despite mixing, could never be reached. Because of the mentioned reasons only the first values of FF-C and FF-D series were taken into account to define the reaction rate constant. Considering the first four points the reaction rate constant would be equal to k = 0,062 M/min and taking first five points the value would be the same as k = 0,07 M/min. In the experiment done by Gangl the valuation brought the outcome of k = 0,061 M/min.

As it comes to the quantum yield in the batch reactor, its value was decreasing at the time. The maximum, achieved after 3 minutes, was equal to Φ_λ = 0,63 and after 15 minutes was reduced to Φ_λ = 0,45 and after 45 minutes to Φ_λ = 0,17. That situation could be again explained with ED3A formation. Gangl [26] calculated the quantum yield of Fe(III)-EDTA as equal to 0,37.

9.3. EDTA degradation with Anox/H$_2$O$_2$^{Cath}/UV method

In Anox/H$_2$O$_2$^{Cath}/UV investigations the EDTA was degraded through •OH radicals, which came from UV irritated hydrogen peroxide that had been produced on the cathode (see Chatpter 5.4), and also through anodic oxidiation. Two types of the experiment were carried out with different reactors: the CSTR and the large PFR. To prove the reproducibility of the study each test was done twice.

A 0,5 M Na$_2$SO$_4$ and 1,34 mM EDTA solution with a circulation flow rate of 15 l/h was used as the electrolyte. Output current of 0,26 A corresponded to a current density of 27,6 A/m^2 on the anode and 1,7 A/m^2 on the cathode. The solution was aerated with an air flow rate of 20 l/h (STP) and the start pH = 3 ± 0,1.

9.3.1. Anox/H$_2$O$_2$^{Cath}/UV process in the CSTR

In the laboratory tests AOP_4_EzR4 and AOP_5_EzR4 the UV lamp was immersed in the CSTR, from which the solution was pumped into the electrolysis cell and after that again back to the reactor. The CSTR was wrapped in aluminum foil to prevent the surroundings from the UV radiation. A gas frit, a pH electrode and a temperature measurement were fixed in the CSTR.
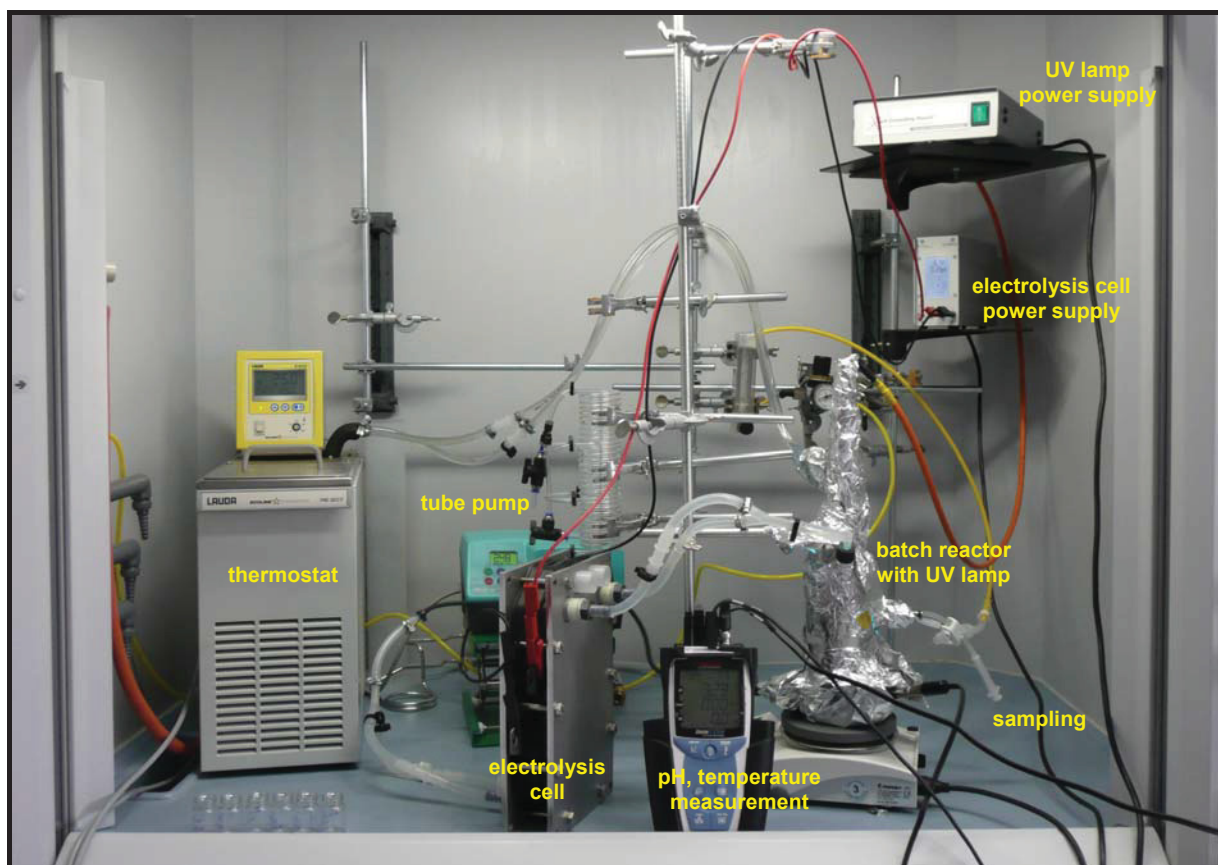
Figure 9.9: Experimental setup in AOP_4_EzR4 and AOP_5_EzR4 tests

Figure 9.10 presents Anox/$H_2O_2^{Cath}$/UV experimental results with comparison to the tests done by Zelenka [22] EUVP-IoxGC_20 at similar laboratory conditions.
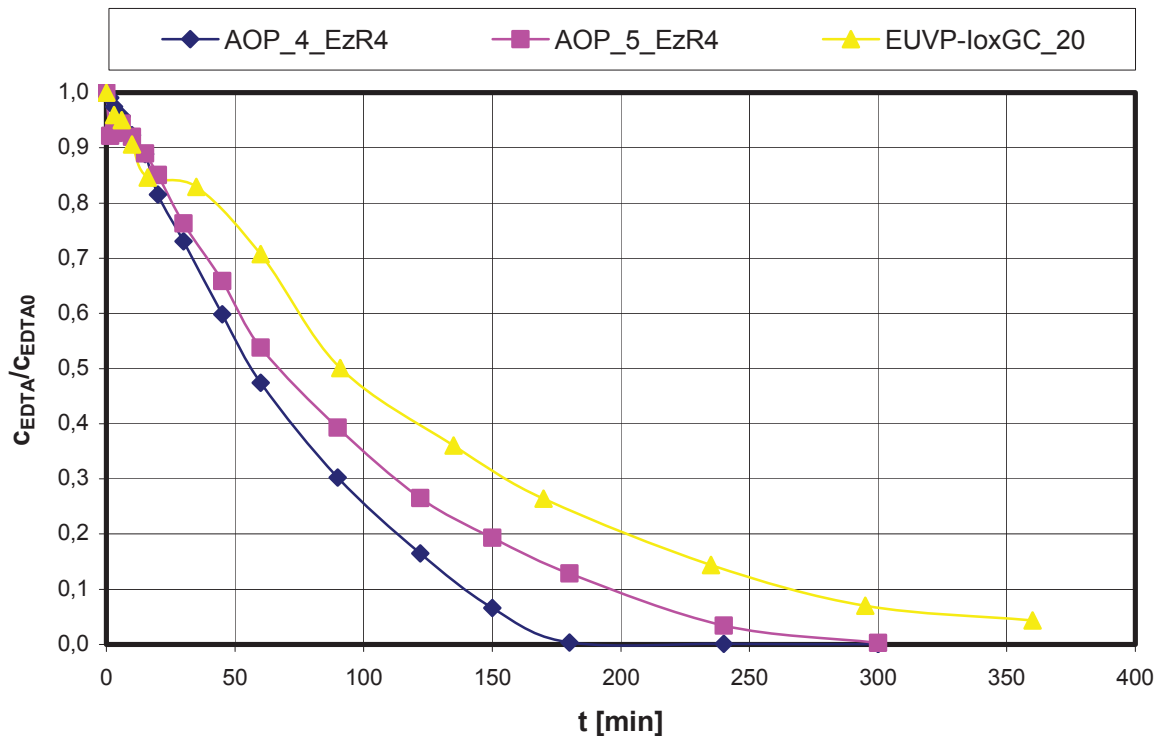
Figure 9.11: Anox/$H_2O_2^{Cath}$/UV tests with the CSTR. EDTA degradation vs time. Low-pressure lamp (35 W), λ = 254 nm, Φ_P = 2,34*10^{-6} einstein/s, Anode: IrO_2 ($A_{specific}$ = 0,096m^2), Cathode: Stainless steel ($A_{specific}$ = 0,096m^2) with glassy carbon filling ($A_{specific}$ = 0,147m^2), I = 0,26 A, j_{anode} = 27,6 A/m^2, Electrolyte solution: c_{Na2SO4} = 0,05 M, c_{EDTA} = 1,34 mM, pH_{start} = 3 ± 0,1, V_{total} = 1,1 l, $\dot{V}$ = 15 l/h, $\dot{V}_{Air}$ = 20 l/h (STP), T = 25 ^{o}C.

Although at the beginning the AOP_5_EzR4 decomposition curve had nearly the same run as the AOP_4_EzR4 one, the complete decomposition of EDTA ended after 300 minutes, while in the second case only 150 minutes were required. In the experiment done by Zelenka after 6 hours c_{EDTA}/c_{EDTA0} = 0,044. In the investigation done by Gangl [26] 180 minutes were necessary for 95 % decomposition of the EDTA. The reaction rate constants calculated according to 1st order reaction run are equal to 0,018 $^-$min in the first experiment and 0,014 $^-$min in the second one.

Differences in the EDTA degradation curves at both experiments could have been caused by various particles distribution in the reactor what meant also unequal irradiation of the particles during both tests. What is more, the pH-value run at both experiments was not identical, which is shown in Figure 9.12.
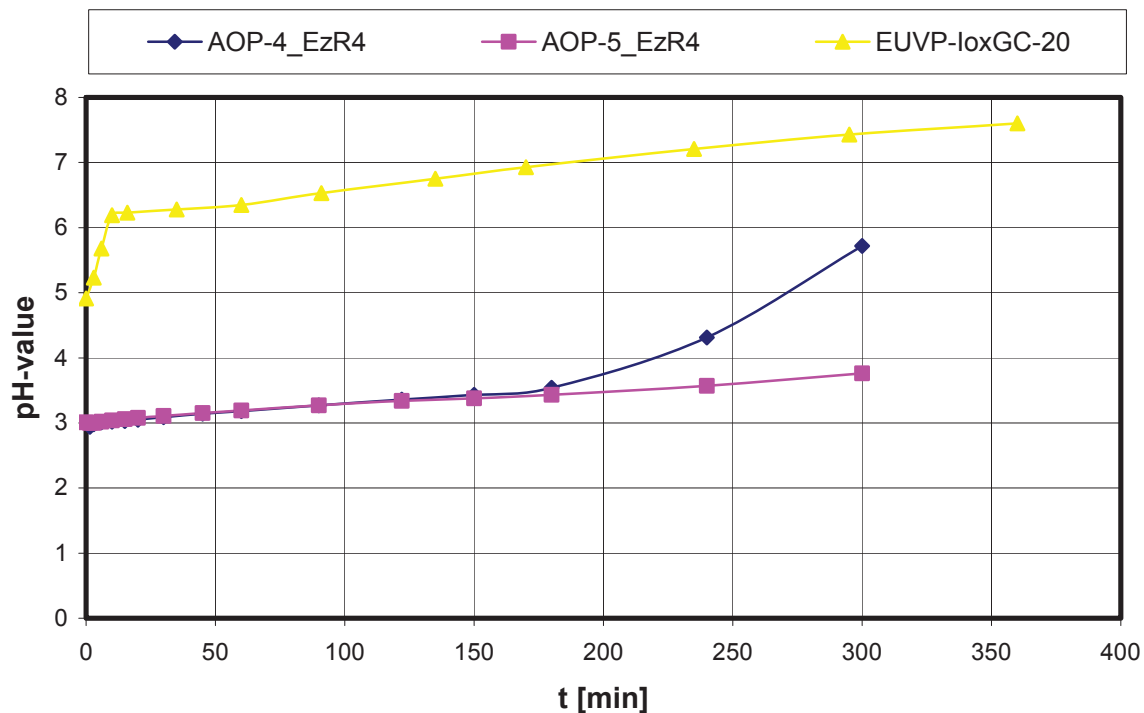
Figure 9.12: pH run in H_2O_2/UV/Anode tests with the CSTR. Low-pressure lamp (35 W), λ = 254 nm, Φ_P = 2,34*10^{-6} einstein/s, Anode: IrO_2 ($A_{specific}$ = 0,096m^2), Cathode: Stainless steel ($A_{specific}$ = 0,096m^2) with glassy carbon filling ($A_{specific}$ = 0,147m^2), I = 0,26 A, j_{anode} = 27,6 A/m^2, Electrolyte solution: c_{Na2SO4} = 0,05 M, c_{EDTA} = 1,34 mM, pH$_{start}$ = 3 ± 0,1, V$_{total}$ = 1,1 l, $\dot{V}$ = 15 l/h, $\dot{V}$ $_{AIr}$ = 20 l/h (STP), T = 25 ^{o}C.

At Figure 9.12 the pH-value run in all three tests is presented. In the AOP_4_EzR4 experiment, after the EDTA was completely degraded, the pH-value had risen to pH = 5,7. In the AOP_5_EzR4 test the pH-value was increasing continuously till pH = 3,76. In case of the experiment done by Zelenka, the start pH was greater, pH = 5, and grew rapidly to pH = 6,2 further run was slightly rising till pH = 7,6.

9.3.2. Anox/$H_2O_2^{Cath}$/UV process in the large PFR

The experimental setup in tests AOP_7 and AOP_8 consisted of a mixing tank from which the solution was pumped into the large PFR with an immersed UV lamp and after that led into the electrolysis cell, from which it returned in the tank. A gas frit was attached in the reactor, a pH and temperature measuring instrument in the tank. The experimental setup scheme is presented at Figure 9.13.
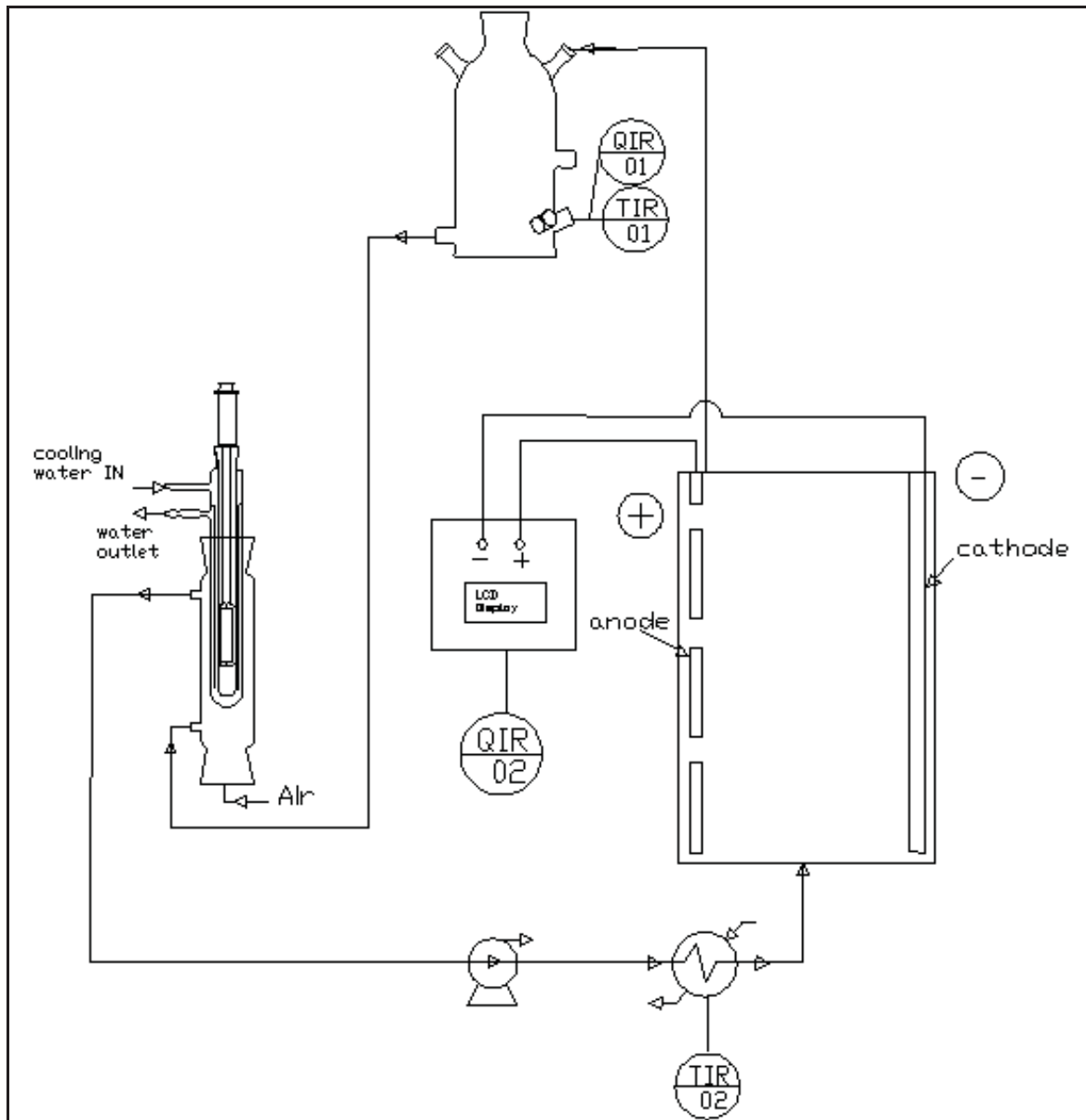
Figure 9.13: Experimental setup in Anox/H$_2$O$_2$^{Cath}/UV test with the large PFR

The experiments were carried out for 5 hours and the achieved EDTA degradation results are presented at Figure 9.14.
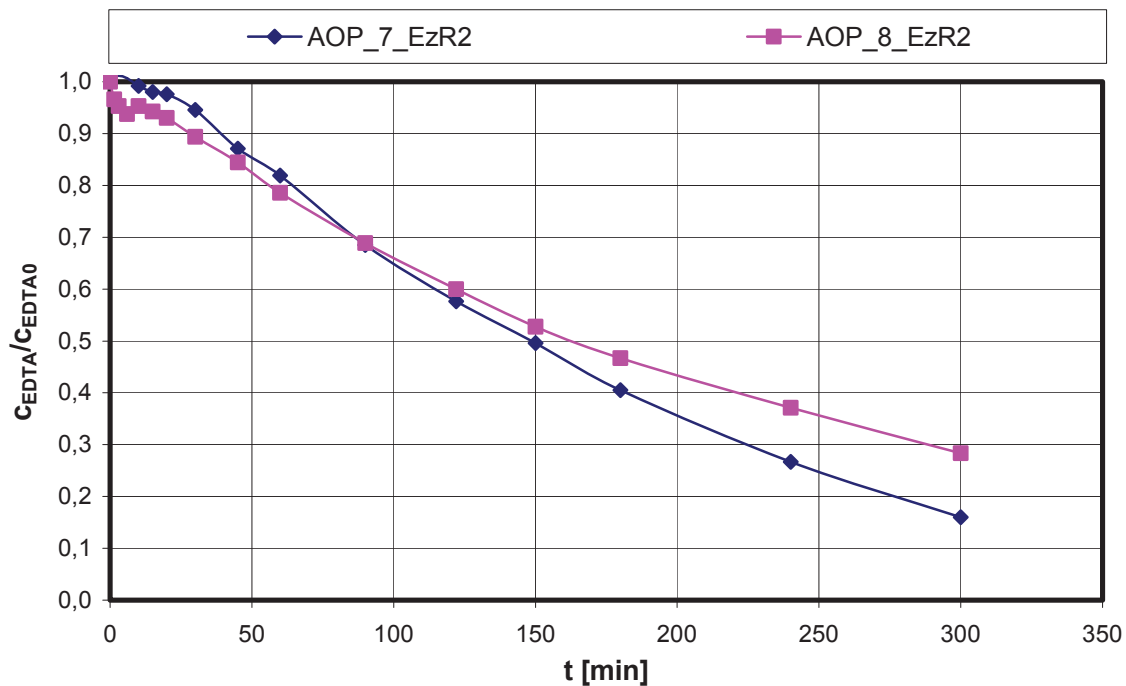
Figure 9.14: Results from Anox/$H_2O_2^{Cath}$/UV tests in the large PFR. Low-pressure lamp (35 W), λ = 254 nm, Φ_P = 4,1*10^{-7} einstein/s, Anode: IrO_2 ($A_{specific}$ = 0,096m^2), Cathode: Stainless steel ($A_{specific}$ = 0,096m^2) with glassy carbon filling ($A_{specific}$ = 0,147m^2), I = 0,26 A, j_{anode} = 27,6 A/m^2, Electrolyte solution: c_{Na2SO4} = 0,05 M, c_{EDTA} = 1,34 mM, pH_{start} = 3 ± 0,1, V_{total} = 1,1 l, $\dot{V}$ = 15 l/h, $\dot{V}_{Air}$ = 20 l/h (STP), T = 25 ^{o}C, 250 rmp.

The EDTA degradation curve in the first experiment had a slightly steeper run than in the second one. In AOP_7_EzR2 test the synthetic water was decomposed in 84 %, in the AOP_8_EzR2 only in 78%. The reaction rate constants calculated according to 1st order reaction run were equal to 0,006 $^-$min in the first experiment and 0,004 $^-$min in the second one.

The possible reason of the differences in the EDTA degradation curve runs were explained in Chapter 9.3.1. The pH-value run at both experiments was also not identical, which presents Figure 9.15.
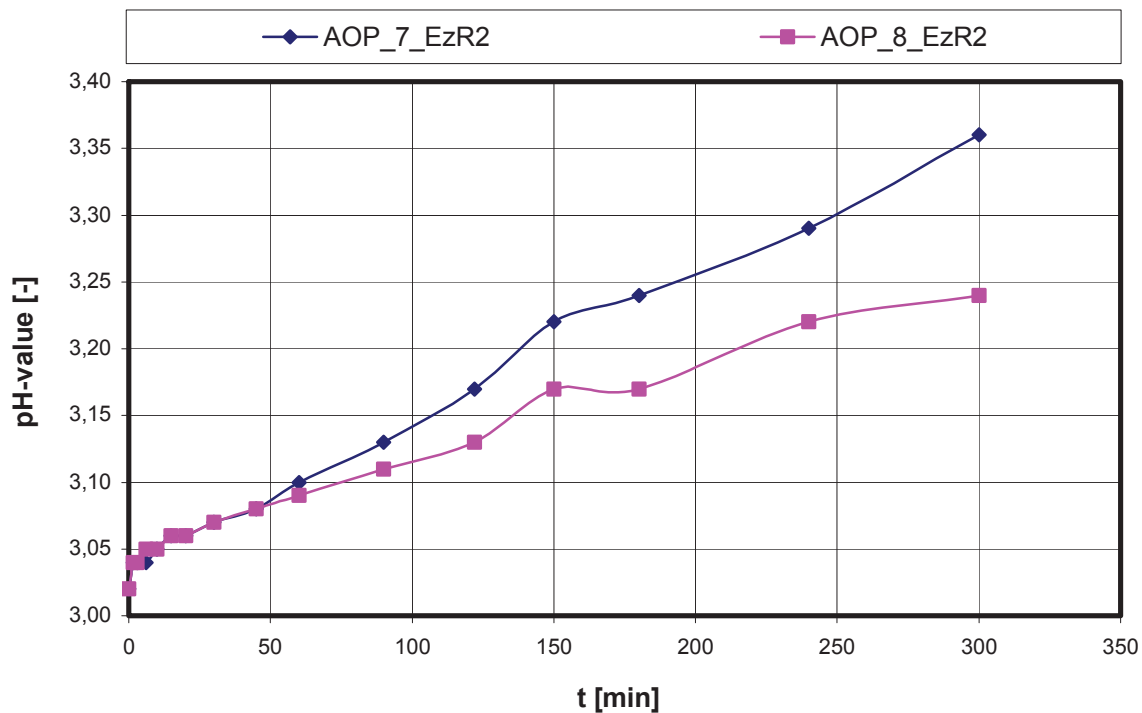
Figure 9.15: pH-value run in Anox/$H_2O_2^{Cath}$/UV tests with the large PFR. Low-pressure lamp (35 W), λ = 254 nm, Φ_P = 4,1*10^{-7} einstein/s, Anode: IrO_2 ($A_{specific}$ = 0,096m^2), Cathode: Stainless steel ($A_{specific}$ = 0,096m^2) with glassy carbon filling ($A_{specific}$ = 0,147m^2), I = 0,26 A, j_{anode} = 27,6 A/m^2, Electrolyte solution: c_{Na2SO4} = 0,05 M, c_{EDTA} = 1,34 mM EDTA, pH$_{start}$ = 3 ± 0,1, V$_{total}$ = 1,1 l, $\dot{V}$ = 15 l/h, $\dot{V}_{Air}$ = 20 l/h (STP), T = 25 ^{o}C.

After 50 minutes the pH-curve of AOP_7_EzR2 test started increasing much faster than that of the AOP_8_EzR2 and at the end reached pH = 3,36. In the second case this value was equal to 3,24. That would be another explanation of various EDTA degradation rates in both experiments: as it was mentioned before (Chapter 1.1 and 9.1), EDTA has 4 dissociation grades, which influence the reaction constant rates.

9.4.   Specific energy demand

To enable the comparison of various AOP techniques and different reactors the specific energy demand was calculated according to Chapter 2.4 and 3.6. In Table 16 the specific energy demands of all investigated EDTA-degradation methods are shown together.

Table 16: Specific energy demand in various reactors at Fe(II)-EDTA degradation.

AOP method		Specific energy demand [kWh g^{-1}]
Direct oxidation		0,0287
Fe(II)-EDTA Photolyse	Coil reactor (10 l/h)	0,0202
	Coil reactor - circulation	0,0548
	Small PFR (10 l/h)	0,0198
	CSTR	0,0454
Anox/H$_2$O$_2$/UV	EC + Large PFR	0,4161
	EC + CSTR	0,3368

The specific energy demand of the anodic oxidation and Anox/H$_2$O$_2$^{Cath}/UV method was calculated for the time span equal to 300 minutes. When it comes to the Fe(II)-EDTA photolysis investigation for the coil reactor experiment the best achieved result was taken into account, what related to the flow rate of 10 l/h. The same flow value was considered in case of the small PFR. The experiment with the coil reactor with circulation flow was treated the same way as a CSTR test with the volume of 0,82 l. The specific energy demand of the CSTR experiment was calculated for 30 minutes and 98 % Fe(II)-EDTA decomposition.

The Fe(II)-EDTA photolysis emerged as the most effective method with regards to the specific energy demand, especially while using the small PFR and the coil reactor. The CSTR process involved a double value of specific energy demand. Even more was necessary in case of the circulation flow in the coil reactor. The specific energy demand value of the direct anodic oxidation remained at a relatively low level, however the low reaction constant rate of EDTA-degradation has to be considered. The Anox/H$_2$O$_2$^{Cath}/UV methods, despite their high rate constants, require a lot of energy effort, which was ten times higher in comparison to other processes. At Figure 9.16 those differences are even more visible.
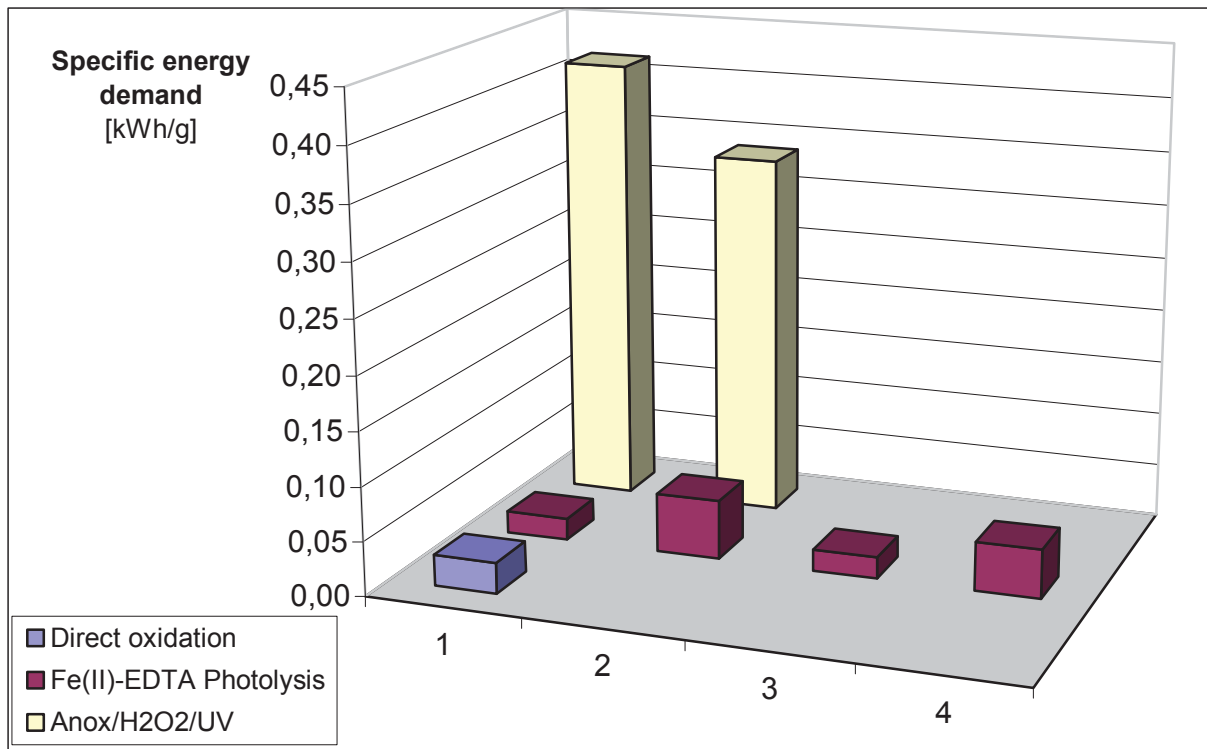
Figure 9.16: The specific energy demand for EDTA-degradation in various AOP methods, where c_{EDTA} = 1,34 mM. X-achse at Fe(II)-EDTA Photolysis: 1 - coil reactor (10 l/h); 2 - Coil reactor – circulation, 3 - small PFR (10 l/h); 4 - CSTR. X-achse at Anox/H_2O_2/UV: 1 – EC + large PFR; 2 – EC + CSTR

10. Summary

The goals of this master thesis were to characterise the bench scale unit built up at VTU Technology laboratory including the comparison of the four different reactor types, as well as various AOPs methods application to find the most efficient instrument for EDTA degradation. In the following chapters, the results of each field of investigation are summarized.

10.1. Bench scale unit characterisation

The characterisation of the bench scale unit consisted of three parts: RTD and effective radiant power description in various reactors and the ability of the hydrogen peroxide generation on the granulate glassy carbon cathode.

10.1.1. Residence time distribution

The RTD investigation in the reactors was done with the application of the step input method and as a mark tracer fluid a coloured solution was used. The RTD was characterised as a change of its concentration in the solution. The content of the coloured medium in the flowing solution was determined with the absorbance value, measured in a spectrophotometer.

According to the results achieved from the investigation, the coil reactor and the CSTR have the closest run to the ideal ones. Although the values of RTD and HRT in both reactors have shown considerable differences at times, their *F(t)* function could be described without doubt as a typical plug flow and CSTR residence time distribution curve. The RTD in case of both PFRs strongly depended on the flow rate, especially in the large reactor. The flow rate of 3 l/h was obviously too low for that laboratory unit as many disruptions were noticed and the *F(t)* function was more alike the CSTR one. The same problem of too low flow rate occurred in the tests with the CSTR. That is why further application of those reactors at such a low flow rate would not be recommended.

Another interesting observation was the existence of two fluid flows in PFRs: the one situated close to the UV lamp cooling coat surface and slower that the second one, set at a distance from the cooling coat (see Figure 8.7).

The electrolysis cell could not have been compared to any of the well-known theoretical reactor models because of its specific construction. The space between the electrode plates was filled with granulate glassy carbon, which restricted the applied flow rate in the *EC Electro MP Cell* to the minimal value of 10 l/h. Otherwise, the fluid would flow only through the anode's tube system.

The entire data concerning the RTD investigation in various reactors with the comparison to their HRT could be found in Table 12.

10.1.2. Radiant power

Photon irradiance measurements in various reactors were done with the use of a chemical actinometer, which in this case was a potassium iodide/iodate solution. The photon irradiance was determined from the concentration of created triiodide. The actinometer experiments were run in all reactor types with various flow rates as a continuous process. The batch reactor was tested in discontinuous conditions with mixing at 250 rpm.

The effective radiant power in the reactors was limited because of the UV lamp cooling coat set-up. From the theoretical value of 10 W guaranteed by the producer, only 2,9 W was recovered in the coil reactor, 3,6 W in the large PRF and 3,75 W in the small PFR. In case of the batch reactor that value was equal to 1,08 W.

The best radiant power efficiency was presented by the coil reactor at flow rates exceeding 5 l/h. The achieved value in those conditions was equal to 1,4 W, which corresponded to nearly 50% of the theoretical value. The radiant power below 5 l/h was relatively low, situated under 1 W, and increasing exponentially with growing speed. That allowed an assumption, that a higher fluid turbulence in the reactor causes better particles irradiation.

In PFRs the radiant power efficiency was much lower. In the large PFR it was oscillating in the range of 0,2 W, independently of the applied flow rate, which corresponded to about 6 % of the theoretical value. In case of the small PFR radiant power reached a value of 0,4 W at its highest flow rates: 15 l/h and 20 l/h, which related to 11 % of the hypothetical values.

The photon irradiance in the batch reactor was measured as a discontinuous process and the concentration of triiodide was increasing as the time elapsed. The experiment was carried out twice with various mixer speeds: 250 and 500 rpm. Higher turbulence of the fluid in the reactor caused better irradiation of the particles in the actinometer solution. The radiant power in the batch reactor at 500 rpm achieved 1,08 W and its efficiency varied between 38-47 % (for details see Chapter 1.1.1).

10.1.3. Cathodic hydrogen peroxide generation

The laboratory tests proved that the best output current to achieve the optimal cathode potential of U_c = -0,5 V would be situated in the range of 0,26...0,29 A, which related to 1,8…2 A/m^2.

The investigation was primarily done at three different current densities: 1,1; 2,2; 4,4 A/m^2 and the flow rate of 10 l/h and the pH-value of 3. The experiments revealed very little cathode ability to hydrogen peroxide production. The obtained values represented less than 10 % recovery of the theoretical calculated values. Further experiments have shown the best efficiency at 2,2 A/m^2, the flow rate at 24 l/h and pH-value of 2 – the hydrogen peroxide increase within 135 minutes was equal to 16,8 mg/l.

The last step of the investigation concerned tests run in the range of 2 ± 0,2 A/m^2 at a flow rate of 24 l/h and a pH-value of 2. The concentration of generated H_2O_2 at that conditions were equal to 20 ± 5 mg/l.

10.2.   AOPs in the EDTA degradation

10.2.1.   Direct anodic oxidation of EDTA

Direct anodic oxidation of the EDTA did not yield the expected results. Basing on the investigation done by Zelenka [22] the chosen current density on the anode was equal to 20 A/m^2 and a pH-value to 5. Those laboratory conditions should assure the best current efficiency. In fact, only about 20 % of EDTA was decomposed after 300 minutes in both carried experiments. The current efficiency, β, in the first experiment AOP_6 brought out the value of 53 % and in case of the second experiment only 37 %. Comparing the results to those achieved by Zelenka in similar laboratory conditions (see Chapter 1.1), a further investigation and optimisation of the anodic oxidation in the *EC Electro MP-Cell* would be recommended.

10.2.2.   Photochemical degradation of Fe(II)-EDTA

Bench scale experiments of the Fe(II)-EDTA photolysis investigated in the coil and the small PFR, and also in the batch reactor yielded very good results with a total Fe(II)-EDTA degradation within 20 minutes. The ratio between Fe(II) and EDTA in the solution was equal to 2:1 and the concentration of the outlet solution consisted of 1,34 mM EDTA and 0,67 mM $Fe_2SO_4*7H_2O$ mixture. All of the experiments had a starting pH-value of 3 ± 0.1 and were aerated with an air flow rate of 20 l/h (STP).

The best results were achieved in the batch reactor, where the rate constant of the Fe(II)-EDTA degradation was situated between 0,062 – 0,07 M/min. The 1,34 mM Fe(II)-EDTA solution was decomposed in 85% within 15 minutes and in 99% within 30 minutes. The experiment with the coil reactor and a circulation flow of the Fe(II)-EDTA solution produced very good effect: at the flow rate of 20 l/h, 90% of Fe(II)-EDTA was degraded within 15 minutes.

The coil reactor and the small PFR had the same rate constant of 0,012 M/min at the flow rate of 10 l/h, however after one flow through the coil reactor the Fe(II)-EDTA was degraded only in 35 %, in the PFR that figure was equal to 65 %. Although the rate constants of the Fe(II)-EDTA decomposition were much lower at smaller flow rates, the degradation grade after one flow through the plug reactor was greater. For example in the coil reactor at flow rate of 3 l/h, the constant rate was equal to 0,006 M/min, but the Fe(II)-EDTA would be degraded in 100%. In the small PFR at the flow rate of 1 l/h 90 % of the Fe(II)-EDTA was decomposed. The choice of the flow rate and the reactor should be considered according to its application in the planned laboratory plant.

The quantum yields, Φ_λ, of the Fe(III)-EDTA photolysis were situated in the range of 0,5. In the coil reactor that value was equal to 0,43 at the flow rate of 10 l/h and in case of the small PFR it exceeded the value of 0,55. The quantum yield measurements in the batch reactor were not as accurate, but the approximate value could be found between 0,45...0,63.

10.2.3.   AEOPs processes

In present work the Anox/$H_2O_2^{Cath}$/UV process was investigated in two combinations: the electrolysis cell was combined with the CSTR or the large PFR. In the *EC Electro MP-Cell the* direct oxidation took place on the anode, while the hydrogen peroxide was generated on the cathode. In the reactors the UV radiation led to the EDTA photolysis or to H_2O_2 irradiation and •OH radicals formation. The combination with the CSTR was much more effective – the total EDTA degradation was achieved after 150 minutes in the first run of the experiment, in the second run at that time a value of 80% EDTA-decomposition was reached. In case of the large PFR after 300 minutes only 70 % of EDTA was degraded in the first run and 82 % in the second one.

To sum up, the investigations performed with the application of various AOPs showed, that the Fe(II)-EDTA photolysis seemed to be the most effective method for EDTA degradation, mainly because of its high extinction coefficient and the ability to absorb UV radiation. The Anox/H_2O_2/UV method with a combination of *EC Electro MP-Cell* and the CSTR with its high reaction rate constant seems to be efficient, however its relatively large specific energy demand has to be taken into account. Direct oxidation on the anode did not yield expected results. Although the specific energy demand in this case is situated in a reasonable range, a very low rate constant of the EDTA-degradation excludes this method from being recommended.

11. Indices

11.1. Abbreviations

Abbreviation	Explanation
AOP	advanced oxidation process
CSTR	continuous stirred-tank reactor
ED3A	ethylenediaminetriacetate
EDTA	ethylene diamine tetraacetic acid
HPLC	high-performance liquid chromatography
HRT	hydraulic residence time
LD50	median lethal dose
MTD	mean time distribution
PFR	plug flow reactor
PVC	polyvinyl chloride
rpm	rotation per minute
RTD	residence time distribution

11.2.   Bibliography

[1]   *European Union Risk Assessment Report. Tetrasodium ethylenediaminetetraacetate (Na$_4$EDTA). CAS No: 64-02-8 EINECS No: 200-573-9 PL-1, 51,* Institute for Health and Consumer Protection. European Chemicals Bureau

[2]   *EU Wasserrahmenrichtlinie 2000/60/EG. Österreichischer Bericht der IST – Bestandsaufnahme.* Anhang – Tabellen, www.lebensministerium.at

[3]   Oppenländer T.: *Photochemical Purification of Water and Air: Advanced Oxidation Processes (AOPs) : Principles, Reaction Mechanisms, Reactor Concepts,* Wiley-VCH, 2003

[4]   Brillas E., Arias C., Cabot P.-L., Centellas F., Garrido J.A., Rodriguez R.M.: *Degradation of Organic Contaminants by Advanced Electrochemical Oxidation Methods*; Portugaliae Electrochimica Acta 24 (2006) 159-189

[5]   Schmidt, V. M.: *Elektrochemische Verfahrenstechnik. Grundlagen, Reaktionstechnik, Prozessoptimierung*; Wiley-VCH GmbH & Co. KGaA, 2003

[6]   Atkins, P.W., Baeran, J.A.: *General chemistry. Second edition, updated version*; Scientific American Books, 1990

[7]   Hibbert, D.B.: *Introduction to electrochemistry*, The Macmillan Press LTD, 1993

[8]   Brett, C.M.A., Brett A. M. O.: *Electrochemistry. Principles, methods and applications*; Oxford University Press, 1993

[9]   Schmidt, A.: *Angewandte Elektrochemie. Grundlagen der elektrolytischen Produktionsverfahren;* Verlag Chemie, 1976

[10]   Bagotsky, V. S.: *Fundamentals of electrochemistry.* Second edition; Wiley-Interscience, 2006

[11]   Atkins, P., de Paul, J. : *Physical chemistry.* Eighth edition; Oxford University Press. 2006

[12]   *Ullmann's Encyclopedia of industrial chemistry;* Sixth, completely revised edition. Volume 11, WILEY-VCH Verlag GmbH&co., 2003, Weinheim

[13]   Ebert, H.: *Elektrochemie. Grundlagen und Anwendungsmoeglichkeiten*; Vogel-Verlag, 1972

[14]   http://www.iupac.org/goldbook/P04633.pdf

[15]   *Ullmann's Encyclopedia of industrial chemistry.* Sixth, completely revised edition. Volume 26; WILEY-VCH Verlag GmbH&co., 2003, Weinheim

[16]   Brillas E., Arias C., Cabot P.-L., Centellas F., Garrido J.A., Rodriguez R.M.: *Degradation of Organic Contaminants by Advanced Electrochemical Oxidation Methods*; Portugaliae Electrochimica Acta 24 (2006) 159-189

[17]   http://en.wikipedia.org/wiki

[18]   http://homepages.ius.edu/DSPURLOC/

[19]   Manahan, S. E.: *Environmental chemistry*; Lewis Publishers, 1994

[20]   Menapace, H., interview on 17.12.2008

[21]   Fryda, M., Matthée, T.: *„Diamantelektroden in der Elektrochemie oder "diamonds are the electrochemist's best friend?!"";* Die Aktuelle Wochenschau der GDCh-Fachgruppe Angewandte Elektrochemie, http://www.aktuelle-wochenschau.de/2006/index06.htm

[22]   Zelenka, J.: *Electrochemical Advanced Oxidation Processes-EAOP Verfahrenstechnische Grundlagen für die Prozessentwicklung*; Dissertation an der TU Graz, 2006

[23]   M. Sörensen M., Zurell S., Frimmel F.H.: *Degradation Pathway of the Photochemical Oxidation of Ethylendiaminetetraacetate (EDTA) in the UV/H_2O_2-process;* Acta hydrochim. hydrobiol. 26 (1998) 2

[24]   Kocot P., Karocki A., Stasicka Z.: *Photochemistry of the Fe(III)-EDTA complexes. A mechanistic study.;* Journal of Photochemistry and Photobiology A: Chemistry 179 (2006) 176-183

[25]   Andreozzi, R., Caprio, V., Insola, A., Marotta, R.: *Advanced oxidation processes (AOP) for water purification and recovery;* Catalysis Today 53 (1999), p 51-59

[26]   Gangl, W.: *Advanced Oxidation Processes (AOPs/AEOPs); Grundlagen, Verfahrensvergleich und -entwicklung am Beispiel des Komplexbildners Ethylendiamintetraacetat (EDTA);* Dissertation an der TU Graz, 2006

[27]   Levenspiel, O.: *Chemical reaction engineering*; Wiley, 1999

[28]   Siebenhofer, M.: *Einfluss der Verweilzeitverteilung (VZV oder RTD) auf die Reaktorleistung (den Umsatz);* Vorlesungsskriptum, TU Graz, 2007

[29]   Hagen, J.: *Chemische Reaktionstechnik. Eine Einfuhrung mit Ubungen*; VCH Verlagsgesellschaft mbH, 1993

[30]   Rahn, R. O.: *Potassium Iodide as a Chemical Actinometer for 254 nm Radiation: Use of Iodate as an Electron Scavanger*; Photochemistry and Photobiology, 1997 66(4): 450-455

[31]   Zhimin Qiang, Jih-Hsing Chang, Chin-Pao Huang: *Electrochemical generation of hydrogen peroxide from dissolved oxygen in acidic solutions;* Water research 36(2002) 85-94, www.elsevier.com/locate/watres

[32]   Kellner, R. [Hrsg.]: *Analytical chemistry;* Wiley-VCH, 1998

[33]   http://www.thermo.com/com/cda/product/detail/0,1055,10121790,00.html

[34]   http://www.cienytec.com/PDFS/Espec_VisionLite_opman.pdf

[35]   Dane, E., Willie, Wille, F. Laatsch, H.: *Kleines chemisches Praktikum,* 10.Auflage; Wiley-VHC Verlag GmbH, 2004

[36]   Christian, G. D., *Analytical chemistry*; Wiley-VHC Verlag GmbH; 2004

[37]   http://www.heraeus-noblelight.com/

[38]   http://www.uv-consulting.de/

[39]   http://www.electrocell.co/

[40]   http://www.htw-germany.com/

[41]   http://www.bolz-electronic.de/download/TG30-2.pdf

[42]   http://www.watson-marlow.com/pdfs-global/wd-323esudud-uk-03.pdf

[43]   http://www.thermo.com/eThermo/CMA/PDFs/Product/productPDF_7652.pdf

[44]   http://lauda.de/

[45]   http://www.brinkmann.com/products/stirrer_HotPlate_de.asp

11.3.   Tables

11.4.   Figures

12. Annexure

Appendix 1 – Actinometer measurement

Table 17: Actinometer solution characteristic during tests in the large PFR. Experimental runs: AKT-F, AKT-G, AKT-H, AKT-I, AKT-J.

Reactor type: **Large PFR**

Actinometer solution characteristic:

	c_{req}	M	m_{req}	m_{eff}	c_{eff}
	[mol/l]	[g/mol]	[g]	[g]	[g/mol]
KI	0,4	166,01	265,60	265,6	0,60
KIO_3	0,10	214,00	85,606	85,61	0,10
Borat	0,01	381,37	8,049	8,05	0,01
H_2O	-	-	4000	4000	-

Table 18: Chemical actinometer measurement data and its evaluation in the large PFR test run: AKT-F

Experimental run: **AKT-F**

λ	$\Phi=f(T,c)$	$P_{theor.}$	$\dot{V}$	pH_{in}	pH_{out}	T
[nm]	[-]	[W]	[l/h]	[-]	[-]	[°C]
254	0,781	3,6	3	9,22	9,27	25

Sample	Time	Abs_{352nm}	Delution 1:x	$c_{Triiodid}$	$\Delta c_{Triiodid}$	$\dot{V}_{BR}$	Φ_P	$P_{eff.}$
[Nr]	[min:sec]	[-]	[-]	[mol/l]	[mol/l]	[mol/h]	[einstein/s]	[W]
AKT-F-00		0,003	1	1,095E-07				
AKT-F-01	00:00	0,943	10	3,442E-04	3,441E-04	0,0010	3,669E-07	0,17
AKT-F-02	07:30	0,507	10	1,850E-04	1,849E-04	0,0006	1,972E-07	0,09
AKT-F-03	15:00	0,793	10	2,894E-04	2,893E-04	0,0009	3,086E-07	0,15
AKT-F-04	22:30	0,85	10	3,102E-04	3,101E-04	0,0009	3,307E-07	0,16

Mean value **0,16**

0,14

Table 19: Chemical actinometer measurement data and its evaluation in the large PFR. Experimental run: AKT-G

Experimental run: AKT-G

λ	Φ=f(T,c)	$P_{theor.}$	$\dot{V}$	pH_{in}	pH_{out}	T
[nm]	[-]	[W]	[l/h]	[-]	[-]	[°C]
254	0,781	3,6	6	9,26	9,28	25

Sample	Time	Abs_{352nm}	Delution 1:x	$c_{Triiodid}$	$\Delta c_{Triiodid}$	$\dot{V}_{BR}$	Φ_P	$P_{eff.}$
[Nr]	[min:sec]	[-]	[-]	[mol/l]	[mol/l]	[mol/h]	[einstein/s]	[W]
AKT-G-00		0,317	10	1,157E-04				
AKT-G-01	0	0,807	10	2,945E-04	1,788E-04	0,0011	3,815E-07	0,18
AKT-G-02	03:45	1,056	10	3,854E-04	2,697E-04	0,0016	5,753E-07	0,27
AKT-G-03	07:30	0,772	10	2,818E-04	1,661E-04	0,0010	3,542E-07	0,17
AKT-G-04	11:15	0,806	10	2,942E-04	1,785E-04	0,0011	3,807E-07	0,18
							Mean value	**0,1753**
								0,1992

Table 20: Chemical actinometer measurement data and its evaluation in the large PFR. Experimental run: AKT-H

Experimental run: AKT-H

λ	Φ=f(T,c)	$P_{theor.}$	$\dot{V}$	pH_{in}	pH_{out}	T
[nm]	[-]	[W]	[l/h]	[-]	[-]	[°C]
254	0,781	3,6	10	9,28	9,30	25

Sample	Time	Abs_{352nm}	Delution 1:x	$c_{Triiodid}$	$\Delta c_{Triiodid}$	$\dot{V}_{BR}$	Φ_P	$P_{eff.}$
[Nr]	[min:sec]	[-]	[-]	[mol/l]	[mol/l]	[mol/h]	[einstein/s]	[W]
AKT-H-00		0,714	10	2,606E-04				
AKT-H-01	0	1,618	10	5,905E-04	3,299E-04	0,0033	1,173E-06	0,55
AKT-H-02	02:15	1,046	10	3,818E-04	1,212E-04	0,0012	4,308E-07	0,20
AKT-H-03	04:30	1,014	10	3,701E-04	1,095E-04	0,0011	3,893E-07	0,18
AKT-H-04	06:45	1,072	10	3,912E-04	1,307E-04	0,0013	4,645E-07	0,22
							Mean value	**0,20**
								0,29

Table 21: Chemical actinometer measurement data and its evaluation in the large PFR test run: AKT-I

Experimental run: AKT-I

λ	Φ=f(T,c)	$P_{theor.}$	$\dot{V}$	pH_{in}	pH_{out}	T
[nm]	[-]	[W]	[l/h]	[-]	[-]	[^{o}C]
254	0,781	3,6	15	9,29	9,30	25

Sample	Time	Abs_{352nm}	Delution 1:x	$c_{Triiodid}$	$\Delta c_{Triiodid}$	$\dot{V}_{BR}$	Φ_P	$P_{eff.}$
[Nr]	[min:sec]	[-]	[-]	[mol/l]	[mol/l]	[mol/h]	[einstein/s]	[W]
AKT-I-00		0,970	10	3,540E-04				
AKT-I-01	0	1,205	10	4,398E-04	8,577E-05	0,0013	4,574E-07	0,22
AKT-I-02	01:30	1,204	10	4,394E-04	8,540E-05	0,0013	4,554E-07	0,21
AKT-I-03	03:00	1,178	10	4,299E-04	7,591E-05	0,0011	4,048E-07	0,19
AKT-I-04	04:30	1,172	10	4,277E-04	7,372E-05	0,0011	3,931E-07	0,19

Mean value   **0,20**

Table 22: Chemical actinometer measurement data and its evaluation in the large PFR test run: AKT-J

Experimental run: AKT-J

λ	Φ=f(T,c)	$P_{theor.}$	$\dot{V}$	pH_{in}	pH_{out}	T
[nm]	[-]	[W]	[l/h]	[-]	[-]	[^{o}C]
254	0,781	3,6	20	9,39	-	25

Sample	Time	Abs_{352nm}	Delution 1:x	$c_{Triiodid}$	$\Delta c_{Triiodid}$	$\dot{V}_{BR}$	Φ_P	$P_{eff.}$
[Nr]	[min:sec]	[-]	[-]	[mol/l]	[mol/l]	[mol/h]	[einstein/s]	[W]
AKT-J-00		1,161	10	4,237E-04				
AKT-J-01	0	1,352	10	4,934E-04	6,971E-05	0,0014	4,956E-07	0,23
AKT-J-02	01:10	1,343	10	4,901E-04	6,642E-05	0,0013	4,723E-07	0,22
AKT-J-03	02:20	1,325	10	4,836E-04	5,985E-05	0,0012	4,256E-07	0,20
AKT-J-04	03:30	1,341	10	4,894E-04	6,569E-05	0,0013	4,671E-07	0,22

Mean value   **0,22**

Table 23: Actinometer solution characteristic during tests in the small PFR. Experimental runs: AKT-K, AKT-L, AKT-M, AKT-N, AKT-O

Reactor type: **Small PFR**

Actinometer solution characteristic

	c_{req}	M	m_{req}	m_{eff}	c_{eff}
	[mol/l]	[g/mol]	[g]	[g]	[g/mol]
KI	0,4	166,01	199,212	199,19	0,40
KIO_3	0,10	214,00	64,240	64,20	0,10
Borat	0,01	381,37	6,040	6,06	0,01
H_2O	-	-	3000	3000	-

Table 24: Chemical actinometer measurement data and its evaluation in the small PFR. Experimental run: AKT-K

Experimental run: **AKT-K**

λ	$\Phi=f(T,c)$	$P_{theor.}$	$\dot{V}$	pH_{in}	pH_{out}	T
[nm]	[-]	[W]	[l/h]	[-]	[-]	[^{o}C]
254	0,781	3,75	3	9,22	9,27	25

Sample	Time	Abs_{352nm}	Delution 1:x	$c_{Triiodid}$	$\Delta c_{Triiodid}$	$\dot{V}_{BR}$	Φ_P	$P_{eff.}$
[Nr]	[s]	[-]	[-]	[mol/l]	[mol/l]	[mol/h]	[einstein/s]	[W]
AKT-K-00		0,001	1	3,650E-08				
AKT-K-01	0	1,225	10	4,471E-04	4,470E-04	0,0013	4,768E-07	0,22
AKT-K-02	150	1,262	10	4,606E-04	4,605E-04	0,0014	4,912E-07	0,23
AKT-K-03	300	1,251	10	4,566E-04	4,565E-04	0,0014	4,869E-07	0,23
AKT-K-04	450	1,262	10	4,606E-04	4,605E-04	0,0014	4,912E-07	0,23

Mean value   **0,23**

Table 25: Chemical actinometer measurement data and its evaluation in the small PFR.
Experimental run: AKT-L

Experimental run: **AKT-L**

λ	Φ=f(T,c)	$P_{theor.}$	$\dot{V}$	pH_{in}	pH_{out}	T
[nm]	[-]	[W]	[l/h]	[-]	[-]	[^{o}C]
254	0,781	3,75	6	9,22	9,27	25

Sample	Time	Abs_{352nm}	Delution 1:x	$c_{Triiodid}$	$\Delta c_{Triiodid}$	$\dot{V}_{BR}$	Φ_P	$P_{eff.}$
[Nr]	[s]	[-]	[-]	[mol/l]	[mol/l]	[mol/h]	[einstein/s]	[W]
AKT-L-00		0,005	10	1,825E-06				
AKT-L-01	0	0,844	10	3,080E-04	3,062E-04	0,0018	6,532E-07	0,31
AKT-L-02	90	0,808	10	2,949E-04	2,931E-04	0,0018	6,251E-07	0,29
AKT-L-03	180	1,235	10	4,507E-04	4,489E-04	0,0027	9,576E-07	0,45
AKT-L-04	270	0,826	10	3,015E-04	2,996E-04	0,0018	6,392E-07	0,30

Mean value   **0,30**

0,33

Table 26: Chemical actinometer measurement data and its evaluation in the small PFR. Test
run: AKT-M

Experimental run: **AKT-M**

λ	Φ=f(T,c)	$P_{theor.}$	$\dot{V}$	pH_{in}	pH_{out}	T
[nm]	[-]	[W]	[l/h]	[-]	[-]	[^{o}C]
254	0,781	3,75	6	9,22	9,27	25

Sample	Time	Abs_{352nm}	Delution 1:x	$c_{Triiodid}$	$\Delta c_{Triiodid}$	$\dot{V}_{BR}$	Φ_P	$P_{eff.}$
[Nr]	[s]	[-]	[-]	[mol/l]	[mol/l]	[mol/h]	[einstein/s]	[W]
AKT-M-00		0,692	10	2,526E-04				
AKT-M-01	0	1,187	10	4,332E-04	1,807E-04	0,0018	6,423E-07	0,30
AKT-M-02	60	1,275	10	4,653E-04	2,128E-04	0,0021	7,564E-07	0,36
AKT-M-03	120	1,274	10	4,650E-04	2,124E-04	0,0021	7,551E-07	0,36
AKT-M-04	180	1,226	10	4,474E-04	1,949E-04	0,0019	6,929E-07	0,33

Mean value   **0,34**

Table 27: Chemical actinometer measurement data and its evaluation in the small PFR.
Experimental run: AKT-N

Experimental run: AKT-N

λ	Φ=f(T,c)	$P_{theor.}$	$\dot{V}$	pH_{in}	pH_{out}	T
[nm]	[-]	[W]	[l/h]	[-]	[-]	[°C]
254	0,781	3,75	15	9,22	9,27	25

Sample	Time	Abs_{352nm}	Delution 1:x	$c_{Triiodid}$	$\Delta c_{Triiodid}$	$\dot{V}_{BR}$	Φ_P	$P_{eff.}$
[Nr]	[s]	[-]	[-]	[mol/l]	[mol/l]	[mol/h]	[einstein/s]	[W]
AKT-N-00		0,942	10	3,438E-04				
AKT-N-01	0	1,381	10	5,040E-04	1,602E-04	0,0024	8,544E-07	0,40
AKT-N-02	90	1,412	10	5,153E-04	1,715E-04	0,0026	9,147E-07	0,43
AKT-N-03	180	1,352	10	4,934E-04	1,496E-04	0,0022	7,980E-07	0,38
AKT-N-04	270	1,387	10	5,062E-04	1,624E-04	0,0024	8,661E-07	0,41

Mean value   **0,40**

Table 28: Chemical actinometer measurement data and its evaluation in the small PFR.
Experimental run: AKT-O

Experimental run: AKT-O

λ	Φ=f(T,c)	$P_{theor.}$	$\dot{V}$	pH_{in}	pH_{out}	T
[nm]	[-]	[W]	[l/h]	[-]	[-]	[°C]
254	0,781	3,75	20	9,22	9,27	25

Sample	Time	Abs_{352nm}	Delution 1:x	$c_{Triiodid}$	$\Delta c_{Triiodid}$	$\dot{V}_{BR}$	Φ_P	$P_{eff.}$
[Nr]	[s]	[-]	[-]	[mol/l]	[mol/l]	[mol/h]	[einstein/s]	[W]
AKT-O-00		1,237	10	4,515E-04				
AKT-O-01	0	1,551	10	5,661E-04	1,146E-04	0,0023	8,148E-07	0,38
AKT-O-02	30	1,591	10	5,807E-04	1,292E-04	0,0026	9,186E-07	0,43
AKT-O-03	60	1,564	10	5,708E-04	1,193E-04	0,0024	8,486E-07	0,40
AKT-O-04	90	1,602	10	5,847E-04	1,332E-04	0,0027	9,472E-07	0,45

8,82E-07   **0,42**

Table 29: Actinometer solution characteristic during tests in the coil reactor. Experimental runs: AKT-T, AKT-U AKT-W AKT-Z.

Reactor type: **Coil reactor**

Actinometer solution characteristic

	c_{req}	M	m_{req}	m_{eff}	c_{eff}
	[mol/l]	[g/mol]	[g]	[g]	[g/mol]
KI	0,60	166,01	298,82	298,7	0,60
KIO_3	0,10	214,00	64,20	64,21	0,10
Borat	0,01	381,37	11,44	11,44	0,01
H_2O	-	-	3000	3000	-

Table 30: Chemical actinometer measurement data and its evaluation in the coil reactor. Experimental run: AKT-T

Experimental run: AKT-T

λ	$\Phi=f(T,c)$	$P_{theor.}$	$\dot{V}$	pH_{in}	pH_{out}	T
[nm]	[-]	[W]	[l/h]	[-]	[-]	[°C]
254	0,815	2,9	0,3	9,04	10,50	25

Sample	Time	Abs_{352nm}	Delution 1:x	$c_{Triiodid}$	$\Delta c_{Triiodid}$	$\dot{V}$	Φ_P	$P_{eff.}$
[Nr]	[min]	[-]	[-]	[mol/l]	[mol/l]	[mol/h]	[einstein/s]	[W]
AKT-T-00		0,003	1	1,095E-07				
AKT-T-01	0	1,223	125	5,579E-03	5,579E-03	0,0017	5,705E-07	0,27
AKT-T-02	10	1,224	125	5,584E-03	5,584E-03	0,0017	5,709E-07	0,27
AKT-T-03	20	1,269	125	5,789E-03	5,789E-03	0,0017	5,919E-07	0,28

Mean value **0,27**

Table 31: Chemical actinometer measurement data and its evaluation in the coil reactor, test run: AKT-U

Experimental run: **AKT-U**

λ	Φ=f(T,c)	$P_{theor.}$	$\dot{V}$	pH_{in}	pH_{out}	T
[nm]	[-]	[W]	[l/h]	[-]	[-]	[°C]
254	0,815	2,9	0,75	9,04	10,50	25

Sample	Time	Abs_{352nm}	Delution 1:x	$c_{Triiodid}$	$\Delta c_{Triiodid}$	$\dot{V}$	Φ_P	$P_{eff.}$
[Nr]	[min]	[-]	[-]	[mol/l]	[mol/l]	[mol/h]	[einstein/s]	[W]
AKT-U-00		0,000	1	0,000E+00				
AKT-U-01	0	1,055	125	4,813E-03	4,813E-03	0,0036	1,230E-06	0,58
AKT-U-02	5	1,113	125	5,078E-03	5,078E-03	0,0038	1,298E-06	0,61
AKT-U-03	10	1,155	125	5,269E-03	5,269E-03	0,0040	1,347E-06	0,63

Mean value **0,61**

Table 32: Chemical actinometer measurement data and its evaluation in the coil reactor, test run: AKT-W

Experimental run: **AKT-W**

λ	Φ=f(T,c)	$P_{theor.}$	$\dot{V}$	pH_{in}	pH_{out}	T
[nm]	[-]	[W]	[l/h]	[-]	[-]	[°C]
254	0,815	2,9	1,0	9,04	10,40	25

Sample	Time	Abs_{352nm}	Delution 1:x	$c_{Triiodid}$	$\Delta c_{Triiodid}$	$\dot{V}$	Φ_P	$P_{eff.}$
[Nr]	[min]	[-]	[-]	[mol/l]	[mol/l]	[mol/h]	[einstein/s]	[W]
AKT-W-00		0,000	1	0,000E+00				
AKT-W-01	0	1,268	125	5,785E-03	5,785E-03	0,0058	1,972E-06	0,93
AKT-W-02	3	1,241	125	5,661E-03	5,661E-03	0,0057	1,930E-06	0,91
AKT-W-03	6	1,261	125	5,753E-03	5,753E-03	0,0058	1,961E-06	0,92

1,95E-06   **0,92**

Table 33: Chemical actinometer measurement data and its evaluation in the coil reactor test run: AKT-Z

Experimental run: AKT-Z

λ	Φ=f(T,c)	$P_{theor.}$	$\dot{V}$	pH_{in}	pH_{out}	T
[nm]	[-]	[W]	[l/h]	[-]	[-]	[°C]
254	0,815	2,9	1,5	9,04	10,13	25

Sample	Time	Abs_{352nm}	Delution 1:x	$c_{Triiodid}$	$\Delta c_{Triiodid}$	$\dot{V}$	Φ_P	$P_{eff.}$
[Nr]	[min]	[-]	[-]	[mol/l]	[mol/l]	[mol/h]	[einstein/s]	[W]
AKT-Z-00		0,000	1	0,000E+00				
AKT-Z-01	0	0,867	150	4,746E-03	4,746E-03	0,0071	2,427E-06	1,14
AKT-Z-02	2	0,868	150	4,752E-03	4,752E-03	0,0071	2,429E-06	1,14
AKT-Z-03	4	0,859	150	4,703E-03	4,703E-03	0,0071	2,404E-06	1,13

Mean value   **1,14**

Table 34: Actinometer solution characteristic during tests in the coil reactor. Experimental runs: AKT-A, AKT-B, AKT-C, AKT-D, AKT-E.

Reactor type: **Coil reactor**

Actinometer solution characteristic

	c_{req}	M	m_{req}	m_{eff}	c_{eff}
	[mol/l]	[g/mol]	[g]	[g]	[g/mol]
KI	0,60	166,01	298,82	298,7	0,60
KIO_3	0,10	214,00	64,20	64,20	0,10
Borat	0,01	381,37	11,44	11,44	0,01
H_2O	-	-	3000	3000	-

Table 35: Chemical actinometer measurement data and its evaluation in the coil reactor, test run: AKT-A

Experimental run: **AKT-A**

λ	$\Phi=f(T,c)$	$P_{theor.}$	$\dot{V}$	pH_{in}	pH_{out}	T
[nm]	[-]	[W]	[l/h]	[-]	[-]	[^{o}C]
254	0,815	2,9	3	9,26	9,3	25

Sample	Time	Abs_{352nm}	Delution 1:x	$c_{Triiodid}$	$\Delta c_{Triiodid}$	$\dot{V}$	Φ_P	$P_{eff.}$
[Nr]	[s]	[-]	[-]	[mol/l]	[mol/l]	[mol/h]	[einstein/s]	[W]
AKT-A-00		0,007	1	2,555E-07				
AKT-A-01	0	1,408	50	2,569E-03	2,569E-03	0,0077	2,628E-06	1,24
AKT-A-02	30	1,544	50	2,818E-03	2,817E-03	0,0085	2,882E-06	1,36
AKT-A-03	60	1,390	50	2,536E-03	2,536E-03	0,0076	2,595E-06	1,22
AKT-A-04	90	1,415	50	2,582E-03	2,582E-03	0,0077	2,642E-06	1,24
AKT-A-05	120	1,493	50	2,724E-03	2,724E-03	0,0082	2,787E-06	1,31

Mean value   **1,25**

1,27

Table 36: Chemical actinometer measurement data and its evaluation in the coil reactor, test run: AKT-B

Experimental run: AKT-B

λ	Φ=f(T,c)	$P_{theor.}$	$\dot{V}$	pH_{in}	pH_{out}	T
[nm]	[-]	[W]	[l/h]	[-]	[-]	[^{o}C]
254	0,815	2,9	6	9,26	9,3	25

Sample	Time	Abs_{352nm}	Delution 1:x	$c_{Triiodid}$	$\Delta c_{Triiodid}$	$\dot{V}$	Φ_P	$P_{eff.}$
[Nr]	[s]	[-]	[-]	[mol/l]	[mol/l]	[mol/h]	[einstein/s]	[W]
AKT-00-00		0,007	1	2,555E-07				
AKT-B-00	0	0,731	50	1,334E-03	1,334E-03	0,0080	2,729E-06	1,29
AKT-B-01	30	0,806	50	1,471E-03	1,471E-03	0,0088	3,009E-06	1,42
AKT-B-02	60	0,808	50	1,474E-03	1,474E-03	0,0088	3,017E-06	1,42
AKT-B-03	90	0,769	50	1,403E-03	1,403E-03	0,0084	2,871E-06	1,35
AKT-B-04	120	0,782	50	1,427E-03	1,427E-03	0,0086	2,919E-06	1,38
AKT-B-05	150	0,794	50	1,449E-03	1,449E-03	0,0087	2,964E-06	1,40

Mean value   **1,39**

1,37

Table 37: Chemical actinometer measurement data and its evaluation in the coil reactor, test run: AKT-C

Experimental run: AKT-C

λ	Φ=f(T,c)	$P_{theor.}$	$\dot{V}$	pH_{in}	pH_{out}	T
[nm]	[-]	[W]	[l/h]	[-]	[-]	[^{o}C]
254	0,815	2,9	10	9,26	9,3	25

Sample	Time	Abs_{352nm}	Delution 1:x	$c_{Triiodid}$	$\Delta c_{Triiodid}$	$\dot{V}$	Φ_P	$P_{eff.}$
[Nr]	[s]	[-]	[-]	[mol/l]	[mol/l]	[mol/h]	[einstein/s]	[W]
AKT-C-00		0,185	50	3,376E-04				
AKT-C-01	0	0,686	50	1,252E-03	9,142E-04	0,0091	3,118E-06	1,47
AKT-C-02	30	0,672	50	1,226E-03	8,887E-04	0,0089	3,031E-06	1,43
AKT-C-03	60	0,671	50	1,224E-03	8,869E-04	0,0089	3,025E-06	1,42
AKT-C-04	90	0,663	50	1,210E-03	8,723E-04	0,0087	2,975E-06	1,40
AKT-C-05	120	0,675	50	1,232E-03	8,942E-04	0,0089	3,049E-06	1,44

Mean value   **1,43**

Table 38: Chemical actinometer measurement data and its evaluation in the coil reactor, test run: AKT-D

Experimental run: AKT-D

λ [nm]	Φ=f(T,c) [-]	$P_{theor.}$ [W]	$\dot{V}$ [l/h]	pH_{in} [-]	pH_{out} [-]	T [°C]
254	0,815	2,9	15	9,39	9,40	25

Sample [Nr]	Time [s]	Abs_{352nm} [-]	Delution 1:x [-]	$c_{Triiodid}$ [mol/l]	$\Delta c_{Triiodid}$ [mol/l]	$\dot{V}$ [mol/h]	Φ_P [einstein/s]	$P_{eff.}$ [W]
AKT-D-00		1,075	25	9,808E-04				
AKT-D-01	0	1,729	25	1,578E-03	5,967E-04	0,0090	3,053E-06	1,44
AKT-D-02	30	1,719	25	1,568E-03	5,876E-04	0,0088	3,006E-06	1,42
AKT-D-03	60	1,695	25	1,547E-03	5,657E-04	0,0085	2,894E-06	1,36
AKT-D-04	90	1,709	25	1,559E-03	5,785E-04	0,0087	2,959E-06	1,39
AKT-D-05	120	1,715	25	1,565E-03	5,839E-04	0,0088	2,987E-06	1,41

Mean value **1,40**

Table 39: Chemical actinometer measurement data and its evaluation in the coil reactor, test run: AKT-E

Experimental run: AKT-E

λ [nm]	Φ=f(T,c) [-]	$P_{theor.}$ [W]	$\dot{V}$ [l/h]	pH_{in} [-]	pH_{out} [-]	T [°C]
254	0,815	2,9	20	9,39	9,50	25

Sample [Nr]	Time [s]	Abs_{352nm} [-]	Delution 1:x [-]	$c_{Triiodid}$ [mol/l]	$\Delta c_{Triiodid}$ [mol/l]	$\dot{V}$ [mol/h]	Φ_P [einstein/s]	$P_{eff.}$ [W]
AKT-E-00		0,678	50	1,237E-03				
AKT-E-01	0	0,911	50	1,662E-03	4,252E-04	0,0085	2,900E-06	1,37
AKT-E-02	30	0,944	50	1,723E-03	4,854E-04	0,0097	3,311E-06	1,56
AKT-E-03	60	0,935	50	1,706E-03	4,690E-04	0,0094	3,199E-06	1,51
AKT-E-04	90	0,909	50	1,659E-03	4,215E-04	0,0084	2,875E-06	1,35
AKT-E-05	120	0,914	50	1,668E-03	4,307E-04	0,0086	2,937E-06	1,38

Mean value **1,43**

Table 40: Chemical actinometer measurements and its evaluation in the batch reactor, test run: AKT-R

Reactor type: **Batch reactor**

Outlet solution:

	V	T	pH_{in}	pH_{out}
	[l]	[°C]	[-]	[-]
	1,5	25	9,24	9,46

	c_{req}	M	m_{req}	m_{eff}	c_{eff}
	[mol/l]	[g/mol]	[g]	[g]	[g/mol]
KI	0,60	166,01	149,41	149,4	0,60
KIO_3	0,10	214,00	32,10	32,1	0,10
Borat	0,01	201,22	3,02	3,0175	0,01

Sample	Time	Abs_{352nm}	Delution 1:x	$c_{Triiodid}$	$\Delta c_{Triiodid}$	V_{BR}	Φ_P	$P_{eff.}$
[Nr]	[s]	[-]	[-]	[mol/l]	[mol/l]	[l]	[einstein/s]	[W]
AKT-R-01	0	1,055	1	0,000E+00		0,82		
AKT-R-02	180	0,527	10	1,923E-04	1,923E-04	0,81	1,108E-06	0,52
AKT-R-03	360	0,913	10	3,332E-04	3,332E-04	0,80	9,477E-07	0,45
AKT-R-04	540	1,466	10	5,350E-04	5,350E-04	0,79	1,002E-06	0,47
AKT-R-05	720	1,872	10	6,832E-04	6,832E-04	0,78	9,473E-07	0,45
AKT-R-06	900	1,485	15	8,130E-04	8,130E-04	0,77	8,902E-07	0,42
AKT-R-07	1080	1,713	15	9,378E-04	9,378E-04	0,76	8,446E-07	0,40
AKT-R-08	1800	1,983	20	1,447E-03	1,447E-03	0,75	7,719E-07	0,36

	Mean value	0,46
		0,44

Table 41: Chemical actinometer measurements and its evaluation in the batch reactor, test run: AKT-S.

Reactor type: **Batch reactor**

Outlet solution:

	V	T	pH$_{in}$	pH$_{out}$
	[l]	[^{o}C]	[-]	[-]
	3	25	9,23	9,81

	c$_{req}$	M	m$_{req}$	m$_{eff}$	c$_{eff}$
	[mol/l]	[g/mol]	[g]	[g]	[g/mol]
KI	0,40	166,01	199,21	149,4	0,40
KIO$_3$	0,10	214,00	64,24	32,1	0,10
Borat	0,01	201,22	6,04	3,0175	0,01

Sample	Time	Abs$_{352nm}$	Delution 1:x	c$_{Triiodid}$	Δc$_{Triiodid}$	V$_{BR}$	Φ_P	P$_{eff.}$	P$_{theor.}$
[Nr]	[s]	[-]	[-]	[mol/l]	[mol/l]	[l]	[einstein/s]	[W]	[W]
AKT-S-00		0,014	1	5,109E-07					
AKT-S-01	0	0,524	1	1,912E-05		0,8300			3,5
AKT-S-02	180	1,058	10	3,861E-04	3,670E-04	0,8275	2,071E-06	0,98	3
AKT-S-03	360	1,561	15	8,546E-04	8,354E-04	0,8250	2,351E-06	1,11	2,9
AKT-S-04	540	1,770	20	1,292E-03	1,273E-03	0,8225	2,380E-06	1,12	2,8
AKT-S-05	720	1,858	25	1,695E-03	1,676E-03	0,8200	2,344E-06	1,10	2,7
AKT-S-06	900	1,146	50	2,091E-03	2,072E-03	0,8175	2,311E-06	1,09	2,6
AKT-S-07	1080	1,349	50	2,462E-03	2,443E-03	0,8150	2,263E-06	1,07	2,5
AKT-S-08	1800	0,961	100	3,507E-03	3,488E-03	0,8125	1,933E-06	0,91	2,4
AKT-S-09	9900	1,382	150	7,566E-03	7,547E-03	0,8100	7,581E-07	0,36	2,3

Mean value   1,08

0,97

Appendix 3 – Hydrogen peroxide generation

Table 42: Hydrogen peroxide concentration in the test run OMa1

Electrolysis cell characteristic:

A_{Cath}	A_{Anod}	I	j
$[m^2]$	$[m^2]$	[A]	$[A/m^2]$
0,13081	0,000096	0,14	1,1

Electrolyte characteristic

c_{Na2SO4}	V_{Na2SO4}	$\dot{V}_{Na2SO4}$	$\dot{V}_{Air\,(STP)}$	T
[M]	[l]	[l/h]	[l/h]	$[^0C]$
0,05	1,20	10,0	20,0	25,0

Sample	t	pH-value	U	δ	$Na_2S_2O_3$	c_{H2O2}	c_{H2O2}
[Nr]	[s]	[-]	[V]	[mS/cm]	[ml]	[mmol/l]	[mg/l]
OMa1-00	0	3,12	0,7	8,44			
OMa1-01	15	3,16	0,7	8,43	0,42	0,21	7,12
OMa1-02	45	3,19	0,7	8,43	0,32	0,16	5,43

Table 43: Hydrogen peroxide concentration in the test run OMa2

Electrolysis cell characteristic:

A_{Cath}	A_{Anod}	I	j
$[m^2]$	$[m^2]$	[A]	$[A/m^2]$
0,13081	0,000096	0,29	2,2

Electrolyte characteristic

c_{Na2SO4}	V_{Na2SO4}	$\dot{V}_{Na2SO4}$	$\dot{V}_{Air\,(STP)}$	T
[M]	[l]	[l/h]	[l/h]	$[^0C]$
0,05	1,20	10,0	20,0	25,0

Sample	t	pH-value	U	δ	$Na_2S_2O_3$	c_{H2O2}	c_{H2O2}	$c_{H2O2\,teor.}$
[Nr]	[s]	[-]	[V]	[mS/cm]	[ml]	[mmol/l]	[mg/l]	[mg/l]
OMa1-00	0	3,12	0,7	8,44				
OMa1-01	15	3,16	0,7	8,43	0,36	0,18	6,17	38,3
OMa1-02	45	3,19	0,7	8,43	0,41	0,20	6,93	115,0

Table 44: Hydrogen peroxide concentration in the test run OMa3

Electrolysis cell characteristic:

A_{Cath}	A_{Anod}	I	j
$[m^2]$	$[m^2]$	[A]	$[A/m^2]$
0,13081	0,000096	0,58	4,4

Electrolyte characteristic

c_{Na2SO4}	V_{Na2SO4}	$\dot{V}_{Na2SO4}$	$\dot{V}_{Air\,(STP)}$	T
[M]	[l]	[l/h]	[l/h]	$[^0C]$
0,05	1,20	10,0	20,0	25,0

Sample	t	pH-value	U	δ	$Na_2S_2O_3$	c_{H2O2}	c_{H2O2}	$c_{H2O2\,teor.}$
[Nr]	[s]	[-]	[V]	[mS/cm]	[ml]	[mmol/l]	[mg/l]	[mg/l]
OMa3-00	0	3,26	1,8	8,42				
OMa3-01	15	3,24	1,8	8,42	0,30	0,15	4,97	76,6
OMa3-02	45	3,23	2	8,42	0,29	0,15	5,02	229,9
OMa3-03	75	3,26	2,2	8,43	0,44	0,22	7,34	383,2
OMa3-04	105	3,29	2,2	8,43	0,52	0,26	8,67	536,5
OMa3-05	135	3,33	2,3	8,42	0,77	0,38	13,08	689,8
OMa3-06	165	3,37	2,3	8,40	0,74	0,37	12,56	843,1

Table 45: Hydrogen peroxide concentration in the test run OMa24

Electrolysis cell characteristic:

A_{Cath}	A_{Anod}	I	j
[m²]	[m²]	[A]	[A/m²]
0,13081	0,000096	0,14	1,1

Electrolyte characteristic

c_{Na2SO4}	V_{Na2SO4}	$\dot{V}_{Na2SO4}$	$\dot{V}_{Air\,(STP)}$	T
[M]	[l]	[l/h]	[l/h]	[°C]
0,05	1,15	24,0	20,0	23,0

Sample	t	pH-value	U	δ	$Na_2S_2O_3$	c_{H2O2}	c_{H2O2}	$c_{H2O2\,teor.}$
[Nr]	[s]	[-]	[V]	[mS/cm]	[ml]	[mmol/l]	[mg/l]	[mg/l]
OMa24-00	0	1,98	0,6	11,44				
OMa24-01	15	1,98	0,7	11,45	0,44	0,26	8,77	18,5
OMa24-02	45	1,97	0,8	11,4	0,29	0,17	5,70	55,5
OMa24-03	75	1,97	0,8	11,35	0,32	0,18	6,16	92,5
OMa24-04	105	1,97	0,8	11,3	0,41	0,23	7,95	129,5
OMa24-05	135	1,96	0,8	11,28	0,25	0,14	4,90	166,5

Table 46: Hydrogen peroxide concentration in the test run OMb24

Electrolysis cell characteristic:

A_{Cath}	A_{Anod}	I	j
[m²]	[m²]	[A]	[A/m²]
0,13	0,000096	0,29	2,2

Electrolyte characteristic

c_{Na2SO4}	V_{Na2SO4}	$\dot{V}_{Na2SO4}$	$\dot{V}_{Air\,(STP)}$	T
[M]	[l]	[l/h]	[l/h]	[°C]
0,05	1,00	24,0	20,0	23,0

Sample	t	pH-value	U	δ	$Na_2S_2O_3$	c_{H2O2}	c_{H2O2}	$c_{H2O2\,teor.}$
[Nr]	[s]	[-]	[V]	[mS/cm]	[ml]	[mmol/l]	[mg/l]	[mg/l]
OMb24-00	135	1,96	1,3	11,26			4,90	
OMb24-01	150	1,96	1,5	11,26	0,36	0,18	6,13	383,2
OMb24-02	180	1,96	1,6	11,21	0,58	0,29	9,81	459,9
OMb24-03	210	1,97	1,6	11,15	0,92	0,46	15,72	536,5
OMb24-04	240	1,97	1,6	11,15	1,27	0,63	21,39	613,1
OMb24-05	270	1,97	1,6	11,1	1,26	0,64	21,72	689,8

Table 47: Hydrogen peroxide concentration in the test run OMf24

Electrolysis cell characteristic:

A_{Cath}	A_{Anod}	I	j
[m^2]	[m^2]	[A]	[A/m^2]
0,13	0,000096	0,58	4,4

Electrolyte characteristic

c_{Na2SO4}	V_{Na2SO4}	$\dot{V}_{Na2SO4}$	$\dot{V}_{Air (STP)}$	T
[M]	[l]	[l/h]	[l/h]	[^{0}C]
0,05	1,15	24,0	20,0	25,0

Sample	t	pH-value	U	δ	Na$_2$S$_2$O$_3$	c$_{H2O2}$	c$_{H2O2}$	c$_{H2O2\ teor.}$
[Nr]	[s]	[-]	[V]	[mS/cm]	[ml]	[mmol/l]	[mg/l]	[mg/l]
OMf24-00	270	1,97	2	11,1			21,72	
OMf24-01	285	1,98	2	11,04	1,25	0,62	21,24	1456,2
OMf24-02	315	1,98	2,1	11,03	1,51	0,74	25,24	1609,5
OMf24-03	345	1,99	2,1	10,96	1,49	0,74	25,03	1762,8
OMf24-04	375	1,99	2,1	10,94	1,36	0,68	23,19	1916,1
OMf24-05	405	2	2,1	10,9	1,46	0,73	24,80	2069,3

Table 48: Hydrogen peroxide concentration in the test run OMc24

Electrolysis cell characteristic:

A_{Cath}	A_{Anod}	I	j
[m^2]	[m^2]	[A]	[A/m^2]
0,13081	0,000096	1,15	8,8

Electrolyte characteristic

c_{Na2SO4}	V_{Na2SO4}	$\dot{V}_{Na2SO4}$	$\dot{V}_{Air (STP)}$	T
[M]	[l]	[l/h]	[l/h]	[^{0}C]
0,05	1,00	24,0	20,0	23,0

Sample	t	pH-value	U	δ	Na$_2$S$_2$O$_3$	c$_{H2O2}$	c$_{H2O2}$	c$_{H2O2\ teor.}$
[Nr]	[s]	[-]	[V]	[mS/cm]	[ml]	[mmol/l]	[mg/l]	[mg/l]
OMc24-00	0	1,99	2,7	11,1				
OMc24-01	15	1,98	3	11,04	0,52	0,26	9,00	152,0
OMc24-02	45	1,99	2,9	11,03	0,60	0,30	10,15	455,9
OMc24-03	75	2	3	10,96	0,85	0,43	14,67	759,8
OMc24-04	105	2	3	10,94	0,90	0,45	15,40	1063,7
OMc24-05	135	2,01	2,9	10,9	0,90	0,45	15,37	1367,7

Table 49: Hydrogen peroxide concentration in the test run OMd24

Electrolysis cell characteristic:

A_{Cath}	A_{Anod}	I	j
[m^2]	[m^2]	[A]	[A/m^2]
0,13081	0,000096	0,26	2,0

Electrolyte characteristic

c_{Na2SO4}	V_{Na2SO4}	$\dot{V}_{Na2SO4}$	$\dot{V}_{Air\,(STP)}$	T
[M]	[l]	[l/h]	[l/h]	[^{0}C]
0,05	1,00	24,0	20,0	25,0

Sample	t	pH-value	U	δ	$Na_2S_2O_3$	c_{H2O2}	c_{H2O2}	$c_{H2O2\,teor.}$
[Nr]	[s]	[-]	[V]	[mS/cm]	[ml]	[mmol/l]	[mg/l]	[mg/l]
OMd24-00	0	1,99	2,1	11,84	0,56	0,28	9,69	
OMd24-01	15	1,99	2,1	11,76	0,48	0,24	8,25	34,4
OMd24-02	45	2	2	11,69	0,50	0,25	8,59	103,1
OMd24-03	75	2	2	11,65	0,62	0,30	10,20	171,8
OMd24-04	105	2	2	11,61	0,74	0,38	12,76	240,5
OMd24-05	135	2,02	2	11,55	0,86	0,42	14,43	309,2
OMd24-06	165	2,03	2	11,50	0,99	0,50	16,90	377,9

Table 50: Hydrogen peroxide concentration in the test run OMe24

Electrolysis cell characteristic:

A_{Cath}	A_{Anod}	I	j
[m^2]	[m^2]	[A]	[A/m^2]
0,13081	0,000096	0,23	1,76

Electrolyte characteristic

c_{Na2SO4}	V_{Na2SO4}	$\dot{V}_{Na2SO4}$	$\dot{V}_{Air\,(STP)}$	T
[M]	[l]	[l/h]	[l/h]	[^{0}C]
0,05	1,00	24,0	20,0	25,0

Sample	t	pH-value	U	δ	$Na_2S_2O_3$	c_{H2O2}	c_{H2O2}	$c_{H2O2\,teor.}$
[Nr]	[s]	[-]	[V]	[mS/cm]	[ml]	[mmol/l]	[mg/l]	[mg/l]
OMe24-00	0	1,94	1,5	13,43	0,35	0,17	5,78	
OMe24-01	15	1,95	1,6	13,38	0,35	0,18	5,96	30,4
OMe24-02	45	1,95	1,7	13,32	0,73	0,37	12,47	91,2
OMe24-03	75	1,95	1,7	13,35	1,24	0,61	20,71	152,0
OMe24-04	105	1,94	1,6	13,34	1,27	0,65	22,01	212,7
OMe24-05	135	1,94	1,5	13,32	1,05	0,51	17,48	273,5
OMe24-06	165	1,94	1,5	13,29	0,87	0,43	14,58	334,3
OMe24-07	195	1,95	1,6	13,24	0,80	0,40	13,47	395,1

Table 51: Hydrogen peroxide concentration in the test run OMh24

Electrolysis cell characteristic:

A_{Cath}	A_{Anod}	I	j	c_{Na2SO4}	V_{Na2SO4}	$\dot{V}_{Na2SO4}$	$\dot{V}_{Air (STP)}$	T
$[m^2]$	$[m^2]$	[A]	$[A/m^2]$	[M]	[l]	[l/h]	[l/h]	$[^0C]$
0,13081	0,000096	0,26	2,0	0,05	1,00	24,0	20,0	25,0

Electrolyte characteristic

Sample	t	pH-value	U	δ	$Na_2S_2O_3$	c_{H2O2}	c_{H2O2}	$c_{H2O2\ teor.}$
[Nr]	[s]	[-]	[V]	[mS/cm]	[ml]	[mmol/l]	[mg/l]	[mg/l]
OMh24-00	0	2,04	0,9	12,71	2,34	1,15	39,10	
OMh24-01	15	2,04	1,4	12,67	1,89	0,94	32,05	34,4
OMh24-02	45	2,03	1,5	12,65	1,04	0,52	17,57	103,1
OMh24-03	75	2,02	1,6	12,59	0,57	0,29	9,86	171,8
OMh24-04	105	2,02	1,7	12,48	0,48	0,24	8,05	240,5
OMh24-05	135	2,02	1,8	12,44	0,75	0,38	12,77	309,2
OMh24-06	180	2,03	1,8	12,46	1,08	0,55	18,53	412,3
OMh24-07	210	2,03	1,8	12,43	1,17	0,58	19,59	481,0

Table 52: Hydrogen peroxide concentration in the test run OMi24

Electrolysis cell characteristic:

A_{Cath}	A_{Anod}	I	j	c_{Na2SO4}	V_{Na2SO4}	$\dot{V}_{Na2SO4}$	$\dot{V}_{Air}$	T
$[m^2]$	$[m^2]$	[A]	$[A/m^2]$	[M]	[l]	[l/h]	[l/h]	$[^0C]$
0,13081	0,000096	0,26	2,0	0,05	1,00	24,0	20,0	25,0

Electrolyte characteristic

Sample	t	pH-value	U	δ	$Na_2S_2O_3$	c_{H2O2}	c_{H2O2}	$c_{H2O2\ teor.}$
[Nr]	[s]	[-]	[V]	[mS/cm]	[ml]	[mmol/l]	[mg/l]	[mg/l]
OMi24-00	0	2,04	1	11,46	0,77	0,38	12,92	
OMi24-01	15	2,05	1,5	11,43	0,74	0,37	12,55	41,2
OMi24-02	45	2,05	1,6	11,38	0,45	0,22	7,59	123,7
OMi24-03	75	2,06	1,7	11,33	0,58	0,29	9,72	206,1
OMi24-04	105	2,06	1,8	11,28	0,73	0,37	12,46	288,6
OMi24-05	135	2,07	1,9	11,22	0,84	0,42	14,24	371,1
OMi24-06	180	2,08	1,9	11,13	0,89	0,45	15,13	494,7
OMi24-07	210	2,09	1,9	11,10	0,96	0,49	16,63	577,2

Appendix 3 – Anodic oxidation

Electrolysis cell characteristic:

A Cath	A Anod	I	j	d gl.carbon
[m²]	[m²]	[A]	[A/m²]	[µm]
0,13081	0,0096	0,19	20,2	3150-4000

Electrolyte characteristic:

c_{Na2SO4}	EDTA	$\dot{V}_{Na2SO4}$	$\dot{V}_{Air\,(STP)}$
[M]	[mmol/l]	[l]	[l/h]
0,05	1,34	1,10	15,0

Table 53: Data from anodic oxidation of EDTA. Laboratory test runs: AOP_6_Ez20

Sample	t	U	pH-Value	T	Q	c_{EDTA}/c_{0EDTA}
Nr	[min]	[V]	[-]	[°C]	[As]	[-]
AOP-6-00	0,0		4,66	25,0		1,00
AOP-6-01	1,5	3,1	4,61	25,0	17,1	0,98
AOP-6-02	6,0	3,1	4,58	25,0	34,2	0,97
AOP-6-03	10,0	3,1	4,55	25,0	68,4	0,97
AOP-6-04	15,0	3,2	4,54	25,0	114,0	0,97
AOP-6-05	20,0	3,2	4,52	25,0	171,0	0,97
AOP-6-06	30,0	3,3	4,5	25,0	228,0	0,97
AOP-6-07	45,0	3,2	4,47	25,0	342,0	0,97
AOP-6-08	60,0	3,3	4,47	25,0	513,0	0,96
AOP-6-09	90,0	3,4	4,48	25,0	684,0	0,95
AOP-6-10	120,0	3,2	4,49	25,0	1026,0	0,93
AOP-6-11	150,0	3,3	4,51	25,0	1390,8	0,91
AOP-6-12	180,0	3,2	4,52	25,0	1710,0	0,88
AOP-6-13	240,0	3,2	4,55	25,0	2052,0	0,86
AOP-6-14	300,0	3,2	4,58	25,0	2736,0	0,80
AOP-6-15	360,0	3,2	4,61	25,0	3420,0	0,77

Table 54: Data from anodic oxidation of EDTA. Laboratory test: AOP_9_Ez20

Sample	t	U	pH-Value	T	Q	c_{EDTA}/c_{0EDTA}
Nr	[min]	[V]	[-]	[°C]	[As]	[-]
AOP-9-00	0,0		4,78	25,0		1,00
AOP-9-01	1,5	3,3	4,71	25,0	17,1	0,98
AOP-9-02	6,0	3,3	4,69	25,0	68,4	0,98
AOP-9-03	10,0	3,3	4,7	25,0	114,0	0,97
AOP-9-04	15,0	3,3	4,7	25,0	171,0	0,97
AOP-9-05	20,0	3,3	4,69	25,0	228,0	0,96
AOP-9-06	30,0	3,3	4,69	25,0	342,0	0,95
AOP-9-07	45,0	3,3	4,71	25,0	513,0	0,93
AOP-9-08	60,0	3,2	4,72	25,0	684,0	0,94
AOP-9-09	90,0	3,2	4,75	25,0	1026,0	0,92
AOP-9-10	120,0	3,2	4,75	25,0	1368,0	0,91
AOP-9-11	150,0	3,1	4,78	25,0	1710,0	0,87
AOP-9-12	180,0	3,1	4,83	25,0	2052,0	0,88
AOP-9-13	240,0	3,0	4,9	25,0	2736,0	0,86
AOP-9-14	300,0	3,0	4,98	25,0	3420,0	0,84
AOP-9-15	360,0	2,9	5,05	25,0	4104,0	0,81

Appendix 4 – Photochemical degradation of Fe(III)-EDTA

Reactor type   **Batch reactor**

Radiation characteristic

P_e	λ	Φ_P
[W]	[nm]	[Einstein/s]
35	254	2,3400E-06

Dilution characteristic

$c_{FeSO4x7H2O}$	c_{EDTA}	V	$\dot{V}_{Air\,(STP)}$	T
[mmol/l]	[mmol/l]	[l]	[l/h]	[^{0}C]
0,67	1,34	0,82	20,0	25,0

Table 55: Photochemical degradation of Fe(III)-EDTA in the batch reactor. Laboratory test: Ph-FF-C

Sample	t	pH-value	c_{EDTA}/c_{0EDTA}	m_{EDTA}	Φ_λ
[Nr]	[min]	[-]	[-]	[mol/s]	[mol/Einstein]
FF-C-00		3,00			
FF-C-01	0	3,02	1,00	0,0000	
FF-C-02	3	3,05	0,76	0,0003	0,62
FF-C-03	6	3,14	0,55	0,0005	0,59
FF-C-04	10	3,24	0,33	0,0007	0,53
FF-C-05	15	3,52	0,16	0,0009	0,44
FF-C-06	20	4,18	0,08	0,0010	0,36
FF-C-07	30	5,05	0,03	0,0011	0,25
FF-C-08	45	6,49	0,02	0,0011	0,17

Table 56: Photochemical degradation of Fe(III)-EDTA in the batch reactor. Laboratory test: Ph-FF-D

Sample	$\dot{V}$	pH-value	c_{EDTA}/c_{0EDTA}	m_{EDTA}	Φ_λ
[Nr]	[l/h]	[-]	[-]	[mol/s]	[mol/Einstein]
FF-D-00		3,01			
FF-D-01	0	2,99	1,00	0,0000	
FF-D-02	3	3,08	0,76	0,0003	0,63
FF-D-03	6	3,11	0,55	0,0005	0,59
FF-D-04	10	3,28	0,31	0,0008	0,54
FF-D-05	15	3,48	0,14	0,0009	0,45
FF-D-06	20	3,94	0,07	0,0010	0,37
FF-D-07	30	5	0,01	0,0011	0,26
FF-D-08	45	6,37	0,00	0,0011	0,17
FF-D-09	60	6,56	0,00	0,0011	0,13

Reactor type **Small PFR**

Radiation characteristic			*Dilution characteristic*			
P_e	λ	$\Phi_{P(batch\ reactor)}$	$c_{FeSO4x7H2O}$	c_{EDTA}	V_R	$\dot{V}_{Air\ (STP)}$
[W]	[nm]	[Einstein/s]	[mmol/l]	[mmol/l]	[l]	[l/h]
35	254	2,29E-06	0,67	1,34	0,113	20,0

Table 57: Photochemical degradation of Fe(III)-EDTA in the small PFR. Laboratory test run: Ph-FF-G

Sample	$\dot{V}$	pH-value	T	c_{EDTA}/c_{0EDTA}	m_{EDTA}	Φ_λ
[Nr]	[l/h]	[-]	[^{0}C]	[-]	[mol/s]	[mol/Einstein]
FF-G-00		3,06	25,0	1,00		
FF-G-01	0,30	5,8	25,0	0,03	1,08E-07	0,05
FF-G-02	0,75	5,4	25,0	0,09	2,55E-07	0,11
FF-G-03	1,00	5,17	25,0	0,11	3,33E-07	0,15
FF-G-04	1,50	4,84	25,0	0,16	4,67E-07	0,20
FF-G-05	3,00	4,39	25,0	0,27	8,18E-07	0,36
FF-G-06	6,00	3,82	25,0	0,47	1,19E-06	0,52
FF-G-07	10,00	3,36	25,0	0,63	1,39E-06	0,61
FF-G-08	15,00	3,23	25,0	0,78	1,23E-06	0,54

Table 58: Photochemical degradation of Fe(III)-EDTA in the small PFR. Laboratory test run: Ph-FF-H

Sample	$\dot{V}$	pH-value	T	c_{EDTA}/c_{0EDTA}	m_{EDTA}	Φ_λ
[Nr]	[l/h]	[-]	[^{0}C]	[-]	[mol/s]	[mol/Einstein]
FF-H-00		3,05	25,0	1,00		
FF-H-01	0,30	6,23	25,0	0,02	1,10E-07	0,05
FF-H-02	0,75	5,57	25,0	0,05	2,66E-07	0,12
FF-H-03	1,00	5,21	25,0	0,06	3,50E-07	0,15
FF-H-04	1,50	4,76	25,0	0,12	4,89E-07	0,21
FF-H-05	3,00	4,21	25,0	0,28	8,08E-07	0,35
FF-H-06	6,00	3,69	25,0	0,50	1,13E-06	0,49
FF-H-07	10,00	3,42	25,0	0,66	1,26E-06	0,55
FF-H-08	15,00	3,3	25,0	0,76	1,34E-06	0,59

Table 59: Photochemical degradation of Fe(III)-EDTA in the small PFR. Laboratory test run: Ph-FF-I

Sample	$\dot{V}$	pH-value	T	c_{EDTA}/c_{0EDTA}	m_{EDTA}	Φ_λ
[Nr]	[l/h]	[-]	[^{0}C]	[-]	[mol/s]	[mol/Einstein]
FF-I-00		3,05	25,0	1,000		
FF-I-01	0,30	4,63	25,0	0,069	1,04E-07	0,05
FF-I-02	0,75	4,03	25,0	0,206	2,22E-07	0,10
FF-I-03	1,00	4,04	25,0	0,257	2,76E-07	0,12
FF-I-04	1,50	3,7	25,0	0,313	3,84E-07	0,17
FF-I-05	3,00	3,63	25,0	0,367	7,07E-07	0,31
FF-I-06	6,00	3,42	25,0	0,537	1,03E-06	0,45
FF-I-07	10,00	3,3	25,0	0,692	1,14E-06	0,50
FF-I-08	15,00		25,0	0,802	1,10E-06	0,48

XXIV

Reactor type   **Coil reactor**

Radiation characteristic			*Dilution characteristic*			
P_e	λ		$c_{FeSO4x7H2O}$	c_{EDTA}	V_R	$\dot{V}_{Air\,(STP)}$
[W]	[nm]		[mmol/l]	[mmol/l]	[l]	[l/h]
35	254		0,67	1,34	0,028	20,0

Table 60: Photochemical degradation of Fe(III)-EDTA in the coil reactor. Laboratory test run: PhF-FF-E

Sample	$\dot{V}$	pH-value	T	c_{EDTA}/c_{0EDTA}	m_{EDTA}	Φ_P	Φ_λ
[Nr]	[l/h]	[-]	[^{0}C]	[-]	[mol/s]	[Einstein/s]	[mol/Einstein]
FF-E-00		3,02	25,0	1,00			
FF-E-01	0,30	5,01	25,0	0,01	1,11E-07	5,78E-07	0,19
FF-E-02	0,75	4,25	25,0	0,13	2,42E-07	1,29E-06	0,19
FF-E-03	1,00	4,17	25,0	0,21	2,94E-07	1,96E-06	0,15
FF-E-04	1,50	3,89	25,0	0,28	4,00E-07	2,42E-06	0,17
FF-E-05	3,00	3,8	25,0	0,37	7,09E-07	2,66E-06	0,27
FF-E-06	6,00	3,66	25,0	0,49	1,15E-06	2,96E-06	0,39
FF-E-07	10,00	3,38	25,0	0,65	1,30E-06	3,04E-06	0,43

Table 61: Photochemical degradation of Fe(III)-EDTA in the coil reactor. Laboratory test run: PhF-FF-F

Sample	$\dot{V}$	pH-value	T	c_{EDTA}/c_{0EDTA}	m_{EDTA}	Φ_P	Φ_λ
[Nr]	[l/h]	[-]	[^{0}C]	[-]	[mol/s]	[Einstein/s]	[mol/Einstein]
FF-F-00		3,05	25,0	1,00			
FF-F-01	0,30	5,34	25,0	0,01	1,10E-07	5,78E-07	0,19
FF-F-02	0,75	4,47	25,0	0,15	2,38E-07	1,29E-06	0,18
FF-F-03	1,00	4,16	25,0	0,21	2,95E-07	1,96E-06	0,15
FF-F-04	1,50	4,13	25,0	0,29	3,98E-07	2,42E-06	0,16
FF-F-05	3,00	3,88	25,0	0,37	7,04E-07	2,66E-06	0,26
FF-F-06	6,00	3,7	25,0	0,49	1,15E-06	2,96E-06	0,39
FF-F-07	10,00	3,36	25,0	0,66	1,28E-06	3,04E-06	0,42

Reactor type   **Coil reactor closed circulation flow**

Radiation characteristic

P_e	λ	Φ_P
[W]	[nm]	[Einstein/s]
35	254	3,04447E-06

Dilution characteristic

$c_{FeSO4x7H2O}$	c_{EDTA}	V_R	$\dot{V}_{Na2SO4}$	$\dot{V}_{Air\ (STP)}$
[mmol/l]	[mmol/l]	[l]	[l/h]	[l/h]
0,67	1,34	0,028	20,0	20,0

Table 62: Photochemical degradation of Fe(III)-EDTA in the coil reactor with circulating flow. Laboratory test run: PhF-FF-J

Sample	t	pH-value	T	c_{EDTA}/c_{0EDTA}	m_{EDTA}	m_{EDTA}	Φ_λ
[Nr]	[min]	[-]	[^{0}C]	[-]	[mmol/l]	[mmol]	[mol/einstein]
FF-J-00	0	3,05	25,0	1,000	1,34	1,101	
FF-J-01	0,8	3,15	25,0	0,811	1,09	0,893	1,4232
FF-J-02	1	3,16	25,0	0,782	1,05	0,861	0,8920
FF-J-03	2	3,2	25,0	0,710	0,95	0,781	0,4339
FF-J-04	4	3,24	25,0	0,549	0,74	0,605	0,4838
FF-J-05	6	3,29	25,0	0,409	0,55	0,451	0,4218
FF-J-06	8	3,34	25,0	0,295	0,40	0,325	0,3435
FF-J-07	10	3,42	25,0	0,211	0,28	0,232	0,2542
FF-J-08	15	3,81	25,0	0,079	0,11	0,087	0,1589
FF-J-09	20	4,35	25,0	0,038	0,05	0,041	0,0500
FF-J-10	30	5,04	25,0	0,008	0,01	0,009	0,0177

Table 63: Photochemical degradation of Fe(III)-EDTA in the coil reactor with circulating flow. Laboratory test run: PhF-FF-K_6.3

Sample	t	pH-value	T	c_{EDTA}/c_{0EDTA}	m_{EDTA}	m_{EDTA}	Φ_λ
[Nr]	[min]	[-]	[^{0}C]	[-]	[mmol/l]	[mmol]	[mol/einstein]
FF-K-00	0	3,05	25,0	1,000	1,34	1,100	
FF-K-01	0,8	3,15	25,0	0,795	1,07	0,874	1,5410
FF-K-02	1	3,16	25,0	0,727	0,98	0,800	2,0453
FF-K-03	2	3,18	25,0	0,664	0,89	0,730	0,3821
FF-K-04	4	3,25	25,0	0,517	0,69	0,569	0,4413
FF-K-05	6	3,34	25,0	0,382	0,51	0,420	0,4057
FF-K-06	8	3,38	25,0	0,275	0,37	0,302	0,3247
FF-K-07	10	3,46	25,0	0,197	0,26	0,217	0,2321
FF-K-08	15	3,86	25,0	0,083	0,11	0,092	0,1372
FF-K-09	20	4,47	25,0	0,043	0,06	0,048	0,0483
FF-K-10	30	5,3	25,0	0,011	0,01	0,012	0,0195

Appendix 5 – Anox/$H_2O_2^{Cath}$/UV process

Laboratory unit set-up   **Electrolysis cell and CSTR**

Electrolysis cell charactertic			*Electrolyte characteristic*					*Radiation characteristic*		
A_{Anod}	I	j	c_{Na2SO4}	EDTA	V_{Na2SO4}	$\dot{V}_{Na2SO4}$	$\dot{V}_{Air (STP)}$	P_e	λ	Φ_P
[m^2]	[A]	[A/m^2]	[M]	[mmol/l]	[l]	[l/h]	[l/h]	[W]	[nm]	[Einstein/s]
0,0096	0,26	27,6	0,05	1,34	1,10	15,0	20	35	254	2,34E-06

Table 64: Data from EDTA degradation with Anox/$H_2O_2^{Cath}$/UV process operated with the CSTR. Laboratory test run: AOP_4_EzR4

Sample	t	U	pH-value	T	Q	c_{EDTA}/c_{0EDTA}
[Nr]	[min]	[V]	[-]	[^oC]	[As]	[-]
AOP-4-00	0		3,01	25,0		1,00
AOP-4-01	1,5	2,8	2,94	25,0	23,4	0,99
AOP-4-02	3	2,9	2,98	25,0	46,8	0,97
AOP-4-03	6	3,1	3,01	25,0	93,6	0,96
AOP-4-04	10	3,2	3,02	25,0	156,0	0,92
AOP-4-05	15	3,2	3,03	25,0	234,0	0,89
AOP-4-06	20	3,2	3,05	25,0	312,0	0,82
AOP-4-07	30	3,1	3,09	25,0	468,0	0,73
AOP-4-08	45	3,1	3,14	25,0	702,0	0,60
AOP-4-09	60	3,0	3,18	25,0	936,0	0,47
AOP-4-10	90	3,0	3,27	25,0	1404,0	0,30
AOP-4-11	122	3,0	3,36	25,0	1903,2	0,17
AOP-4-12	150	3,3	3,43	25,0	2340,0	0,07
AOP-4-13	180	3,1	3,54	25,0	2808,0	0,00
AOP-4-14	240	3,2	4,31	25,0	3744,0	0,00
AOP-4-15	300	3,2	5,72	25,0	4680,0	0,00

Table 65: Data from EDTA degradation with Anox/$H_2O_2^{Cath}$/UV process operated with the CSTR. Laboratory test run: AOP_5_EzR4

Sample	t	U	pH-value	T	Q	c_{EDTA}/c_{0EDTA}
[Nr]	[min]	[V]	[-]	[°C]	[As]	[-]
AOP-5-00	0		3,01	1,00		1,00
AOP-5-01	1,5	3,3	3	0,92	23,4	0,92
AOP-5-02	3	3	3	0,93	46,8	0,93
AOP-5-03	6	3,1	3,02	0,94	93,6	0,94
AOP-5-04	10	3,2	3,04	0,92	156,0	0,92
AOP-5-05	15	3,3	3,06	0,89	234,0	0,89
AOP-5-06	20	3,4	3,08	0,85	312,0	0,85
AOP-5-07	30	3,3	3,11	0,76	468,0	0,76
AOP-5-08	45	3,3	3,15	0,66	702,0	0,66
AOP-5-09	60	3,3	3,19	0,54	936,0	0,54
AOP-5-10	90	3,3	3,27	0,39	1404,0	0,39
AOP-5-11	122	3,1	3,34	0,27	1903,2	0,27
AOP-5-12	150	3,2	3,38	0,19	2340,0	0,19
AOP-5-13	180	3,2	3,43	0,13	2808,0	0,13
AOP-5-14	240	3,2	3,57	0,03	3744,0	0,03
AOP-5-15	300	3,4	3,76	0,00	4680,0	0,00

Laboratory unit set-up   **Electrolysis cell and large PFR**

Electrolysis cell charactertic			*Electrolyte characteristic*					*Radiation characteristic*		
A_{Anod}	I	j	c_{Na2SO4}	EDTA	V_{Na2SO4}	$\dot{V}_{Na2SO4}$	$\dot{V}_{Air\,(STP)}$	P_e	λ	Φ_P
[m²]	[A]	[A/m²]	[M]	[mmol/l]	[l]	[l/h]	[l/h]	[W]	[nm]	[Einstein/s]
0,0096	0,26	27,6	0,05	1,34	1,10	15,0	20	35	254	4,10E-07

Table 66: Data from EDTA degradation with Anox/$H_2O_2^{Cath}$/UV process operated with the the large PFR. Laboratory test run: AOP_7_EzR2

Sample	t	U	pH-value	T	Q	c_{EDTA}/c_{0EDTA}
[Nr]	[min]	[V]	[-]	[°C]	[As]	[-]
AOP-7-00	0		3,02	1,00		1,00
AOP-7-01	1,5	3,1	3,04	0,92	23,4	1,01
AOP-7-02	3	3,1	3,04	0,93	46,8	1,01
AOP-7-03	6	3,1	3,04	0,94	93,6	1,01
AOP-7-04	10	3,2	3,05	0,92	156,0	0,99
AOP-7-05	15	3,3	3,06	0,89	234,0	0,98
AOP-7-06	20	3,3	3,06	0,85	312,0	0,98
AOP-7-07	30	3,3	3,07	0,76	468,0	0,95
AOP-7-08	45	3,3	3,08	0,66	702,0	0,87
AOP-7-09	60	3,4	3,1	0,54	936,0	0,82
AOP-7-10	90	3,4	3,13	0,39	1404,0	0,68
AOP-7-11	122	3,4	3,17	0,27	1903,2	0,58
AOP-7-12	150	3,4	3,22	0,19	2340,0	0,50
AOP-7-13	180	3,4	3,24	0,13	2808,0	0,41
AOP-7-14	240	3,5	3,29	0,03	3744,0	0,27
AOP-7-15	300	3,5	3,36	0,00	4680,0	0,16

Table 67: Data from EDTA degradation with Anox/$H_2O_2^{Cath}$/UV process operated with the large PFR. Laboratory test run: AOP_8_EzR2

Sample	t	U	pH-value	T	Q	c_{EDTA}/c_{0EDTA}
[Nr]	[min]	[V]	[-]	[^oC]	[As]	[-]
AOP-8-00	0		3,02	1,00		1,00
AOP-8-01	1,5	3,1	3,04	0,92	23,4	0,97
AOP-8-02	3	3	3,04	0,93	46,8	0,95
AOP-8-03	6	3	3,05	0,94	93,6	0,94
AOP-8-04	10	3,1	3,05	0,92	156,0	0,95
AOP-8-05	15	3,1	3,06	0,89	234,0	0,94
AOP-8-06	20	3,1	3,06	0,85	312,0	0,93
AOP-8-07	30	3,1	3,07	0,76	468,0	0,89
AOP-8-08	45	3,1	3,08	0,66	702,0	0,84
AOP-8-09	60	3	3,09	0,54	936,0	0,79
AOP-8-10	90	3,1	3,11	0,39	1404,0	0,69
AOP-8-11	122	3,1	3,13	0,27	1903,2	0,60
AOP-8-12	150	3,1	3,17	0,19	2340,0	0,53
AOP-8-13	180	3,1	3,17	0,13	2808,0	0,47
AOP-8-14	240	3,1	3,22	0,03	3744,0	0,37
AOP-8-15	300	3,2	3,24	0,00	4680,0	0,28